Quantitative Evaluation of Mesoscale Eddies in the North Atlantic Using Satellite Altimetry and Ocean Reanalyses

Paolo Mauriello[1,2], Gregory C. Smith[3], Andrea Storto[1], Chunxue Yang[1]

[1]Institute of Marine Science, National Research Council of Italy, Rome, Italy
[2] Department of Physics "E.R. Caianiello", University of Salerno, Fisciano, Italy
[3] Meteorological Research Division, Environment and Climate Change Canada (ECCC), Dorval, Canada

Correspondence to: Paolo Mauriello (pmauriello@unisa.it – paolo.mauriello@artov.ismar.cnr.it)

Abstract. Ocean mesoscale eddies (10–250 km) play a key role in transporting heat, momentum, and nutrients. Accurately evaluating their representation in ocean reanalysis becomes important given that ocean reanalysis is widely used in ocean and climate research due to their temporal and spatial consistent coverage. This study aims to assess two global ocean reanalysis products GLORYS12V1 (1/12° resolution) and GLORYS2V4 (1/4° resolution) available from the Copernicus Marine Service against satellite altimetry observations. We have used both AVISO DUACS (1/8°) and SWOT MIOST Science product (1/8°), as reference datasets that allow us to understand better the advantage of high-resolution altimetry data and have a fair evaluation for eddy-resolving ocean reanalysis (1/12°). The evaluation approach is based on a feature-based eddy-verification method to compare eddy properties for example amplitude, radius, centroid position using a cost-function metric. Probability of Detection (POD) and False Alarm Ratio (FAR) are then used to quantify the reanalysis skill. GLORYS12V1 demonstrates better agreement with observations than GLORYS2V4, especially for eddies with amplitudes >10 cm. For both AVISO DUACS 1/8° and SWOT MIOST Science, the POD increases by more than 30% when moving from GLORYS2V4 to GLORYS12V1, while the FAR also rises by about 20%, mainly due to the detection of more small eddies. For matched eddies, GLORYS12V1 shows a lower matching cost than GLORYS2V4 for both satellite products, with reductions of approximately 26%. The mean errors in amplitude, radius, and centroid distance are reduced by approximately 35%, 32%, and 13%, respectively. GLORYS12V1 achieves POD values of about 62% with both references, compared with about 46% for GLORYS2V4. FAR ranges from approximately 18% for GLORYS2V4 to 24% for GLORYS12V1. The results underline the added value of high model resolution for the representation mesoscale eddies in ocean reanalyses and highlight the value of wide-swath altimetry for model verification in regions as North Atlantic.

1 Introduction

Ocean mesoscale features with spatial scales from tens to hundreds of kilometers and time scales from weeks to months were first observed in the early 1930s by Columbus Iselin and colleagues during Montauk-to-Bermuda Cruises, as in Cullen (2005).

Since 1992, the launch of satellite altimetry missions has enabled global, high-resolution monitoring of sea level and ocean currents, significantly improving our understanding of ocean features, particularly mesoscale dynamics, as in Le Traon and Morrow (2001). Over the past decades, numerous studies have explored the dynamics and impacts of eddies, given their significant roles in transporting water masses, heat, salt and nutrients (Rhines and Young, 1982; Richardson, 1983; Stephens & Marshall, 1999; Chenillat et al., 2016; Yang et al., 2022). Recognizing their important role, several studies in recent years have investigated the predictability of eddies (Xu et al., 2018; Thoppil et al., 2021).

However, satellite altimetry only measures the surface signature of the eddy features. In contrast, ocean reanalyses produced by combining numerical models with observations through data assimilation schemes provides the evolution of four-dimensional ocean state estimates, enabling us to study the ocean mesoscale eddy structures not only at the surface but the subsurface. Therefore, it is important to evaluate how well ocean reanalyses represent mesoscale eddies to better understand the uncertainty inherent in these products. In recent years, the spatial resolution of ocean models has increased allowing a greater representation of smaller ocean features. The first aim of this study is to evaluate the ability of ocean reanalyses with different spatial resolutions (1/4° and 1/12°) to represent mesoscale eddies in the North Atlantic. Second, we assess how the verification results change when using two different satellite reference products, AVISO DUACS 1/8° and SWOT MIOST Science, in order to understand whether the additional fine-scale information from SWOT modifies the evaluation of reanalysis performance.

Several studies have investigated mesoscale eddy properties, such as population, duration, lifetime, and trajectories, in numerical models and reanalyses (de Vos et al., 2018; Mason et al., 2019; Xie et al., 2020; Bonaduce et al., 2021; Smith and Fortin, 2022). Eddy detection methods commonly used in these studies include approaches based on the Okubo-Weiss parameter, wavelet analysis of the relative vorticity field, and the geometry of streamlines (Souza et al., 2011). Another widely used approach, introduced by Chelton et al. (2011), relies on satellite-altimetry fields to identify coherent eddy structures. The py-eddy-tracker package developed by Mason et al. (2014) is also widely used to detect and track eddies at regional and global scales, as in de Vos et al. (2018) and López-Álzate et al. (2022). In the present study, we use py-eddy-tracker to perform the eddy detection and tracking process. This step is applied independently to each dataset and provides the eddy catalogues, including eddy position, amplitude, radius, polarity, and trajectories. However, evaluating the skill of an ocean reanalysis requires an additional step beyond detecting and tracking eddies independently in each dataset. In particular, it is necessary to determine whether an eddy detected in a reanalysis corresponds to the same eddy observed in satellite altimetry at a given time and location (a feature-matching and verification problem). To fill the gap, Smith and Fortin (2022) developed a verification method to evaluate the capability of ocean reanalyses in representing the eddy features at exact locations and time detected in satellite altimetry data. In this study we will adopt this method to evaluate the representation of eddies in two ocean reanalyses, thereby opening the door to a greater exploitation of ocean reanalyses.

A reference dataset is needed to validate and evaluate the performance of ocean numerical models in representing mesoscale eddies, also as done in previous feature-based eddy verification studies (Smith and Fortin, 2022). The finer spatial resolution of ocean reanalyses creates a problem when using the AVISO DUACS ¼° dataset as a reference, because this dataset cannot capture many small-scale features. Amores et al. (2018) show that signals smaller than about 50 km can be aliased into longer wavelengths in satellite altimetry. Ballarotta et al. (2019) also showed that the effective resolution of AVISO DUACS gridded altimetry maps is lower than their nominal grid spacing. This means that some of the small-scale variability found in high-resolution reanalyses may not be shown correctly in the AVISO DUACS product. For this reason, we did not use the ¼° AVISO DUACS product in this study. Instead, we used the AVISO DUACS dataset at 1/8°, which provides a finer nominal grid spacing and is consistent with the 1/8° grid of the SWOT MIOST product. Its use reduces the nominal grid-spacing mismatch with GLORYS12V1, but it does not overcome the effective-resolution limits of mapped altimetry, which depends on satellite sampling and the mapping procedure rather than on grid spacing alone. Small eddies close to the resolving capability of AVISO DUACS 1/8° are therefore interpreted with caution (Amores et al., 2018; Ballarotta et al., 2019).

The AVISO DUACS 1/8° satellite altimetry dataset, available from 1993 to the present at the global scale, has been widely used as a benchmark to validate and assess numerical models, ocean reanalyses, mesoscale eddy properties in many studies (Taburet et al.,2019; Mason et al., 2019; Xie et al., 2020). In this study, however, we use AVISO DUACS 1/8° only over the period overlapping with SWOT MIOST Science, from 1 August 2023 to 1 May 2025, in order to apply the same verification framework to both satellite reference products.

The availability of observations from the SWOT (Surface Water and Ocean Topography) wide-swath satellite altimetry mission provides another possible reference dataset for evaluating the capability of higher-resolution ocean reanalyses to identify and to track mesoscale eddies over the time in a regional area. SWOT was launched in December 2022 and offers wide-swath measurements of sea surface height, which allows observations of ocean features at much finer spatial scales than traditional altimetry. One of the objectives of SWOT is the observation of two-dimensional ocean surface topography and the characterization of mesoscale and submesoscale ocean circulation. Nevertheless, one important application of SWOT observations is their use in ocean analysis and forecasting systems through data assimilation, since wide-swath SSH observations can help better constrain mesoscale features and smaller-scale variability (Morrow et al., 2019; Fouchet et al., 2025). In the present study, however, we do not use the native SWOT swath observations directly. We use the experimental SWOT MIOST Science product, a global daily Level-4 gridded reconstruction of sea-surface height and derived geostrophic velocities produced by SSALTO/DUACS. MIOST stands for Multiscale Interpolation Ocean Science Topography. It merges irregularly sampled altimeter observations into fields that are continuous in space and time using a linear optimal-interpolation framework in which different covariance functions can be used to represent variability at different spatial and temporal scales. In the configuration considered here, the covariance functions are designed primarily to represent mesoscale geostrophic variability (Ubelmann et al., 2021; CLS and CNES, 2025). SWOT Level-4 sea-level products are not limited to the MIOST reconstruction used in this study. AVISO/DUACS also distributes experimental regional products generated using 4DVarNET and 4DVarQG. The 4DVarNET approach combines a variational data-assimilation formulation with a deep-learning framework to learn both the representation of ocean dynamics and the associated solver (Fablet et al., 2021; Beauchamp et al., 2023). In contrast, 4DVarQG uses a four-dimensional variational scheme constrained by a reduced-order quasi-geostrophic model, introducing an explicit dynamic prior into the reconstruction (Le Guillou et al., 2021).

Comparisons over the North Atlantic indicate that 4DVarNET and 4DVarQG are capable of providing finer effective resolution and improving the reconstruction of the energetic and nonlinear structures of the Gulf Stream compared to MIOST, although their performance may vary spatially and neither method currently provides a global mapping solution (Ballarotta et al., 2025). MIOST is selected because it provides a spatially consistent global reconstruction (such as AVISO DUACS 1/8°) covering the intended validation domain, the North Atlantic, up to the upper mid-latitudes (60°N). The 4DVarNET and 4DVarQG experimental maps, as of the study's final implementation (October and November 2025), were currently regional products covering approximately 25–50° N and 80° W–10° W and therefore do not include the northern part of our study region. However, there are some important limitations that must also be considered. First, because the mission is very recent, the time coverage of SWOT data is limited. Therefore, SWOT data cannot yet be used to study decadal or long-term variability of mesoscale activity. In this study, SWOT is used only for a short-period evaluation of the representation of mesoscale and smaller-scale eddy features in high-resolution reanalyses. Second, since similar nadir altimetry observations are assimilated in some ocean reanalysis products considered in this study, neither AVISO DUACS 1/8° nor SWOT MIOST Science can be regarded as a fully independent verification dataset. DUACS 1/8° is based on multi-mission nadir altimetry, while SWOT MIOST Science combines SWOT wide-swath observations with a multi-mission nadir-altimetry background used to constrain the larger-scale signal. Therefore, both satellite products share, at least partly, observational information with the reanalyses. However, SWOT MIOST Science also introduces additional fine-scale information from SWOT wide-swath measurements, which is not directly assimilated in the reanalysis products considered here. For these reasons, AVISO DUACS 1/8° and SWOT MIOST Science are used as complementary evaluation references rather than as absolute observational truth. The comparison with SWOT provides insight into how well the reanalyses represent fine-scale variability revealed by wide-swath altimetry, whereas the DUACS comparison provides continuity with the longer pre-SWOT altimetry record.

This complementary approach allows us to assess the representation of mesoscale eddies in the reanalyses while explicitly acknowledging the limitations associated with the partial dependence of the reference datasets.

An evaluation over the full period of the reanalyses era (1993 – present), including the uncertainties associated with altimetry constellation and mapping procedures, will be left for a future study.

In the following sections, we will introduce in detail the data and methods we use in this study and present the results of the evaluation (Section 2) and finally provide assessment results in terms of ocean reanalyses in representing ocean mesoscale eddies (Section 3).

2 Data and Methods

In this study, we use two Global Ocean Reanalysis datasets, GLORYS12V1 and GLORYS2V4, and two standard satellite-altimetry gridded-observational products, AVISO DUACS L4 product and SWOT MIOST L4 product. Detailed descriptions are provided below.

2.1 Satellite Altimetry Products

The AVISO DUACS global 1/8° daily gridded product provides sea level anomaly (SLA), absolute dynamic topography (ADT), and geostrophic velocities derived from multi-mission satellite altimetry. The product is generated by the CNES/CLS DUACS system and distributed by the Copernicus Marine Service (Taburet et al., 2019; Ballarotta et al., 2019). Although its nominal grid spacing is 1/8° (approximately 12.5 km), its effective resolution is lower because the optimal-interpolation procedure smooths part of the small-scale variability. Its effective resolving capability is typically between 50 and 100 km, depending on latitude and the observing constellation, which limits the representation of the smallest mesoscale and submesoscale features (Chelton et al., 2011b; Ballarotta et al., 2019; CMEMS Sea Level Product User Manual, 2025).

To complement the standard DUACS product, we also use the experimental global 1/8° SWOT MIOST Science gridded sea-level dataset distributed by AVISO/DUACS (CLS and CNES, 2025). This product combines multi-mission nadir altimetry with SWOT observations and uses the MIOST framework to reconstruct fields that are continuous in space and time through a multiscale optimal-interpolation approach designed to represent mesoscale geostrophic variability (Ubelmann et al., 2015; Rogé et al., 2017; CLS and CNES, 2025). However, SWOT MIOST remains a daily Level-4 mapped product and should not be interpreted as a direct representation of the native KaRIn observations. Its smallest-scale variability is still affected by observational noise, filtering, interpolation, and the spatial and temporal sampling of the observing system. In addition, its relatively short temporal coverage limits its use for investigating decadal or longer-term variability.

The SWOT Level-4 products over the North Atlantic are not limited to MIOST. There are, as noted in Introduction, other experimental regional products, such as 4DVarNET and 4DVarQG, are also available and use different data-driven or dynamically constrained mapping approaches (Le Guillou et al., 2021; Beauchamp et al., 2023; Ballarotta et al., 2025). As explained in Introduction, we select MIOST because it provides a spatially consistent global reconstruction covering the complete verification domain, differently from these other products that don’t include the whole study area.

The AVISO DUACS 1/8° product used in this study corresponds to the Copernicus Marine Service product SEALEVEL_GLO_PHY_L4_MY_008_047, dataset cmems_obs-sl_glo_phy-ssh_my_allsat-l4-duacs-0.125deg_P1D, DOI: 10.48670/moi-00148. This product was accessed and downloaded on 31 October 2025.

The SWOT MIOST Science product used in this study corresponds to the AVISO/DUACS Experimental Multimission Gridded Level-4 Sea Surface Heights and Velocities product including SWOT observations, generated using the MIOST mapping method, version 2.0.1, DOI: 10.24400/527896/A01-2025.001. This product was accessed and downloaded from the v_2_0_1/miost/science directory on 1 November 2025.

2.2 Global Ocean Reanalysis products

To evaluate the impact of the spatial resolution on reanalysis skills, we used two Global Ocean Reanalysis products, distributed by CMEMS: GLORYS2V4 and GLORYS12V1. These products are part of the CMEMS multi-year reanalysis portfolio and are designed to deliver consistent, observation-constrained reconstructions of the ocean state over the satellite altimetry era (1993–present).

GLORYS12V1 is an eddy-resolving reanalysis, developed by Mercator Ocean International. It provides a global ocean reanalysis at 1/12° horizontal resolution (~8 km), with 50 vertical levels. The system is based on the NEMO ocean general circulation model (v3.1) coupled with the LIM2 sea-ice model and uses Arakawa C-grid discretization, as explained in Madec, G., & the NEMO System Team (2024). The reanalysis assimilates along-track delayed-time sea-level anomaly (SLA) from all altimetric satellites, AVHRR-only Reynolds SST (1/4°), in-situ temperature and salinity profiles from the CORA v4.1 database (Szekely et al., 2019), and sea-ice concentration from CERSAT (Ezraty et al.,2007).

For both comparisons, the study requires the use of the interim extension for GLORYS12V1 (cmems_mod_glo_phy_myint_0.083deg_P1D-m) : daily mean sea surface height fields from the interim archive, matching the same period used for satellite datasets.

GLORYS2V4 is a lower-resolution global ocean reanalysis included in the Copernicus Marine Global Ocean Ensemble Physics Reanalysis product. It is based on the NEMO v3.1 model framework coupled with the LIM2 thermodynamic–dynamic sea ice model, configured on the ORCA025 grid with a nominal horizontal resolution of 1/4° and 75 vertical levels. For the present study, the temporal coverage selected for GLORYS2V4 also matches the period used for the satellite datasets, in order to allow a direct comparison with GLORYS12V1. All details on the main parameters of the two reanalysis products are included in Table 1.

GLORYS12V1 was obtained from the Copernicus Marine Service product GLOBAL_MULTIYEAR_PHY_001_030, DOI: 10.48670/moi-00021. The product was accessed and downloaded on 1 November 2025.

GLORYS2V4 was obtained from the Copernicus Marine Service product GLOBAL_MULTIYEAR_PHY_ENS_001_031, DOI: 10.48670/moi-00024. The product was accessed and downloaded on 1 November 2025.

Parameters	GLORYS12V1	GLORYS2V4
Model version + grid version	LIM2 EVP NEMO 3.1, driven at the surface by ECMWF ERA Interim reanalysis until end of 2018 and ERA5 reanalysis thereafter + ORCA Grid (1/12°)	LIM2 EVP NEMO 3.1 + ORCA1/4°
Domain	Global	Global
Horizontal resolution	1/12°: 4320 X 2041 grid points	1/4°: 1440 X 1021 grid points
Vertical sampling	50 z-levels	75 z-levels
Numerical technique	Primitive equations with finite differences: on Arakawa C native grid	Same as GLORYS12V1
Time integration	Leapfrog explicit, barotropic/baroclinic splitting; baroclinic step: 300 s	Leapfrog explicit, barotropic/baroclinic splitting; baroclinic step: 450 s
Prognostic variables	3D currents, potential temperature, salinity, turbulent kinetic energy (TKE), sea surface height (SSH)	Same variables as GLORYS12V1
Geophysical variables	Bathymetry from ETOPO2 plus some local smoothing to accommodate large tidal currents	Same as GLORYS12V1
Horizontal diffusion	horizontal Laplacian on tracer variables, bi-Laplacian on momentum variables	Same as GLORYS12V1
Surface scheme	ERA-Interim until 2018, ERA5 from 2019, bulk CORE formula with corrections for precipitation and radiative fluxes	No surface nudging precipitation, flux correction Climatological runoff + ice shelf and iceberg melting
Turbulent mixing	TKE scheme with mixing length set to 10 m	Same as GLORYS12V1
Assimilated Satellite observations	Reynolds 0.25° AVHRR-only SST, Delayed Time SLA from all altimetric satellites, in situ T/S profiles from Copernicus Marine CORAv4.1 database, CERSAT Sea Ice Concentration	SST, SLA, T/S profiles, SIC

Table 1. Parameters used in GLORYS12V1 and GLORYS2V4. Both the Reanalysis dataset used the same assimilated scheme: SAM2, a large-scale bias correction 7-day assimilation window Merge MDT (observations + model) Reynolds SST, CORA.

2.3 Verification Period and Domain

As mentioned in 2.2, the analysis was conducted over the period from 1st August 2023 to 1st May 2025. This period corresponds to the availability of daily outputs from both reanalysis systems, and it ensures the overlap with the DUACS 1/8° observational datasets and provides a sufficient window for an eddy statistics evaluation. An evaluation of eddy statistics over the full period of the reanalysis products is left to a future study. Here, our focus is to demonstrate the robustness of the verification approach and to assess the sensitivity of the reanalysis evaluation to the choice of satellite altimetry reference product by using two different satellite datasets. Before the application of the verification method, all products are previously interpolated to a 1/8° regular grid (DUACS 1/8° and SWOT MIOST Science grids), and high-pass filtered using a Bessel filter with a 500 km cutoff, as described in Mason et al. (2014), to isolate the mesoscale signals (see Appendix D for more details about different spatial Bessel filter cutoff wavelength). The same parameters are also used for the eddy detection algorithm. The verification domain is defined as the region bounded by 29.8° N – 59.8° N in latitude and 80.1° W – 30.1° W for longitude, to include the Gulf Stream influence region, as described in Smith and Fortin (2022). This region is known for its intense mesoscale activity and high eddy kinetic energy, making it particularly suitable for validating eddy-resolving capabilities of ocean analysis and reanalysis systems.

2.4 Eddy verification methodology

The detection and tracking of mesoscale eddies in this study follows the standard procedure implemented in PyEddyTracker described in Mason et al. (2014), Mason et al. (2019), Pegliasco et al. (2021) and used in Smith and Fortin (2022) to develop a robust verification methodology, adopted in this study. It is based on identifying closed contours in daily fields of Sea Level Anomaly (SLA) or Sea Surface Height (SSH), and using the associated geostrophic velocities to classify the rotation polarity. We have adopted the approach described by Pegliasco et al. (2021), where the detection is performed on SSH (or Absolute Dynamic Topography) fields rather than SLA to reduce the risk of misidentifying Gulf Stream meanders as eddies, an issue commonly encountered when using SLA in strongly sheared regions. A closed contour is “accepted” as an eddy, in other words, it is considered a “detected” eddy for py-eddy-tracker routine, if it satisfies the following criteria:

- It must contain a single maximum (for Anticyclonic) or minimum (for Cyclonic).
- The shape must be roughly circular, with a contour area not deviating more than 55% from a perfect circle.
- Pixel count 5 pixels = Imin ≤ I ≤ Imax = 2000 pixels: have between 5 and 2000 pixels.
- The amplitude, computed as the difference between the contour extremum and the outermost valid contour, must be at least twice the contour interval. With the 0.2 cm contour interval used here, this gives a minimum algorithmic threshold of 0.4 cm. This low value is used only as a permissive detection criterion and not as a physical threshold for eddies; weak features are assessed later through lifetime filtering and amplitude-dependent verification statistics (see Sect. 3.2 and Appendix C for more details).

After the detection of eddies for each date, eddies are tracked in time using cost function C (Eq. 1), which links eddies on consecutive days based on similarity in amplitude, radius, and centroid position. For a particular eddy, all eddies within a radius of 125 km are identified. The cost function, adopted for each pair of eddies, is based on the difference in amplitude A, in effective radius R and distance D, and it is defined as:

$$C$$

$$C = \sqrt{\frac{(A_1 - A_2)^2}{A_1^2} + \frac{(R_1 - R_2)^2}{R_1^2} + \frac{(D)^2}{(125\ km)^2}} \quad (1)$$

where the subscripts 1 and 2 denote, respectively, the satellite eddy and the candidate reanalysis eddy in the matching procedure. In the tracking procedure, they denote a detected eddy at time t and a candidate continuation at time t+1, respectively (see Appendix D for more details about the use of a different distance threshold of the matching cost function).

A minimum lifetime threshold is applied to reduce the identification of transient or spurious features, like in Mason et al. (2014). In this study, we adopt a 4-day minimum lifetime threshold, requiring each eddy to be detected on consecutive days without observational gaps. This relatively short threshold is used to verify the ability of the reanalyses to represent the full spectrum of mesoscale features detected in the satellite products, including short-lived eddies that may still affect the matching statistics. In addition, we have also introduced a calculation with a minimum lifetime threshold of 7 days and 28 days (see Appendix A, for more details). A lifetime threshold of 7 days is also used for certain evaluations to demonstrate the sensitivity to this choice (e.g 4 days). The 28-day threshold is useful for isolating persistent structures, but it is not our primary choice because the aim is also to evaluate the entire population, including short-lived eddies. Eddy properties such as effective radius, amplitude, trajectory, and lifetime are computed for each track. The effective radius is defined as the radius of a circle with the same area enclosed by the eddy contour.

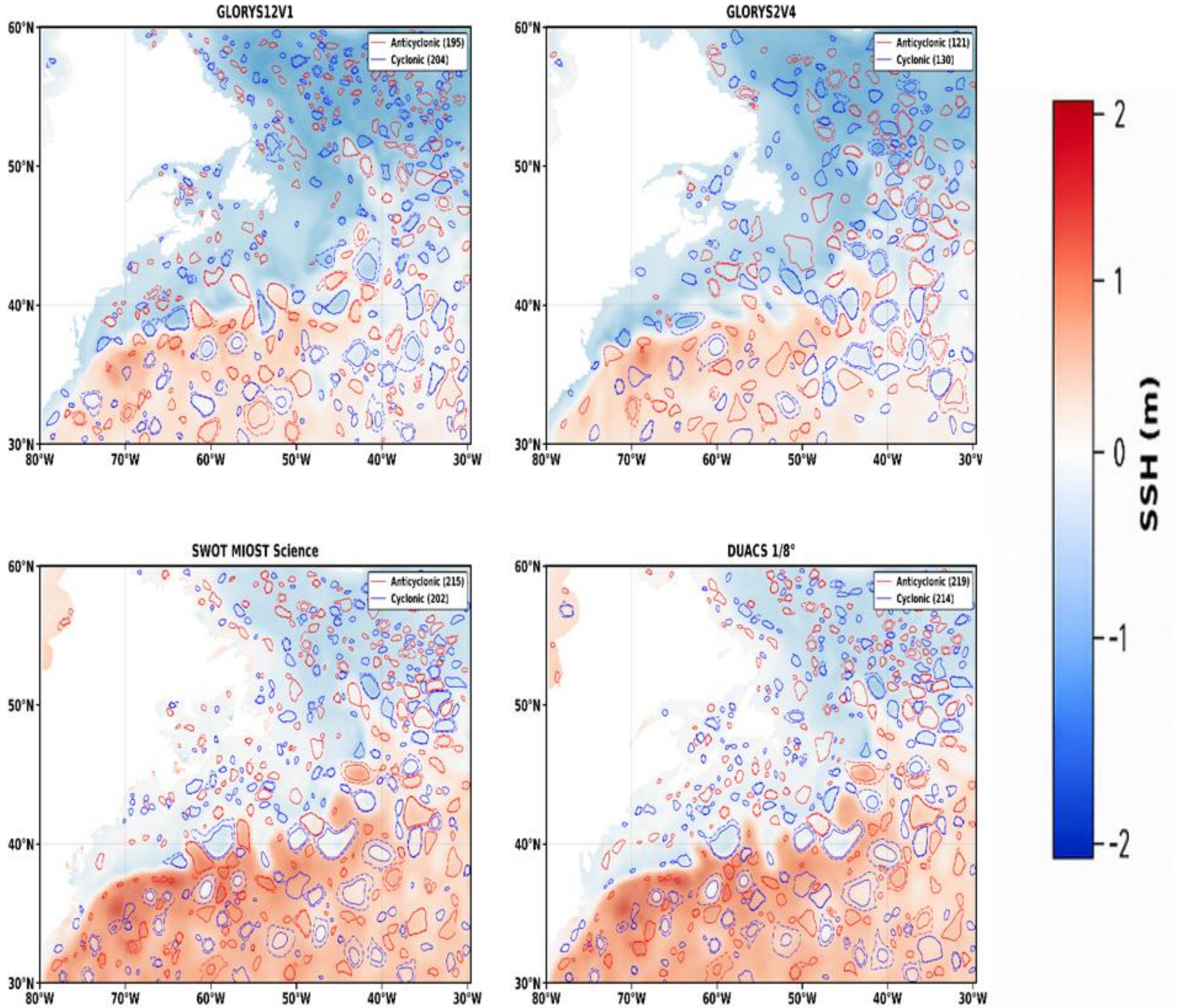

Fig.1.Daily sea-level fields on 1 January 2025 for GLORYS12V1, GLORYS2V4, SWOT MIOST Science, and AVISO DUACS 1/8°, after application of a high-pass Bessel filter with a cutoff wavelength of 500 km. The common colour bar is labelled SSH (m), with SSH used here as a general label for the sea-surface height field. Specifically, the colour shading represents modelled SSH for GLORYS12V1 and GLORYS2V4 and satellite-derived Absolute Dynamic Topography (ADT) for SWOT MIOST Science and AVISO DUACS 1/8°. Although SSH and ADT are not formally identical quantities, they are dynamically comparable and are treated consistently for contour-based eddy detection. Detected anticyclonic and cyclonic eddies are overlaid in red and blue, respectively. Solid contours indicate the contour of maximum circum-averaged geostrophic speed, whereas dashed contours indicate the effective contour used to calculate eddy area and effective radius. All fields were remapped onto the same regular 1/8° grid to allow direct comparison.

This consistent methodology for all datasets ensures that the detected eddies are comparable and that any differences in eddy representation between reanalyses or between them and observations are due to the intrinsic quality of the reanalysis systems and not to processing artifacts (Droghei et al., 2018; Ciani et al., 2019). First, an analysis of the power spectral analysis for the four products considered in this study, using 1 January 2025 as a representative test case. All datasets are remapped onto the same regular 1/8° grid, which is the native grid of both SWOT and DUACS. Figure 1 shows the SSH fields used in this study from GLORYS12V1, GLORYS2V4, SWOT MIOST Science and AVISO DUACS 1/8°. For the two reanalysis products, GLORYS12V1 and GLORYS2V4, SSH represents the modelled sea-surface height above the model geoid or reference equipotential surface, as described in Lellouche et al. (2021). For the satellite altimetry products used in this study, the corresponding SSH field is represented by Absolute Dynamic Topography (ADT), which is the sea-surface height above the geoid and is obtained by adding the Mean Dynamic Topography (MDT) to the Sea Level Anomaly (SLA) (i.e. ADT = SLA + MDT, as explained in Mulet et al. (2021)). Although the reanalysis SSH and satellite ADT are not identical data products, since the former is produced by ocean models constrained by data assimilation and the latter is derived from satellite altimetry and an estimated MDT, they can be considered dynamically comparable, because they provide dynamically comparable representations of sea-surface dynamic topography, from which surface geostrophic currents are derived. As described in Mason et al. (2014), Mason et al. (2019) and Pegliasco et al. (2021), contour-based eddy detection and tracking methods, such as those implemented in py-eddy-tracker, can be consistently applied to both fields because they mainly rely on local extrema, closed contours, spatial gradients, and centre-to-edge height differences. The superimposition of the detected eddies on the SSH/ADT background also allows their sizes and positions to be evaluated in relation to the Gulf Stream pathway.

In analogy to the approach adopted in Droghei et al. (2018) and Ciani et al. (2019), we selected the North-West Atlantic region and computed one-dimensional wavenumber spectra using a fast Fourier transform (FFT) to quantify the spatial scales effectively represented by each dataset. To avoid the latitude-dependent distortion associated with zonal wavenumbers expressed in degrees, all SSH fields were first projected onto a Lambert Azimuthal Equal-Area coordinate system centred on the study domain. The fields were then interpolated onto a regular kilometre-scale grid with dx = dy = 12.5 km. The one-dimensional zonal and meridional spectra were computed on this projected grid using FFTs. The resulting wavenumbers are therefore expressed in cycles / km, with the corresponding wavelengths shown in kilometres.

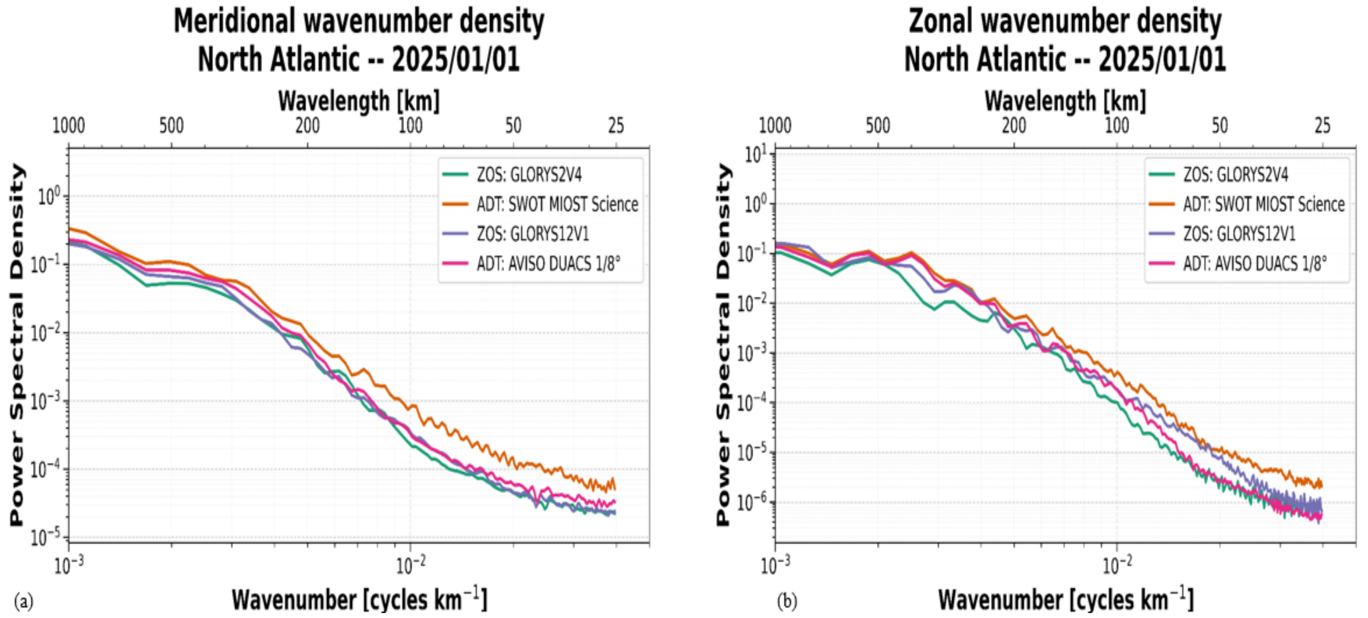

Fig.2. Power spectral density of SSH, corresponding to ADT for the satellite altimetry products, for the four datasets on 1 January 2025 over the selected North Atlantic region. All fields were projected onto a Lambert Azimuthal Equal-Area coordinate system and interpolated onto a regular kilometre-scale grid with dx = dy = 12.5 km, before computing the spectra. Panel (a) shows the meridional spectrum and panel (b) the zonal spectrum. Wavenumbers are expressed in cycles / km, with the corresponding wavelengths shown in kilometres on the upper x-axis.

Fig. 2 reports the comparative spectral analysis of the four SSH fields along the zonal and meridional directions on the projected grid. At large spatial scales, approximately larger than 200 km, all spectra exhibit comparable energy levels, indicating a consistent representation of the dominant mesoscale structures. At shorter wavelengths, differences become more evident. In the meridional direction, SWOT systematically exhibits the highest spectral energy over most of the resolved range, with a clearer separation from the other products below about 100 km. DUACS and GLORYS12V1 show intermediate and broadly similar energy levels, whereas GLORYS2V4 generally displays the weakest small-scale energy. In the zonal direction, the four spectra are also similar at large scales, but a progressive separation emerges toward smaller wavelengths, with SWOT again retaining the highest spectral energy. Over much of the mesoscale range, GLORYS12V1 and DUACS remain relatively close, while GLORYS2V4 decreases more rapidly. At wavelengths shorter than about 50 km, all spectra show a marked decay, but SWOT continues to preserve the largest amount of variance, and GLORYS12V1 generally retains more small-scale zonal energy than GLORYS2V4. Overall, these spectra indicate that the SWOT product better preserves fine-scale variability, while the higher-resolution GLORYS12V1 reanalysis captures small-scale mesoscale energy more effectively than GLORYS2V4.

In Fig.3, we see the dependence between radius and amplitude, in which we note that eddies display similar properties in terms of effective radius and amplitude. Many small eddies are detected with a radius below 50 km and amplitude less than 5 cm. In Fig. 4, most eddies have amplitudes lower than 10 cm. However, their mean lifetime is lower than 50 days (see Appendix C for more details about mean lifetime and eddy amplitude thresholds). However, features with amplitudes of only a few millimetres, should not be interpreted as physically robust eddies. The 0.4 cm value corresponds only to the permissive algorithmic threshold used during the py-eddy-tracker detection step, and is not used here as a physical threshold to define the robust eddy population. It can be noted, generally, that larger amplitude eddies are also found to have larger radius (Fig. 3). The eddy identification and tracking procedure are independently applied for each product and produce plots about physical features and time series of anticyclonic and cyclonic eddies.

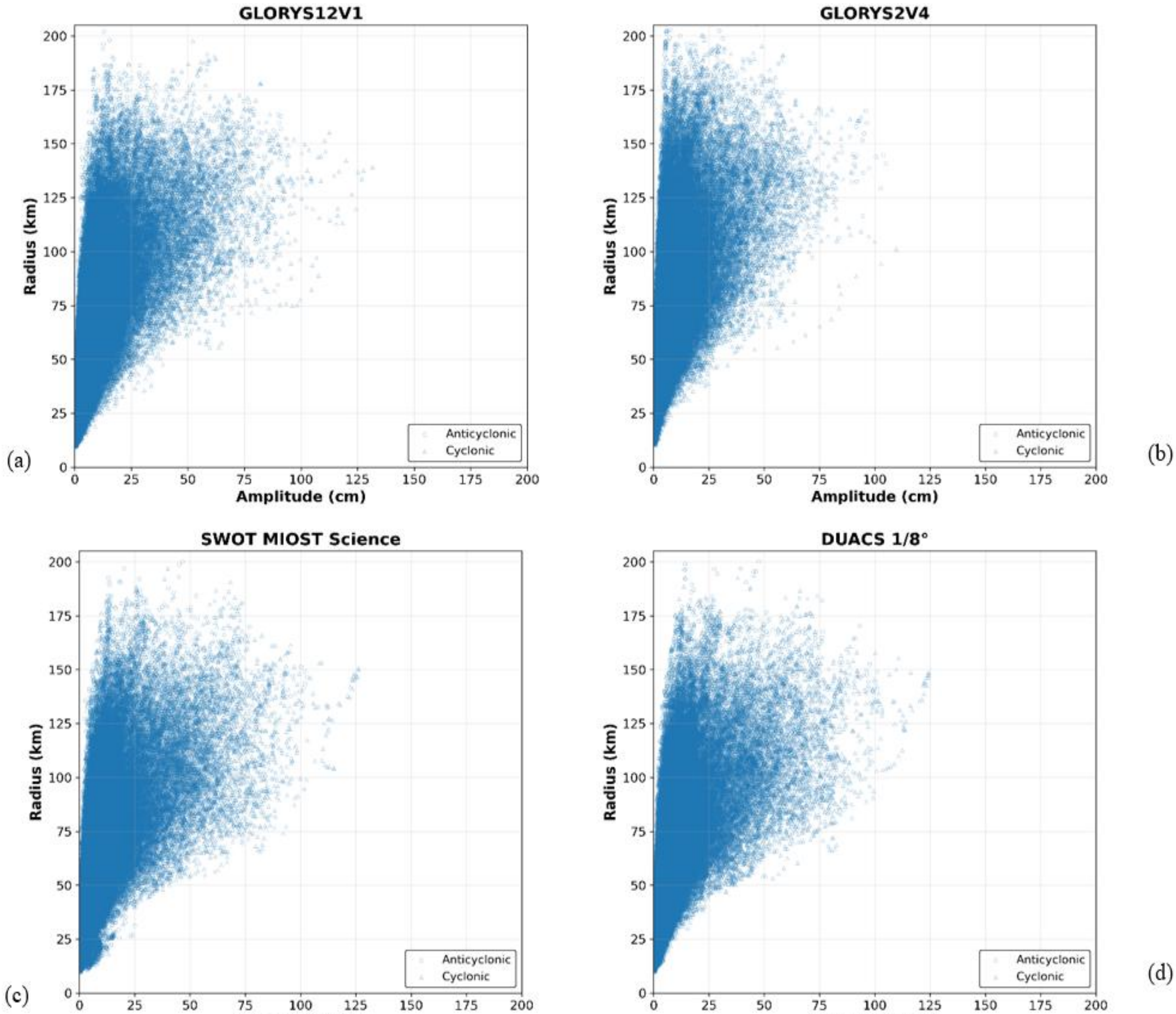

Fig. 3. Scatter plots of detected eddies, with a minimum lifetime threshold of 4 days, between Radius and Amplitude, from 2023-08-01 to 2025-05-01, for (a) GLORYS12V1 (bilinear remapped onto DUACS and SWOT grid), (b) GLORYS2V4 (bilinear remapped onto DUACS and SWOT grid), (c) SWOT MIOST Science, and (d) AVISO DUACS 1/8°. The eddy amplitude and the eddy radius are calculated at the track level, by averaging the amplitude and radius over the entire lifetime of the eddy.

The same cost function (1) used for the tracking procedure is also used to match the eddies between the reanalysis and the observed eddy (satellite). This function allows us to see how the eddies can be matched even if they have different values for radius, amplitude, mean centroid position, and shape. Although one or more of these parameters can vary, for an eddy to be considered matched to the corresponding satellite dataset, the cost function must be minimized, provided that the distance between the eddy centroids does not exceed 125 km (is set to 125 km, i.e., that's slightly greater than the average diameter of eddies in the North Atlantic region; see Ballarota et al., 2019).

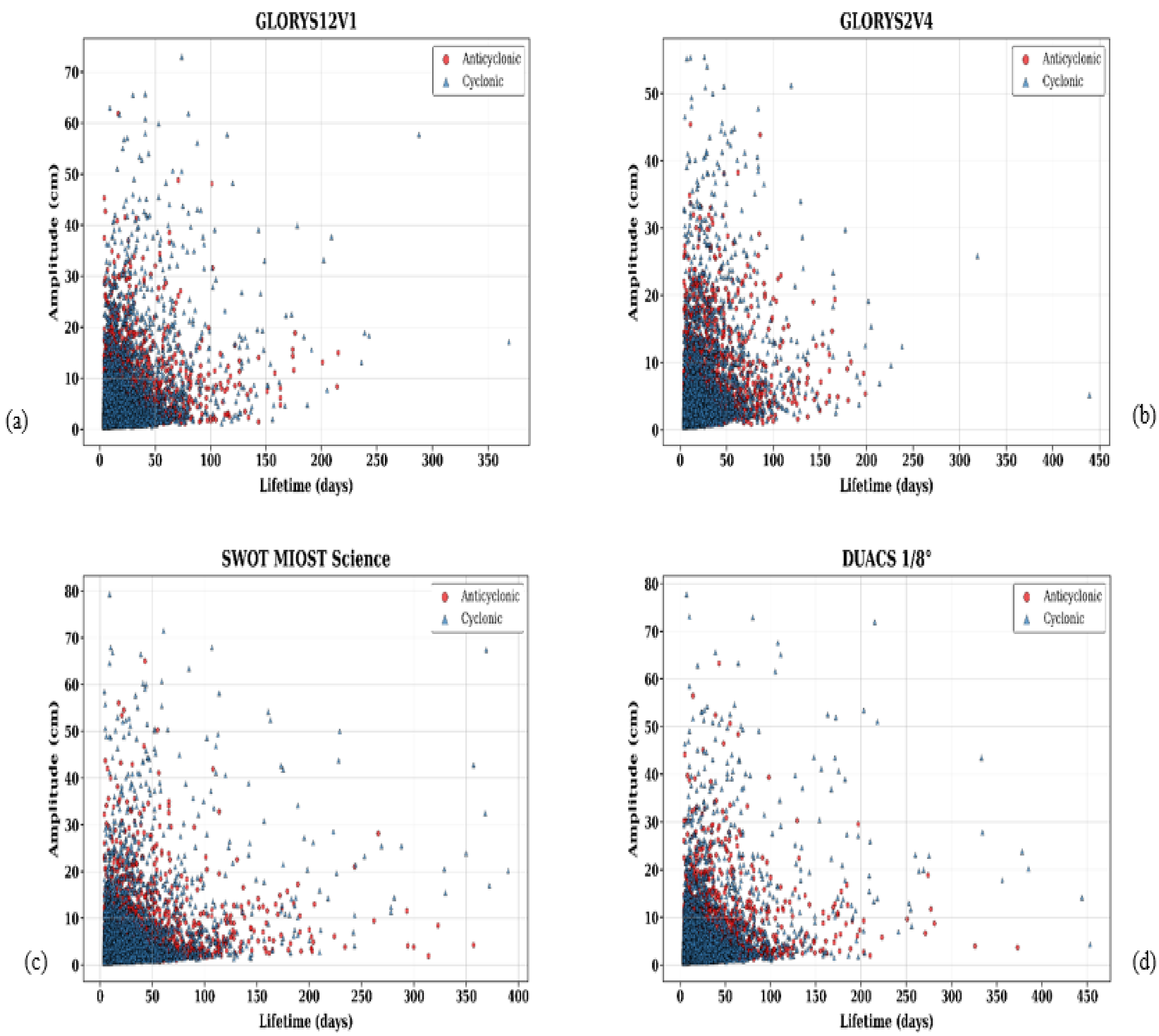

Fig.4. Scatter plots of identified eddies, with a lifetime threshold of 4 days, between Amplitude vs Lifetime of eddies for (a) GLORYS12V1, (b) GLORYS2V4, (c) SWOT, (d) DUACS. Each eddy is counted only once. The amplitude is calculated at the trace level, by averaging the amplitude over the entire lifetime of the eddy.

Therefore, following the application of the matching algorithm, as described in Smith and Fortin (2022), an eddy identified in both the reanalysis (i.e. GLORYS2V4 and GLORYS12V1) and verifying datasets (DUACS and SWOT products) is referred to as ‘‘hit’’. An eddy in the verifying dataset with no corresponding eddy in the reanalysis is referred to as a ‘‘miss”, whereas an eddy present in a reanalysis but not in the verifying dataset, is deemed as a ‘’false alarm’’. In Fig. 5(a) and in Fig. 5(b), we see an example of eddy matching procedure for both comparisons, following the concept of the matching algorithm, described in Smith and Fortin, 2022. The statistics for hits, misses and false alarms can be tabulated over the study area and over the full evaluation period to provide an indication of the skill of two reanalysis products in representing the "observed eddies". It is interesting to consider what fraction of the observed eddies are captured (not excluded) by reanalysis products, using the Probability of Detection (POD), as introduced and explained in Smith and Fortin (2022), defined as:

$$POD = \frac{hits}{(hits + misses)} \quad (2)$$

The POD is the number of matched eddies over the total number of eddies present in the satellite product.

Similarly, one can consider what fraction of the predicted eddies in the model analyses did not occur using the False Alarm Ratio (FAR), as explained in Smith and Fortin (2022), defined as:

$$FAR = \frac{false\ alarms}{(false\ alarms\ +\ hits)} \quad (3)$$

Both POD and FAR have values between [0,1] with perfect values of 1 and 0, respectively.

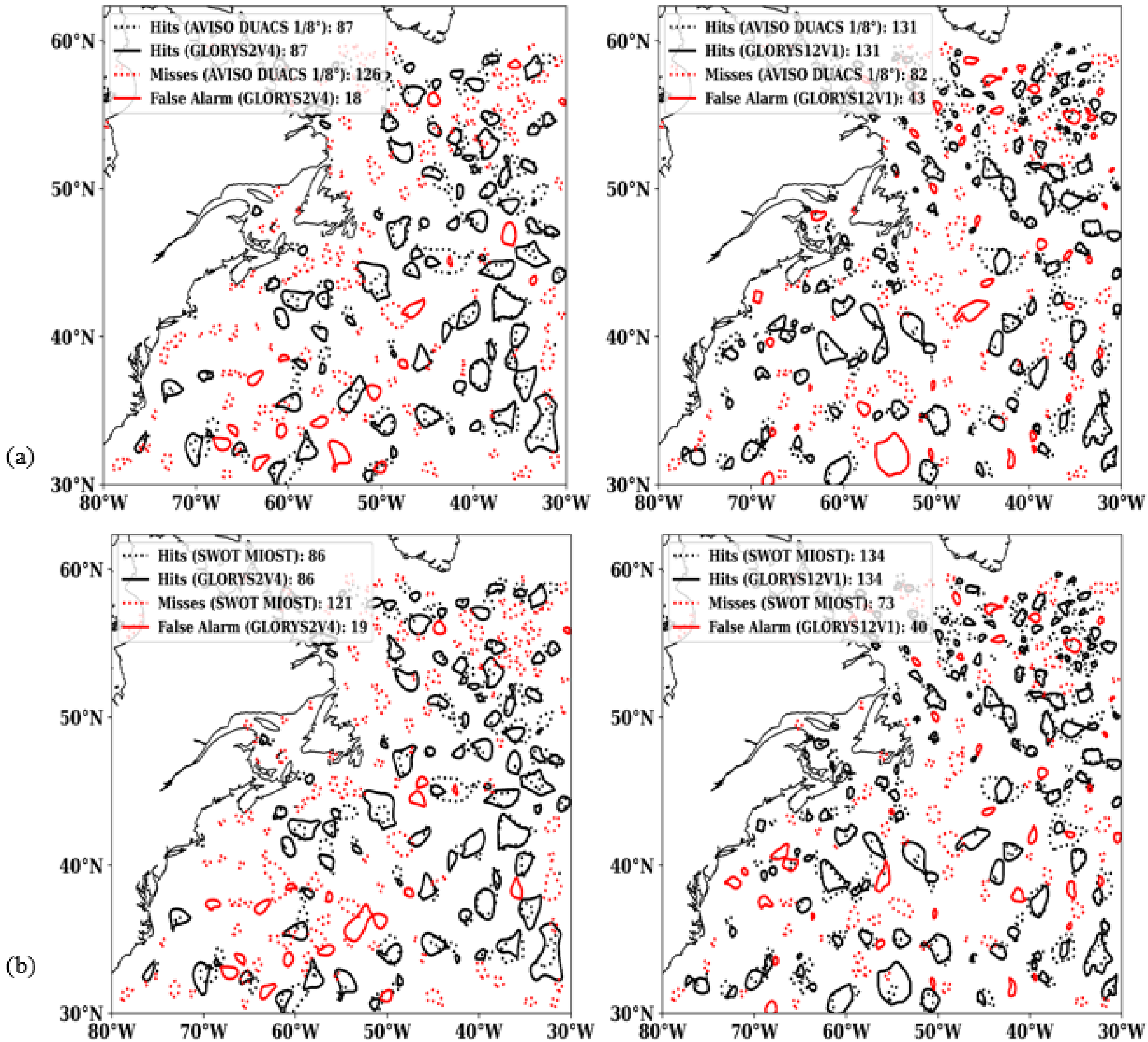

Fig. 5. The first one (a) is an example showing Anticyclonic eddy matching statistics for 1st January 2025 for GLORYS2V4 (left), and GLORYS12V1 (right), compared with DUACS. Eddies for which a corresponding match is found (hits) between DUACS and GLORYS2V4/GLORYS12V1 are shown as dotted and solid black contours. Eddies identified in DUACS (satellite data) with no corresponding eddy in GLORYS2V4/GLORYS12V1 are deemed misses (red dotted contours). Eddies identified in GLORYS2V4/GLORYS12V1 but without a corresponding eddy to DUACS are deemed false alarms. The second one (b) is an example showing Anticyclonic eddy matching statistics for 1st January 2025 for GLORYS2V4 (left), and GLORYS12V1 (right), compared with SWOT (satellite data).

3.Results

In this section, we present the results from the application of the eddy identification, tracking and matching algorithm described above. First, the results of the eddy identification in the four sets of analyses are presented in Section 3.1. We then examine the matching statistics (hits, false alarms, misses, POD and FAR) in terms of eddy radius and amplitude in Sect. 3.2. We also evaluate errors in the properties of matched eddies due to the relative contributions to the matching cost function (hits cost, radius, amplitude, and distance between eddy centroids) in Section 3.3.

3.1 Results of eddy identification

The properties of identified eddies for the four datasets are quite similar (see Fig. 3) over the entire period. In Fig. 3, we see similar trends between radius and amplitude. Many small eddies, with a radius lower than 60 km (see Fig.3 and Fig.4) not far from the threshold of detection, and an amplitude lower than 5 cm, have been identified. We do not clearly see two distinct populations based on an amplitude threshold of 10 cm, compared to the corresponding average lifetime. This is merely a descriptive threshold, intended to show that most of the detected eddies are clustered within a 10-cm amplitude range. For more details, see Appendix C, which provides a more detailed description of the datasets based on specific eddy amplitude thresholds.

In Fig. 4 we see that most have amplitudes below 10 cm, but at the same time there is a moderate positive correlation between amplitude and lifetime, whereby as amplitude increases, so does the average survival time of the eddies. Considering anticyclonic and cyclonic eddies together, the Spearman correlation coefficients are $\rho = 0.422$ for GLORYS12V1, $\rho = 0.518$ for GLORYS2V4, $\rho = 0.464$ for SWOT MIOST Science, and $\rho = 0.455$ for DUACS 1/8°, with $p < 0.001$ in all cases. These results indicate that larger-amplitude eddies tend to persist longer, although a moderate correlation and the amplitude alone does not fully explain the variability in eddy lifetime. The number of identified eddies is sensitive to the choice of the minimum eddy lifetime threshold, as noted in Section 2.4. Tables 2 and 3 show the total number of anticyclonic and cyclonic eddies detected and tracked with a minimum lifetime of 4 days. The total number of identified and tracked eddies is higher in the satellite products than in GLORYS2V4 and GLORYS12V1, for both anticyclonic and cyclonic eddies. Consistent with its higher spatial resolution, GLORYS12V1 detects more eddies than GLORYS2V4. Tables 2 and 3 also show an almost balanced cyclonic/anticyclonic distribution in the satellite products, but a stronger cyclonic dominance in both reanalyses. This difference is likely related to the different nature of the products. Reanalyses combine assimilated observations with model dynamics and can therefore retain or generate small-scale structures, especially in the eddy-resolving GLORYS12V1 system. In contrast, DUACS and SWOT MIOST are Level-4 gridded satellite products derived from along-track altimetry, and their mapping and interpolation procedures may smooth or merge weak small-scale SSH features. Therefore, the cyclonic excess in the reanalyses should be interpreted with caution. It may reflect model dynamics, data-assimilation effects, and the sensitivity of the closed-contour detection method to weak cyclonic SSH minima, rather than a robust observed polarity asymmetry.

3.2 Eddy verification results

For each comparison, hits, misses, and false alarms are tabulated over the full evaluation period (1 year and 9 months for both comparisons). These counts tabulated, meaning that they are evaluated by adding up all the counts of hits, misses, and false alarms for the entire verification period, for both cyclonic and anticyclonic eddies are used to compute the Probability of Detection (POD) and the False Alarm Ratio (FAR) (following the Eqs. (2) and (3)). For the total counts of eddies, the results are reported separately for anticyclonic and cyclonic. The results for DUACS-based comparison are shown in Fig. 6(a), Table 2 and Table 4, while in Fig. 6(b), Table 3 and Table 5 for SWOT comparison results.

Dataset	Anticyclonic	% w.r.t. DUACS	Cyclonic	% w.r.t. DUACS
DUACS	125580 (4 days)	- -	125229 (4 days)	- -
GLORYS2V4	67961 (4 days)	54.12%	72953 (4 days)	58.26%
GLORYS12V1	97788 (4 days)	77.87%	106861 (4 days)	85.33%

Table 2: total number of anticyclonic and cyclonic eddies identified in the region of study over the evaluation period for DUACS, GLORYS2V4, and GLORYS12V1, for a minimum lifetime threshold of 4 days. The percentage of eddies identified in GLORYS2V4 and GLORYS12V1 with respect to AVISO is also provided.

Dataset	Anticyclonic	% w.r.t. SWOT	Cyclonic	% w.r.t. SWOT
SWOT	124154 (4 days)	- -	125676 (4 days)	- -
GLORYS2V4	67961 (4 days)	54.74%	72953 (4 days)	58.05%
GLORYS12V1	97788 (4 days)	78.76%	106861 (4 days)	85.03%

Table 3: total number of anticyclonic and cyclonic eddies identified in the region of study over the evaluation period for SWOT MIOST, GLORYS2V4, GLORYS12V1, for a minimum lifetime threshold of 4 days The percentage of eddies identified in GLORYS2V4 and GLORYS12V1 with respect to SWOT MIOST is also provided.

Verification metric	GLORYS12V1	GLORYS2V4	Diff.	Diff.%
POD	0.628	0.460	0.168	36.52%
FAR	0.230	0.182	0.048	26.37%

Table 4: aggregated eddy verification statistics for the Probability of Detection (POD) and False Alarm Ratio (FAR) evaluated over the period, from 1st August 2023 to 1st May 2025, for the comparison with AVISO DUACS 1/8°, with a minimum lifetime threshold of 4 days.

Verification metric	GLORYS12V1	GLORYS2V4	Diff.	Diff.%
POD	0.624	0.455	0.169	37.14%
FAR	0.237	0.194	0.043	22.16%

Table 5: aggregated eddy verification statistics for the Probability of Detection (POD) and False Alarm Ratio (FAR) evaluated over the period 1st August 2023 to 1st May 2025, for the comparison with SWOT MIOST, with a 4-day minimum lifetime threshold.

There is certainly a slight decrease, when comparing the total number of anticyclonic eddies to that of cyclonic eddies, which is particularly evident for GLORYS12V1. Based on the observed data, the two satellite products show nearly balanced polarity counts, with differences not exceeding 1.3 %. In contrast, cyclonic daily detections exceed anticyclonic detections by approximately 7.3 % in GLORYS2V4 and 9.3 % in GLORYS12V1. As shown in the eddy matching example in Fig. 5, there is a significant difference in terms of hits, misses, and false alarms between the two reanalyses. While the number of hits increases by about 37% when switching from GLORYS2V4 to GLORYS12V1, the number of misses decreases significantly, by about 31%, whereas the number of false alarms increases dramatically, around 77%. This demonstrates how GLORYS12V1 shows greater agreement with both observational datasets, but at the same time generates a significantly higher number of false alarms, which perfectly explains the increase in the FAR, as shown in Fig. 6. Furthermore, the daily POD and FAR fluctuate but remain stationary over time, with no apparent seasonal cycle as shown in Fig. 6(a) and Fig. 6(b). As noted above, the calculation is also applied to the minimum threshold of 7 and 28 days without any observational gaps for each eddy within this time interval, in Appendix A. This sensitivity test shows that short-lived eddies contribute to part of the variability in the verification metrics.

On average values, GLORYS12V1 achieves a POD exceeding 60% and a FAR lower than 24%. For the comparison with GLORYS2V4 FAR is lower than 20%. GLORYS12V1 shows an improvement over GLORYS2V4, that’s greater than 36% for POD, but with high values for FAR increasing, that is 26.37% for DUACS comparison.The same verification approach was applied to the SWOT, yielding a slightly different balance of hits, misses, and false alarms. Mean eddy lifetimes are slightly lower for SWOT than for DUACS for both minimum-lifetime thresholds considered (Appendix B). GLORYS12V1 tends to align more closely with SWOT observations than GLORYS2V4, with the highest values, with a greater relative gain in POD (+37.14%) and a lower FAR increasing (22.16%) than DUACS comparison, for the minimum lifetime of 4 days.

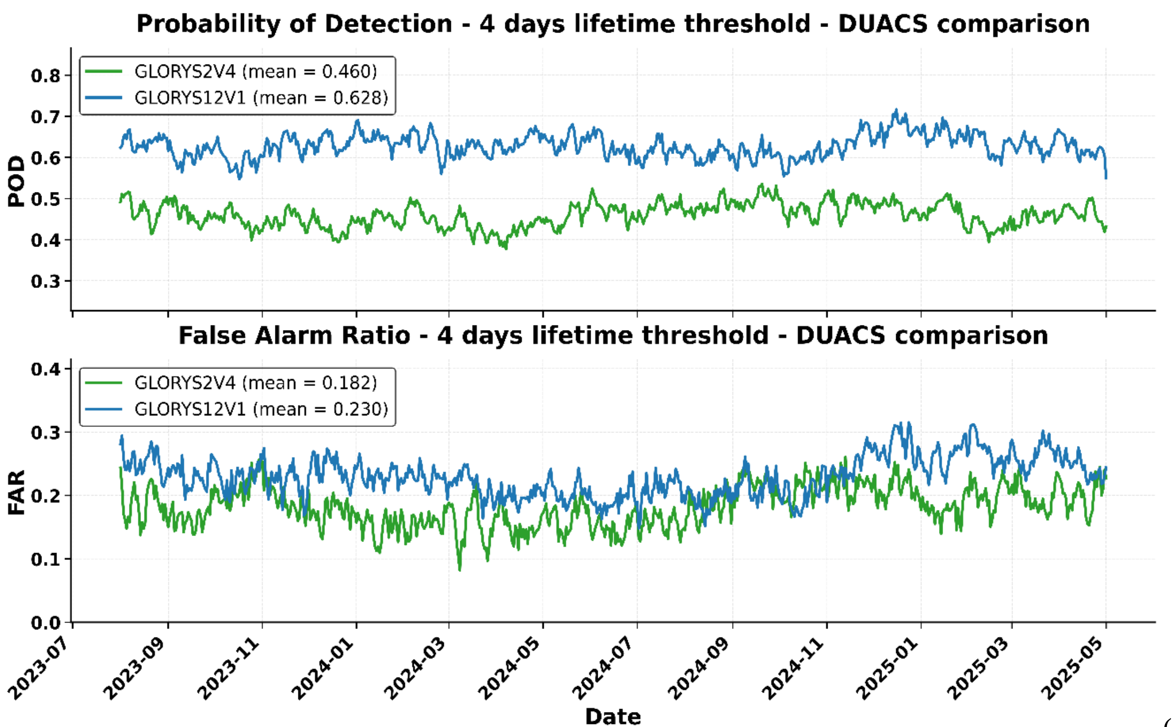

(a)

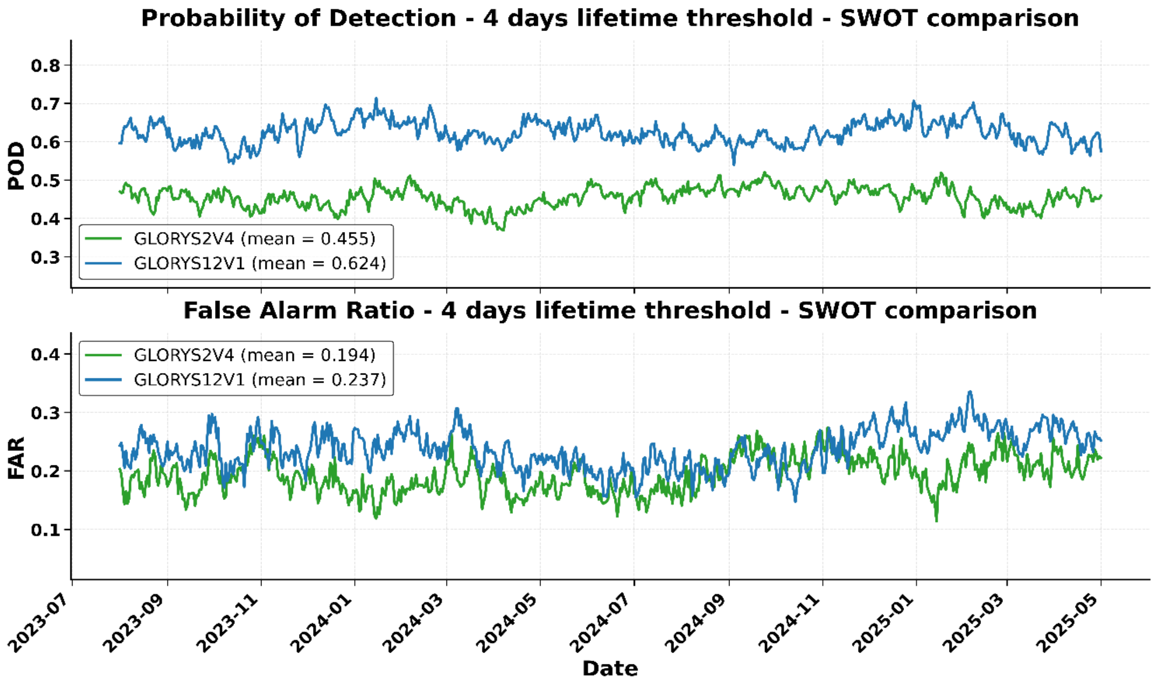

(b)

Fig.6. Time series of matching statistics for GLORYS2V4 and GLORYS12V1, compared with DUACS 1/8°, over the period from 1 August 2023 to 1 May 2025, for a 4-day minimum lifetime threshold (a). In the bottom, the time series with SWOT MIOST Science, over the period from 1 August 2023 to 1 May 2025, for a 4-day minimum lifetime threshold (b).

This indicates that, specifically regarding GLORYS2V4, the POD values are very similar in the DUACS and SWOT comparisons. There is a slight decrease when SWOT is used as reference. The decrease is about 0.005 for the 4-day threshold. GLORYS2V4 can match part of the eddies detected by SWOT, but with slightly lower efficiency than for DUACS. The FAR also slightly increases in the SWOT comparison, by about 0.012, showing a small increase in terms of false alarms. Overall, these differences are small, suggesting that the verification results for GLORYS2V4 are relatively insensitive to the choice between the two satellite reference products. However, the overall POD values, that are around 62%, for both comparisons with GLORYS12V1, show that a significant proportion of observed eddies (around 38%) remains unmatched. It highlights the presence of limitations in their high-resolution applications, such as difficulties in representing small or short-lived features and maintaining eddy-track continuity. As the minimum lifetime threshold increases, the POD improvement of GLORYS12V1 relative to GLORYS2V4 becomes smaller, whereas the reduction in FAR becomes more pronounced. GLORYS12V1 has a higher FAR than GLORYS2V4 for the 4-day and 7-day lifetime thresholds, likely because it detects a larger number of eddies, some of which do not find a corresponding match in the satellite datasets. At the 28-day threshold, this relationship reverses, with GLORYS12V1 showing a lower FAR than GLORYS2V4 (see Appendix A for further details).

To further assess the robustness of these findings, a block bootstrap resampling (95% confidence intervals) was performed using 4-day blocks, consistent with the imposed minimum lifetime threshold. Results for both SWOT and DUACS (Tables 6 and 7) confirm that GLORYS12V1 systematically outperforms GLORYS2V4 in terms of POD (0.618 - 0.620 vs 0.448 -

0.452), with a statistically significant difference (~ 0.17) that is insensitive to block length. This gain is consistently associated with a moderate increase in FAR (~ 0.045 - 0.049), confirming a robust trade-off between detection sensitivity and reliability. The agreement between the two observational references strengthens confidence in the statistical significance of the results, although it does not fully remove uncertainties related to the definition and detectability of small-scale or short-lived eddy structures.

Verification Metric	GLORYS12V1	GLORYS2V4	Difference (12V1 − 2V4)
POD (Mean)	0.618	0.448	0.170
POD (95% CI)	[0.609, 0.627]	[0.441, 0.454]	[0.160, 0.182]
FAR (Mean)	0.235	0.190	0.045
FAR (95% CI)	[0.229, 0.242]	[0.183, 0.198]	[0.038, 0.052]

Table 6. Bootstrap resampling for SWOT MIOST Science comparison, for a minimum lifetime threshold of 4 days, and a block length of 4 days.

Verification Metric	GLORYS12V1	GLORYS2V4	Difference (12V1 − 2V4)
POD (Mean)	0.620	0.452	0.168
POD (95% CI)	[0.610, 0.629]	[0.442, 0.463]	[0.154, 0.180]
FAR (Mean)	0.235	0.187	0.049
FAR (95% CI)	[0.230, 0.237]	[0.181, 0.192]	[0.040, 0.054]

Table 7. Bootstrap resampling for DUACS 1/8° comparison, for a minimum lifetime threshold of 4 days, and a block length of 4 days.

As additional sensitivity tests of the coupled block bootstrap, we also performed the bootstrap resample using 7-day, 20-day and 30-day blocks, and the mean lifetimes of both satellite eddies. The results are reported in Appendix B. The relative ranking of GLORYS12V1 and GLORYS2V4 and the main conclusions of the 4-day analysis remain consistent across the different block lengths, although the estimated confidence intervals vary with the choice of block length. Therefore, the 30-day test is included only as an additional robustness check. Very large block lengths may reduce the variability of the resampling procedure and may partly weaken the main purpose of the block bootstrap, which is to account for temporal dependence in the data when the underlying statistical distribution is unknown.

In general, as the minimum eddy lifetime threshold increases, the FAR and POD values of each reanalysis products, for both satellite comparisons, tend to converge toward similar levels as described in Appendix A for longer-lived eddies (especially for 28-day minimum eddy lifetime threshold). Figures 7 and 9 show the dependence of the eddy matching statistics (hits, misses and false alarms) on the physical properties of the eddies, namely the effective radius and amplitude, respectively. These statistics are calculated to show how eddies are distributed across different ranges of radius and amplitude, and thus to identify the ranges with the highest clustering. For hits and misses, the radius and amplitude were taken from the satellite (the reference) product, because these eddies refer to observed features that are either detected or not detected by the reanalysis. For false alarms, the radius and amplitude are taken from the corresponding reanalysis product. Each bin of the histogram has a width of 10 km and 2 cm, respectively for eddy radius and eddy amplitude. The highest counts of misses and false alarms are associated with small eddies, specifically for those with radii below 50 km and amplitudes below 5 cm.

Figures 8 and 10 show the dependence of the verification metrics in terms of the same physical eddy features.

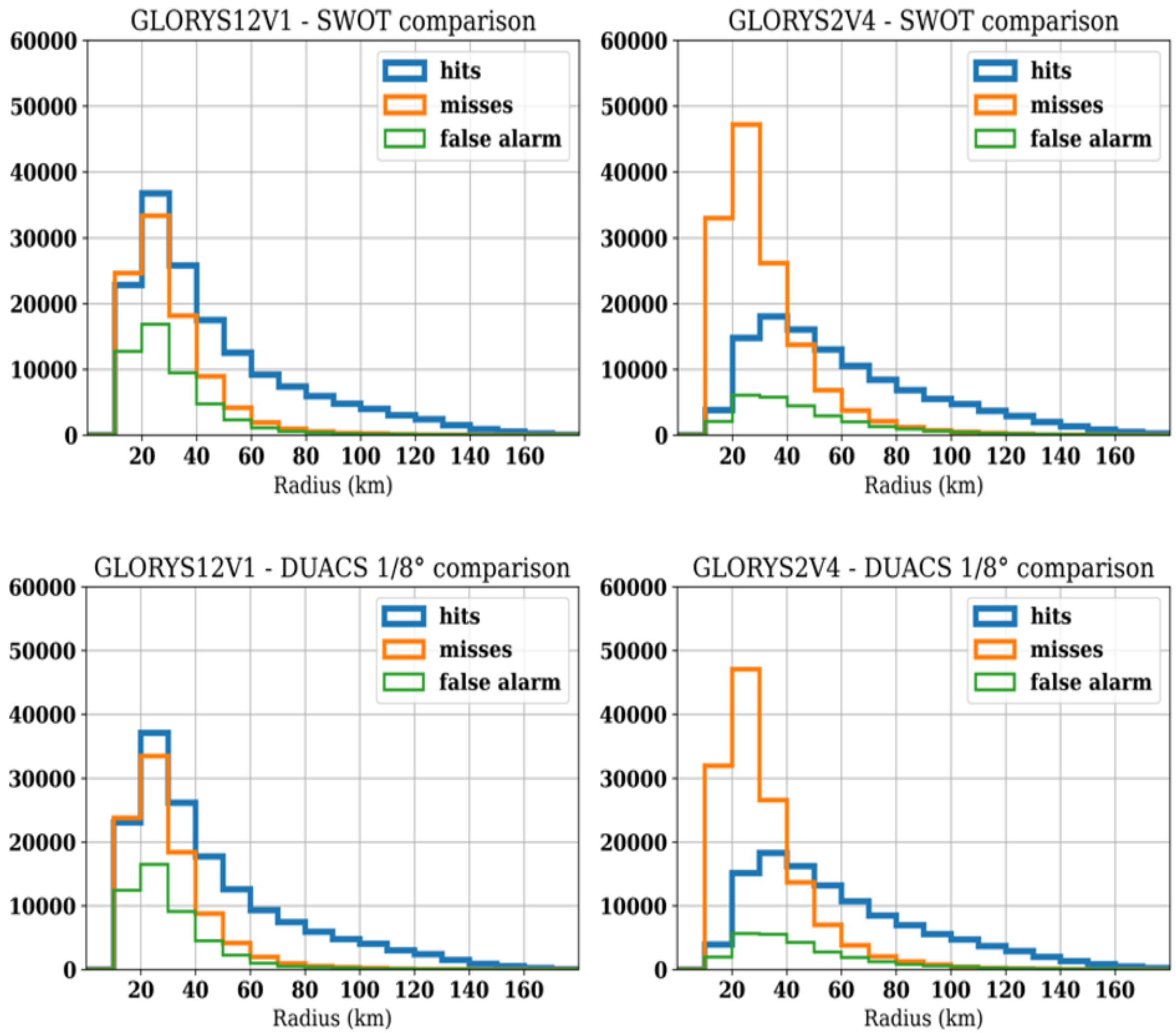

Fig. 7. On the top: eddy matching histograms for the total number of hits (blue), misses (orange), false alarms (green) for GLORYS12V1 (left) and GLORYS2V4 (right), compiled as a function of effective radius (km) over the evaluation period, for SWOT comparison, with a lifetime threshold of 4 days. In the bottom: eddy matching histograms compiled as a function of effective radius (km) over the same evaluation period, for comparison with DUACS, with a lifetime threshold of 4 days. The radius of hits and misses refers to the satellite (reference) eddies, while the radius of false alarms refers to those of unmatched eddies detected in the reanalysis.

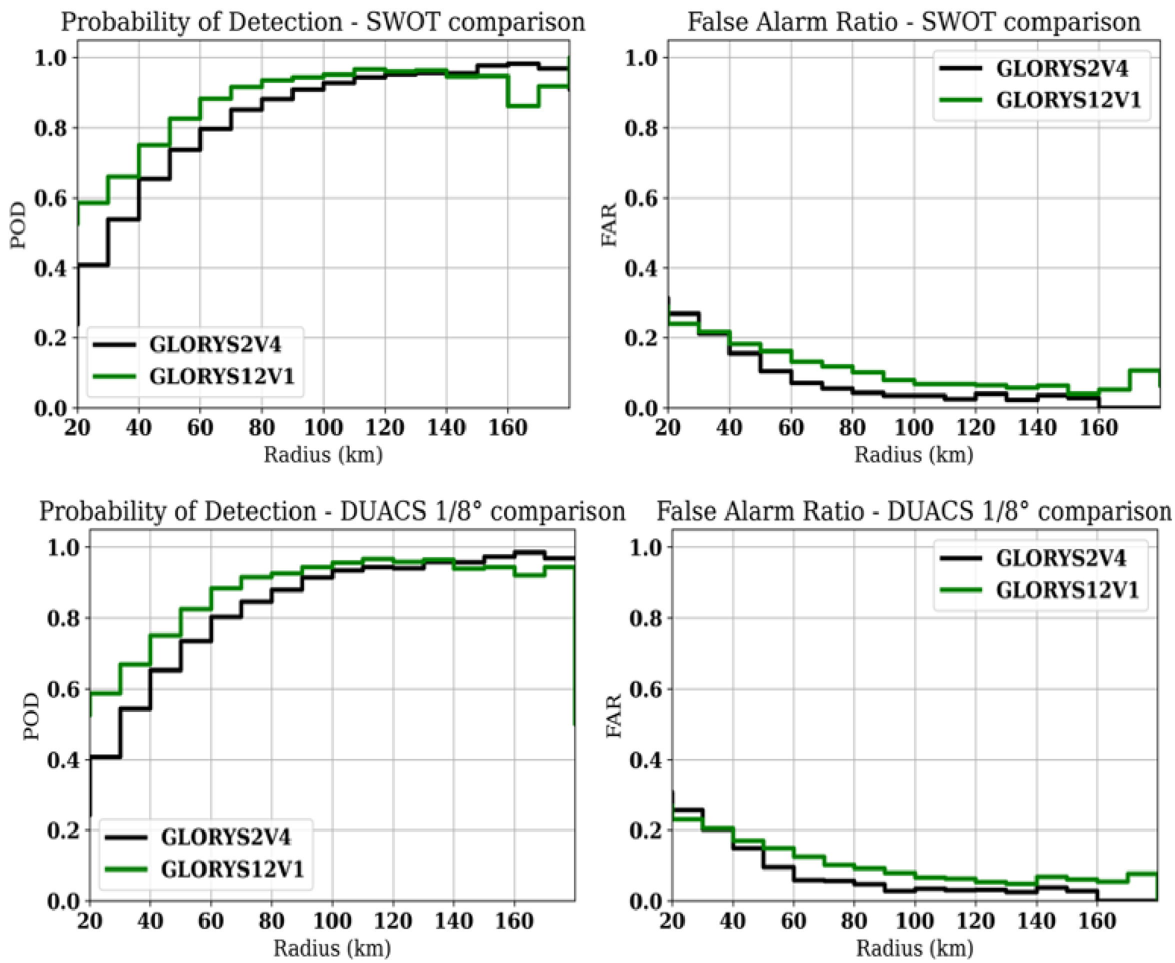

Fig.8. On the top: histograms of the probability of detection (POD; left) and the false alarm ratio (FAR; right), over the evaluation period, evaluated as a function of radius (km) for comparison with SWOT, with a lifetime threshold of 4 days. In the bottom: histograms of the POD and FAR as a function of radius (km), for the comparison with DUACS, with a lifetime threshold of 4 days. The radius of hits and misses refers to the satellite (reference) eddies, while the radius of false alarms refers to those of unmatched eddies detected in the reanalysis.

For the DUACS comparison, Figures 8 and 10 show that FAR is generally higher in the smallest effective-radius and amplitude bins, exceeding 30% in some of these classes and highlighting the greater difficulty in verifying the smallest features in this gridded product. The FAR remains close or higher than 20% until 50 km in terms of effective radius. At the same time, the POD of GLORYS12V1 is close to 60% even for small radius and amplitude values, showing a relevant fraction of small observed eddies is still detected by the reanalyses. The largest proportion of misses is consistently associated with small eddies, specifically those with radii below 50 km and amplitudes under 4 cm. The comparison with SWOT shows a similar dependence on eddy size. The largest differences in the verification metrics are again found for small-radius and small-amplitude eddies. The POD of GLORYS12V1 remains close to 60%, while the GLORYS2V4 FAR is generally higher in the smallest bins. This indicates that the main difficulty is not only the detection of small observed eddies, but also the presence of unmatched (especially for the small eddies) produced by the reanalyses. However, for both satellite comparisons, the verification skills generally improve as eddy radius and amplitude increase. This suggests a better matching capability for larger and stronger mesoscale eddies, which are less affected by small-scale noise or detection uncertainty. The differences between the DUACS and SWOT comparison are most evident for small eddies, while they become smaller for larger eddies. For this reason, Appendix C includes additional analyses of the verification metrics using different amplitude-based subsets, including eddies with amplitudes greater than 5, 10, 15, and 20 cm, as well as eddies with amplitudes below 10 cm. Appendix C also presents the eddy matching histograms using a semi-logarithmic scale for the y-axis, which represents the number of eddies. These additional analyses allow us to assess more clearly how the verification results change when low-amplitude eddies are progressively excluded, when the analysis focuses on stronger mesoscale structures, and when the contribution of the most numerous small-amplitude eddies is examined in greater detail.

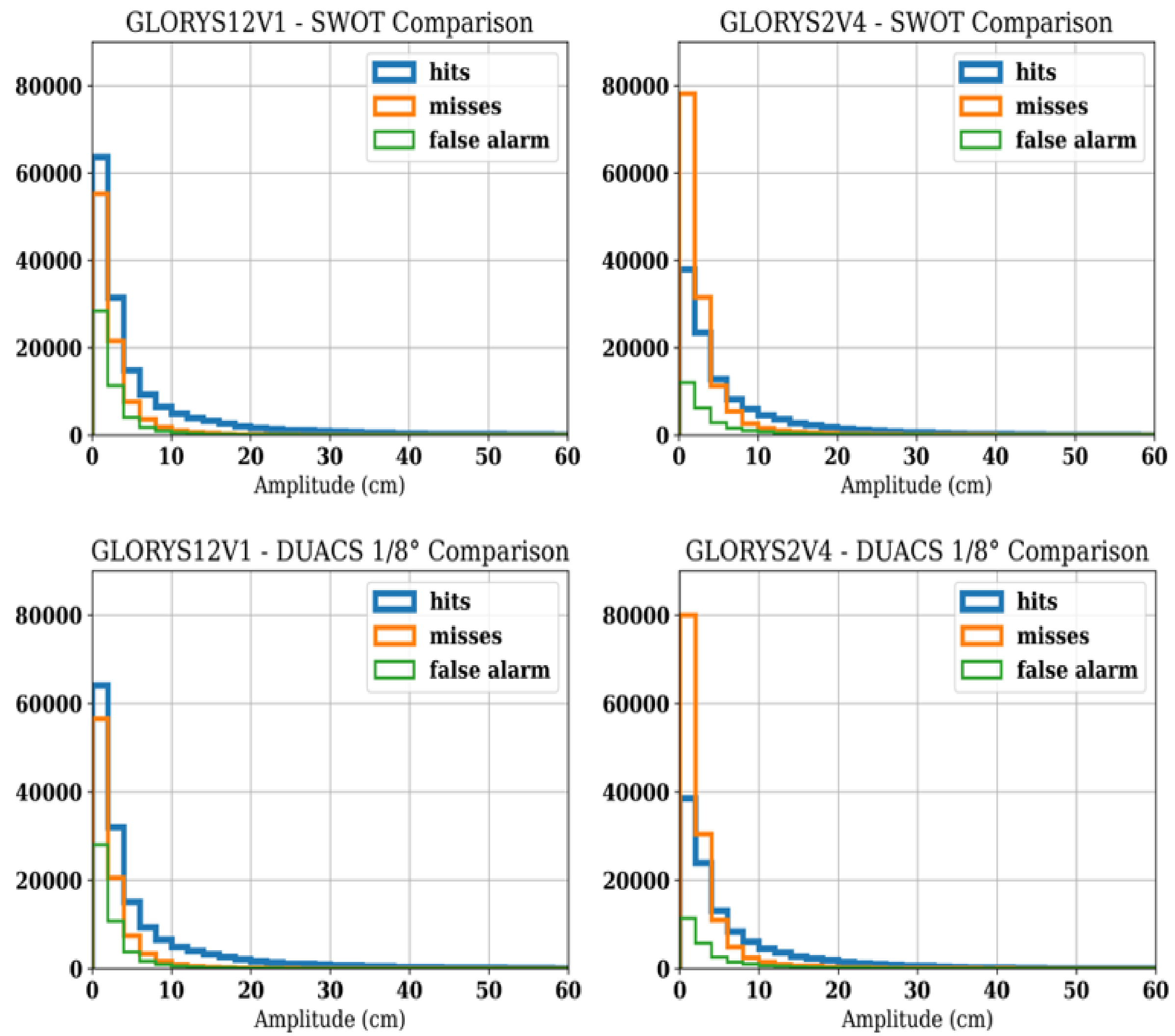

Fig.9. On the top: eddy matching histograms for the total number of hits (blue), misses (orange), false alarms (green) for GLORYS12V1 (left) and GLORYS2V4 (right), compiled as a function of amplitude (cm) over the evaluation period, for SWOT comparison. In the bottom: eddy matching histograms compiled as a function of amplitude (cm) over the evaluation period, for comparison with DUACS 1/8°. The amplitude of hits and misses refers to the satellite (reference) eddies, while the amplitude of false alarms refers to those of unmatched eddies, detected in the reanalysis.

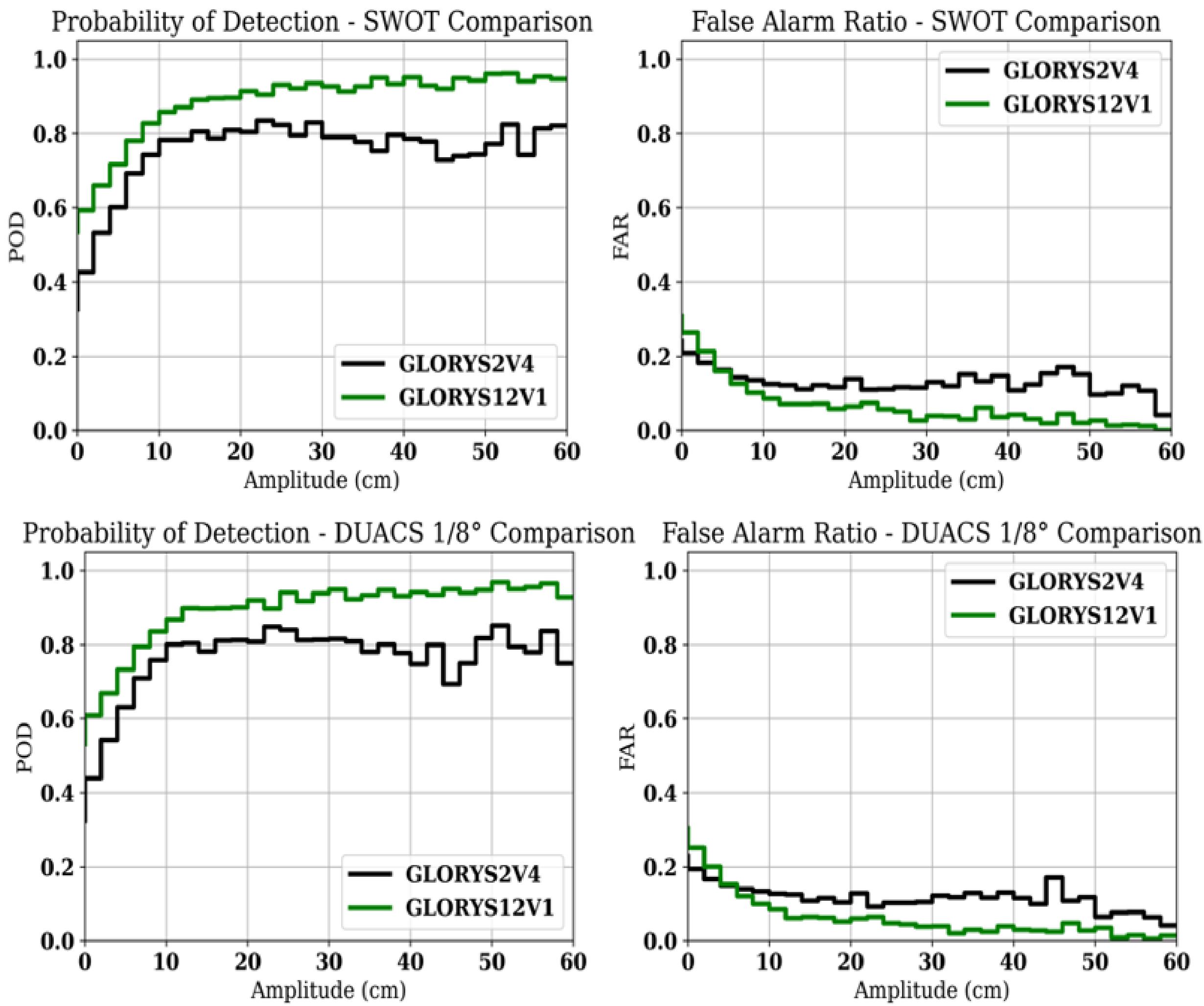

Fig. 10. On the top: histograms of the probability of detection (POD; left) and the false alarm ratio (FAR; right), over the evaluation period, evaluated as a function of amplitude (cm) for comparison with SWOT. In the bottom: histograms of the POD and FAR as a function of amplitude (cm), over the evaluation period, for the comparison with DUACS. The amplitude of hits and misses refers to the satellite (reference) eddies, while the amplitude of false alarms refers to those of unmatched eddies detected in the reanalysis.

Therefore, it can be concluded that many of these small eddies are likely to be spurious features (mesoscale features) that do not provide useful information regarding the quality of the analyses. Since small eddy detections are more sensitive to mapping, filtering, observational noise, model resolution, and the parameters of the detection and tracking algorithms, as noted before. The presence of such features may stem from factors such as the incomplete along-track nadir altimeter coverage in the AVISO gridded analyses, spurious features linked to the covariance structures in the SAM2 data assimilation scheme (Lellouche et al., 2018) used in GLORYS12V1 and GLORYS2V4, enhanced variability in the Gulf Stream, where standard deviations in SSH can exceed 0.2 m in GLORYS2V4, the global SSH rise observed in GLORYS2V4 since 1993, tracking a realistic trend of

~3 mm/year but accompanied by a growing standard deviation of 0.03 m, increasing with this trend, in the post-2020 (Copernicus Marine Service, Bourdallé-Badie R. & Drévillon M., 2024).

For eddies larger than these limits, both comparisons show strong agreement. In DUACS comparison, for radii > 100 km, the POD reaches ~90% and FAR falls to around 10–15%. In the SWOT-based comparison, the performance is quite similar: FAR drops below 10%, while POD rises above 80–95% for amplitudes greater than 10 cm.

An additional perspective on the differences between GLORYS12V1 and GLORYS2V4 can be obtained by examining the integrated matching statistics as a function of eddy radius and amplitude (Fig. 11 and Fig. 12). We focus on two descriptive diagnostics: (i) the radius below which 90% of the false alarms occur and (ii) the percentage of matched eddies with amplitudes greater than 10 cm. The first identifies the size range in which unmatched reanalysis detections are concentrated, whereas the second describes the contribution of high-amplitude eddies to successful matches. These values are used for descriptive comparison and should not be interpreted as physical thresholds defining separate eddy populations or as criteria for filtering detections.

For DUACS comparison (Fig. 11), we can see that:

- 90% of false alarms are concentrated below the 49.9 km radius for GLORYS12V1 and 79.7 km for GLORYS2V4,corresponding to a difference of 29.8 km between the two cumulative distributions. Regarding Amplitude, 95.63% of GLORYS12V1 hits and 86.93% of GLORYS2V4 hits occur below 10 cm.

We can estimate that the 4.27% of GLORYS12V1 hits are above 10 cm versus 13.07% for GLORYS2V4, with a difference of 8.8 in terms of percentage.

For the SWOT comparison, using the results of Fig.12, we can estimate:

- 90% of false alarms fall below 52.70 km radius for GLORYS12V1 and 80.30 km for GLORYS2V4, corresponding to a difference of 27.60 km. In terms of amplitude, 87.1% of GLORYS2V4 hits and 95.55% of GLORYS12V1 hits lie below 10 cm.

For SWOT, the corresponding proportions are 4.45% and 12.9%, respectively, with a difference of −8.45 percentage points.

Thus, the proportion of matched eddies exceeding 10 cm is smaller for GLORYS12V1 in both comparisons. Similar statements could be done for eddy radius.

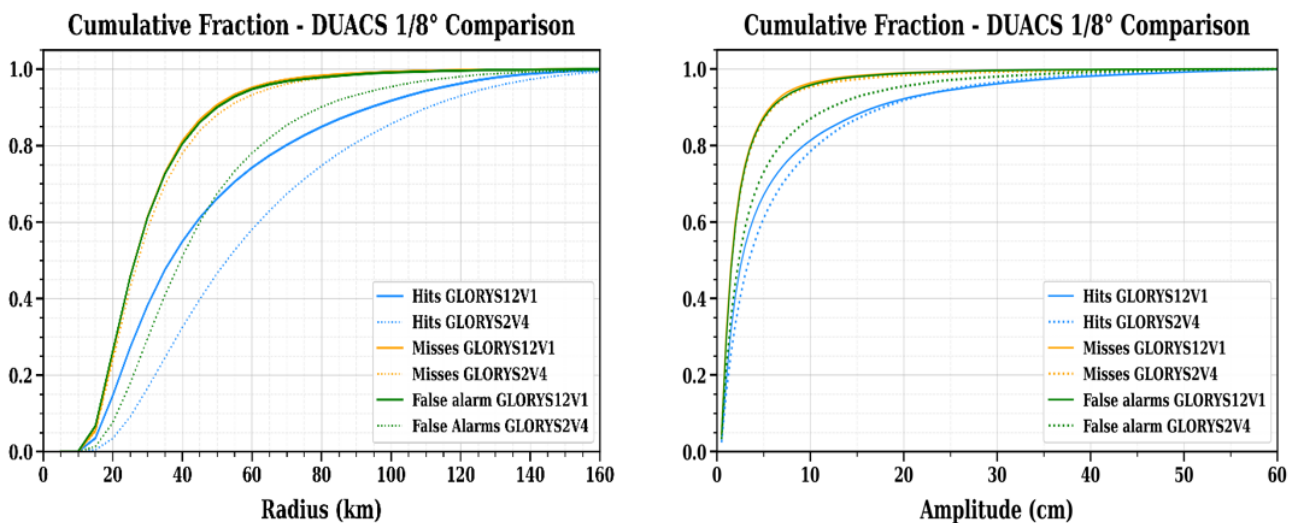

Fig. 11. Cumulative distribution of hits (blue), misses (orange) and false alarms (green) for GLORYS2V4 (dotted) and for GLORYS12V1 (solid) as a function of radius (left) and amplitude (right), for the comparison with DUACS, with a lifetime threshold of 4 days. The radius and the amplitude of hits and misses refers to the satellite (reference) eddies, while the radius and the amplitude of false alarms refers to the unmatched eddies detected in the reanalysis.

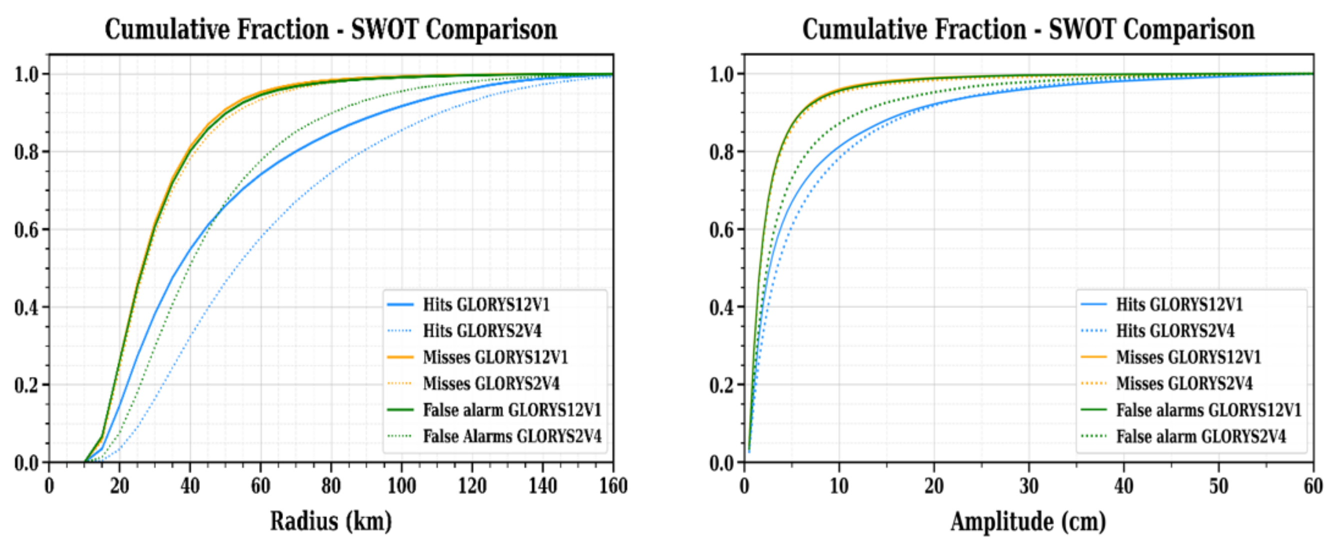

Fig.12. Cumulative distribution of hits (blue), misses (orange) and false alarms (green) for GLORYS2V4 (dotted) and for GLORYS12V1 (solid) as a function of radius (left) and amplitude (right), for the comparison with SWOT, with a lifetime threshold of 4 days. The radius and the amplitude of hits and misses refers to the satellite (reference) eddies, while the radius and the amplitude of false alarms refers to the unmatched eddies detected in the reanalysis.

Overall, these cumulative diagnostics show that most matching errors are associated with small eddies, those with radii below 50 km and amplitude below 4-5 cm. We see differences between DUACS and SWOT comparisons. They should be interpreted only as differences in reanalysis–satellite consistency over the common evaluation period, and not as a ranking of the quality of the two satellite products. However it also confirms a key weakness of GLORYS12V1: although it detects more eddies overall, it also produces more unmatched eddies (small eddies), which increases FAR. These cumulative plots show that both reanalysis systems still struggle to match very small eddies (radius < 50 km and amplitude < 4 – 5 cm), and that many of these features are likely not true eddies but artefacts in either the satellite products or the model. This suggests that future verification studies should apply filters to remove or down-weight small eddies, so that evaluation focuses on dynamically meaningful ocean structures.

3.3 Evaluation of errors in matched eddy properties

Determining whether an observed eddy has a corresponding match in a reanalysis dataset is important, but it does not fully capture how accurately that eddy is represented. As illustrated in Fig. 5, and explained in Section 2.4, some matched eddies exhibit significant differences in terms of radius, amplitude, shape, position, compared to the satellite data, despite correctly identifying the same features (see Eq. 1). These discrepancies are expected to vary between the two reanalysis systems given their differing spatial resolutions, and thus their capacity to resolve mesoscale variability. So, we try to answer the question about the possibility to detect differences in the properties of matched eddies between the two reanalysis systems used in this study. To quantify these differences, we analyze the errors in radius, amplitude, and centre displacements for each “matched” eddy (hit). For each of these properties, we compute binned, normalized histograms that illustrate the distribution of radius error (difference between satellite and reanalysis effective radius), amplitude error (difference in SSH extremum relative to the outer contour between satellite and reanalysis matched eddy), separation distance between satellite and reanalysis matched eddy centroid.

Unlike the tracking cost function (Eq. 1), these quantities are presented without the normalization factors (i.e., not scaled by A_1, R_1, or the 125 km distance), to retain their physical units (km or cm). While this approach no longer allows a direct assessment of their relative contribution to the overall cost function, it provides a clearer, physically interpretable picture of where and how the reanalyses diverge from satellite data (facilitates a physical interpretation of the histograms). The resulting normalized histograms (normalized by the total number of hits) are shown in Fig. 13(a) and Fig. 13(b). The distributions of the cost function and associated errors for matched eddies reveal clear differences between GLORYS2V4 and GLORYS12V1, for all terms of the cost function (Eq. 1). Indeed, from Table 8, the mean cost function values, for DUACS comparison, are 1.76 for GLORYS2V4 and 1.31 for GLORYS12V1, indicating a clear reduction in the cost function for each matched eddy for the eddy-resolving (GLORYS12V1) system. Likewise, the mean errors in effective radius (24.62 km vs. 16.81 km), the mean amplitude errors (5.43 cm vs 3.55 cm) and centroid distance (57.49 km vs. 49.85 km) are quite different with general differences between the two reanalysis systems.

Mean error	Cost	Radius (Km)	Amplitude (cm)	Distance (Km)
GLORYS2V4	1.76	24.62	5.43	57.49
GLORYS12V1	1.31	16.81	3.55	49.85
% diff.	-25.57%	-31.72%	-34.62%	-13.29%

Table 8. Error contributions to the cost function for all hits evaluated over the period 1st August 2023 to 1st May 2025, for DUACS comparison. Mean values for the cost function as well as contributions from radius (km), amplitude (cm), and distance errors (km). The percentage difference crossing from GLORYS2V4 to GLORYS12V1 is provided in the bottom row.

Mean error	Cost	Radius (Km)	Amplitude (cm)	Distance (Km)
GLORYS2V4	1.79	24.92	5.53	57.86
GLORYS12V1	1.33	16.79	3.59	50.29
% diff.	-25.70%	-32.62%	-35.08%	-13.06%

Table 9. Error contributions to the cost function for all hits evaluated over the period 1st August 2023 to 1st May 2025, for SWOT comparison Mean values for the cost function as well as contributions from radius (km), amplitude (cm), and distance errors (km). The percentage difference crossing from GLORYS2V4 to GLORYS12V1 is provided in the bottom row.

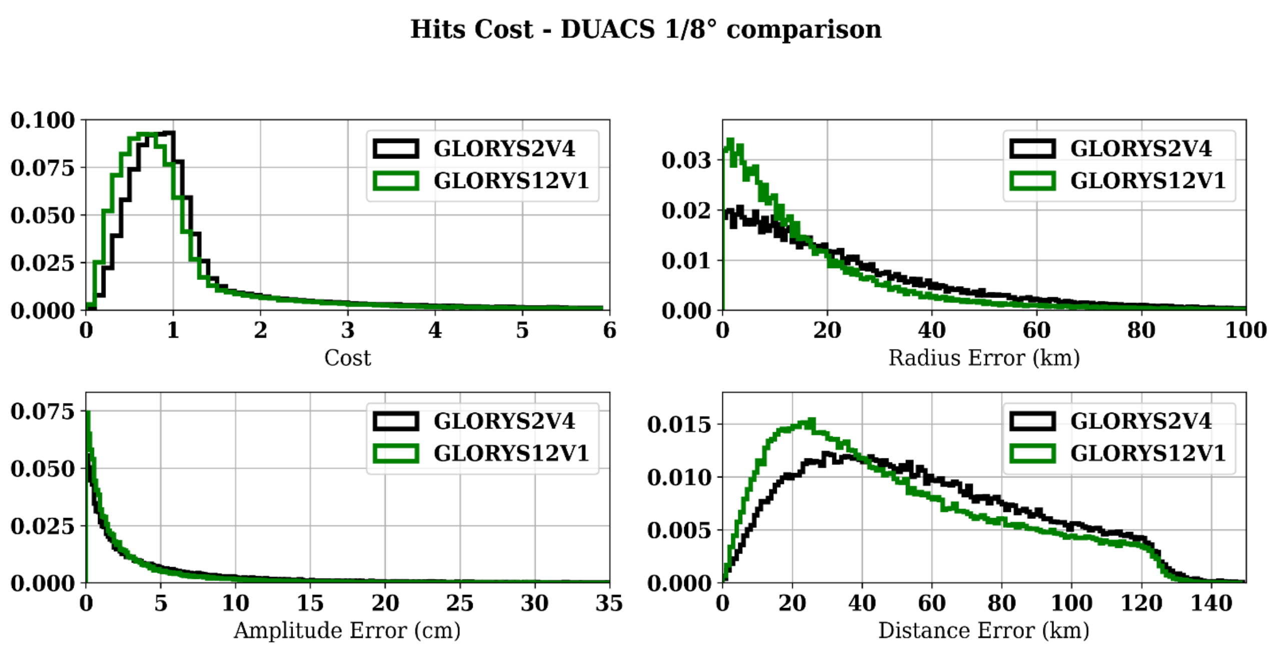

(a)

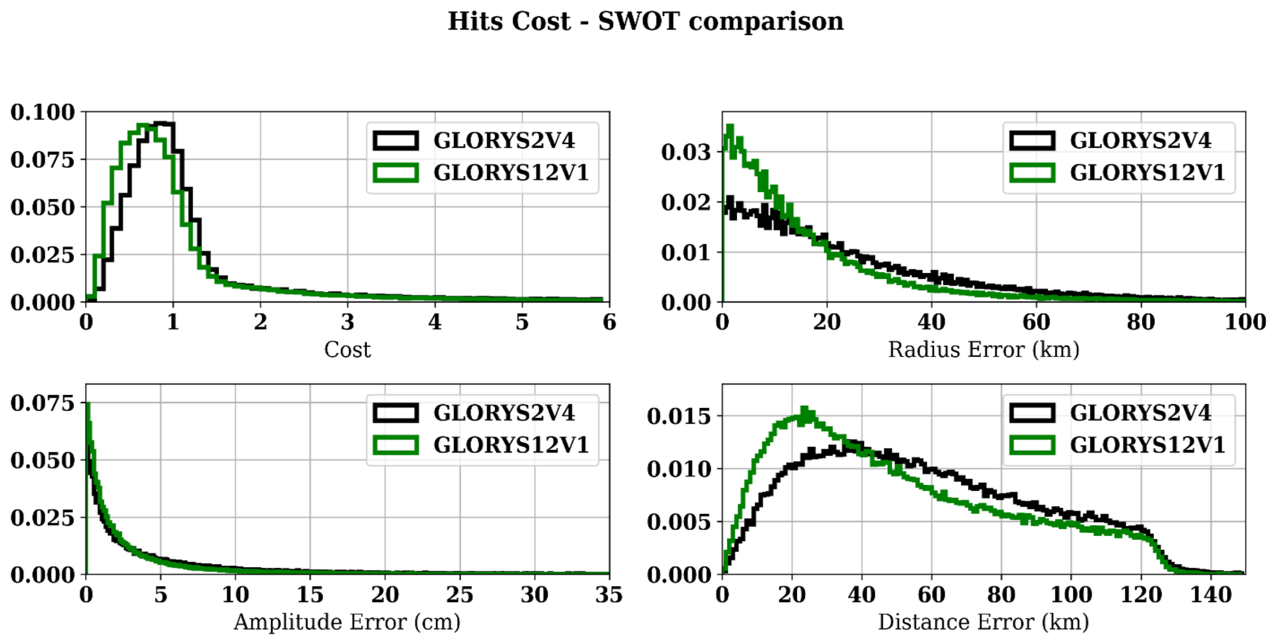

(b)

Fig. 13. In (a), normalized histograms of values for matched eddies between DUACS and GLORYS2V4 (black line) or GLORYS12V1 (green line). While in (b), the comparison between SWOT and GLORYS2V4 (black line) or GLORYS12V1 (green line). The distribution of values for the total cost is shown in the top panel on the left. Also shown are the normalized distributions of differences in terms of radius in the top on the right, amplitude in the bottom on the left, and distance between eddy positions, in the bottom on the right.

For SWOT comparison (see Table 9), the differences between the two reanalyses become somewhat more pronounced than in the DUACS comparison, for all terms of cost function (most notably in the error regarding the effective radius, but except for the distance between the centroid of eddies). The mean cost function is 1.79 for GLORYS2V4 and 1.33 for GLORYS12V1, corresponding to a -25.70% difference, crossing from GLORYS2V4 to GLORYS12V1. The amplitude error is 5.53 cm versus 3.59 cm (-35.08% in difference, from GLORYS2V4 to GLORYS12V1). The effective radius error is 24.92 km versus 16.79 km (-32.62% in difference) and the centroid distance error is 57.86 km vs 50.29 km (-13.06% in difference). These results indicate that, for all terms of the cost function, GLORYS12V1 achieves nearly identical results in both comparisons (Table 8 and Table 9). Meanwhile, GLORYS2V4 shows slightly higher average values for all terms of the cost function when compared to SWOT. These results show that GLORYS12V1 has lower mean errors than GLORYS2V4 for all terms of the cost function in both satellite comparisons. The improvement is particularly evident for the effective radius and amplitude errors, while the reduction in centroid-distance error is smaller but still present. This confirms that the eddy-resolving reanalysis provides a better representation of the physical properties of matched eddies. The advantage of GLORYS12V1 becomes slightly more apparent when the comparison is performed against SWOT. However, the results for the SWOT and DUACS comparisons are very similar. This shows that the relative improvement of GLORYS12V1 over GLORYS2V4 is robust to the choice of satellite reference dataset.

4. Summary and discussion

We have applied a feature-based verification methodology for evaluating ocean reanalysis products, following the verification approach developed and adopted by Smith and Fortin (2022), and we have used the eddy detection and tracking procedures described in Mason et al. (2014) and Pegliasco et al. (2021). This methodology is based on prior work in eddy tracking and leverages open-source tools (py-eddy-tracker) to provide a robust, reproducible framework for assessing the skill of reanalysis datasets in representing observed mesoscale features. As a demonstration, we evaluated eddy properties in two global reanalysis systems of different spatial resolutions, GLORYS2V4 and GLORYS12V1, from 1st August 2023 to 1st May 2025 for both comparisons.

The analysis shows a significant increase in POD for GLORYS12V1 compared with GLORYS2V4, although this improvement is accompanied by a higher FAR under the 4-day reference configuration. The verification results show clear differences between the two reanalysis and the satellite products used as references. When compared with DUACS, GLORYS12V1 achieves a POD of 0.628, compared with 0.460 for GLORYS2V4, corresponding to a relative increase of approximately 37%. However, FAR increases from 0.182 to 0.230, corresponding to a relative increase of approximately 26%. The comparison with SWOT MIOST Science shows similar results: POD is 0.624 for GLORYS12V1 and 0.455 for GLORYS2V4, corresponding to an increase of approximately 37%, while FAR increases from 0.194 to 0.237, or by approximately 22%. The block-bootstrap analysis performed using a 4-day minimum lifetime threshold and 4-day blocks confirms this difference. The mean FAR difference between GLORYS12V1 and GLORYS2V4 is 0.049 for DUACS (95% CI: [0.040, 0.054]) and 0.045 for SWOT MIOST Science (95% CI: [0.038, 0.052]). Further block-bootstrap sensitivity tests, reported in Appendix B, were performed using 7-day, 20-day, and 30-day blocks, as well as block lengths based on the mean lifetimes of the satellite-observed eddies. These tests provide consistent results. In all these tests, the 95% confidence interval of the FAR difference remains above zero. Therefore, the higher FAR of GLORYS12V1 is robust to the choice of block length, although the difference between the two reanalyses becomes smaller when the 7-day minimum lifetime threshold is applied. Small and short-lived eddies play an important role in the verification results. The sensitivity analyses using minimum-lifetime thresholds of 7 and 28 days are reported in Appendix A. The differences between GLORYS12V1 and GLORYS2V4 decrease as the minimum-lifetime threshold increases, particularly for FAR. The FAR gap narrows at the 7-day threshold and reverses at the 28-day threshold: GLORYS12V1 retains higher POD and has lower FAR than GLORYS2V4 for both observational references when only long-lived eddies are retained. This behaviour is associated with the exclusion of many short-lived and less stable eddies, which are among the most difficult features to match across datasets. For matched eddies, GLORYS12V1 also provides a more accurate representation of eddy properties. For both satellite comparisons, its mean matching cost is approximately 26% lower than that of GLORYS2V4, while the mean errors in effective radius, amplitude, and centroid distance are reduced by approximately 32%, 35%, and 13%, respectively.

The concentration of misses and false alarms among small eddies indicates greater uncertainty in their detection and matching. Some of these features may correspond to dynamically relevant eddies, whereas others may be affected by noise, mapping uncertainties, filtering, or unresolved variability. GLORYS12V1 detects a larger number of small features, some of which remain unmatched and contribute to its higher FAR. This highlights the need for a simple and objective approach to limit the influence of very small and short-lived eddies in both satellite products and reanalyses, in order to obtain more reliable verification metrics. The sensitivity tests in Appendix D show that the absolute POD and FAR values depend on the matching-distance threshold and the Bessel-filter cutoff wavelength. Nevertheless, GLORYS12V1 maintains a higher POD than GLORYS2V4 under all the tested configurations.

Both satellite reference products are distributed on a nominal 1/8° grid, while SWOT MIOST Science additionally incorporates wide-swath SWOT observations through the MIOST mapping methodology. However, the Copernicus Marine Service Synthesis Quality Overview Document for Sea Level Products (CMEMS-SL-SQO-008-033-068) notes that the effective resolution of gridded sea-level products remains constrained by altimeter sampling and mapping procedures. Therefore, caution is required when interpreting results close to the effective resolution limit, because very small and short-lived eddies may still be influenced by noise and mapping artefacts. The remapping of all datasets onto the same regular 1/8° grid allows a consistent comparison but does not make their native or effective resolutions equivalent. Despite these limitations, the results support the added value of the eddy-resolving GLORYS12V1 reanalysis compared with the eddy-permitting GLORYS2V4. The amplitude-based analyses show that GLORYS12V1 generally maintains a higher POD than GLORYS2V4. However, progressively excluding low-amplitude eddies does not produce a monotonic improvement in POD and FAR, as shown in Appendix C. False alarms are mainly concentrated among small eddies. In the DUACS comparison, 90% of the false alarms occur below a radius of approximately 50 km for GLORYS12V1 and 80 km for GLORYS2V4. The corresponding thresholds in the SWOT comparison are approximately 53 and 80 km. These results indicate that the false alarms associated with GLORYS12V1 are concentrated at smaller radii; they do not imply a lower total number or ratio of false alarms. In the DUACS comparison, approximately 4.3% of the GLORYS12V1 hits have amplitudes above 10 cm, compared with 13.1% for GLORYS2V4. In the SWOT comparison, the corresponding proportions are approximately 4.5% and 12.9%, respectively. These values describe the amplitude distribution of the matched eddies and should not be interpreted as direct measures of the overall performance of the two reanalyses. The common evaluation period covers less than two years and may therefore not fully sample the interannual variability of the North Atlantic eddy field. This limitation is particularly relevant for large and energetic eddies, which are less frequent and more sensitive to the specific dynamical conditions of the analysed period. Moreover, the results should not be interpreted as a ranking of the quality of the two satellite products. DUACS and SWOT MIOST Science provide complementary observational references with different mapping characteristics and levels of small-scale variability. SWOT MIOST Science provides additional information from wide-swath observations, but it remains a Level-4 mapped product. Furthermore, neither satellite product can be considered a fully independent reference because they share nadir-altimetry information with each other and with observations assimilated into the reanalyses.

Future work should develop objective and scale-aware strategies to filter or down-weight uncertain small features without automatically excluding dynamically relevant eddies. The present matching and verification framework could also be extended to include the "coincidence status" classification described by Ma et al. (2020), distinguishing matched, split, merged, missed, and artefactual eddies. This would provide a more detailed assessment and improve the diagnostic capability of the verification framework. Finally, extending the analysis to longer periods, using satellite products with sufficient temporal coverage, and applying the methodology to other ocean regions would make it possible to better account for interannual variability and different dynamical regimes.

Appendix A

In this appendix we aim to assess how the verification metrics, used to evaluate the ability of global ocean reanalyses to detect eddies observed in satellite datasets over a highly eddy-populated region, change under these different methodological choices.

Eddy detection-tracking and matching results for 7 and 28 minimum lifetime thresholds.

To assess the sensitivity of the verification results to the lifetime criterion, the detection, tracking, and matching analyses were repeated using minimum-lifetime thresholds of 7 and 28 days. Tables A1, A2, A5, and A6 report the numbers of anticyclonic and cyclonic eddies retained in each catalogue, whereas Tables A3, A4, A7, and A8 report POD, FAR, and the differences between GLORYS12V1 and GLORYS2V4. Fig. A1 shows the corresponding time series and power spectra. Increasing the minimum lifetime substantially reduces the number of retained eddies, especially at 28 days. This reduction does not, however, lead to lower FAR values: relative to the 4-day analysis, POD decreases and FAR increases for both reanalyses and both observational references. In Fig. A1, panel (a) shows the time series of the verification metrics over the full study period for both comparisons, while panel (b) shows the power spectra associated with each time series. The aim for the calculation of the power spectra is assessing how the variability of the verification metrics changes as the minimum eddy lifetime threshold is progressively increased.

Dataset	Anticyclonic	% w.r.t. DUACS	Cyclonic	% w.r.t. DUACS
DUACS	116644	-	116295	-
GLORYS2V4	62479	53.56%	67486	58.03%
GLORYS12V1	86976	74.57%	95836	82.40%

Table A1. Total number of anticyclonic and cyclonic eddies identified in the region of study over the evaluation period for DUACS, GLORYS2V4, and GLORYS12V1, for eddies with a minimum lifetime threshold of 7 days. The percentage of eddies identified in GLORYS2V4 and GLORYS12V1 with respect to DUACS is also provided.

Dataset	Anticyclonic	% w.r.t. SWOT	Cyclonic	% w.r.t. SWOT
SWOT	114015	-	116036	-
GLORYS2V4	62479	54.79%	67486	58.15%
GLORYS12V1	86976	76.28%	95836	82.59%

Table A2. Total number of anticyclonic and cyclonic eddies identified in the region of study over the evaluation period for SWOT, GLORYS2V4, and GLORYS12V1, for eddies with a minimum lifetime threshold of 7 days. The percentage of eddies identified in GLORYS2V4 and GLORYS12V1 with respect to SWOT is also provided.

Verification metric	GLORYS12V1	GLORYS2V4	Diff.	Diff.%
POD	0.608	0.449	0.159	35.41%
FAR	0.225	0.196	0.029	14.80%

Table A3. aggregated eddy verification statistics for the Probability of Detection (POD) and False Alarm Ratio (FAR) evaluated over the period, from 1st August 2023 to 1st May 2025, for the comparison with DUACS, with a minimum lifetime threshold of 7 days.

Verification metric	GLORYS12V1	GLORYS2V4	Diff.	Diff.%
POD	0.606	0.447	0.159	35.57%
FAR	0.237	0.209	0.028	13.4%

Table A4. Aggregated eddy verification statistics for the Probability of Detection (POD) and False Alarm Ratio (FAR) evaluated over the period, from 1st August 2023 to 1st May 2025, for the comparison with SWOT, with a minimum lifetime threshold of 7 days.

Dataset	Anticyclonic	% w.r.t. DUACS	Cyclonic	% w.r.t. DUACS
DUACS	67686	-	69657	-
GLORYS2V4	39218	57.94%	43705	62.74%
GLORYS12V1	41768	61.70%	49935	71.69%

Table A5. Total number of anticyclonic and cyclonic eddies identified in the region of study over the evaluation period for DUACS, GLORYS2V4, and GLORYS12V1. The percentage of eddies identified in GLORYS2V4 and GLORYS12V1 with respect to DUACS is also provided, with a lifetime threshold of 28 days.

Dataset	Anticyclonic	% w.r.t. SWOT	Cyclonic	% w.r.t. SWOT
SWOT	67089	-	68842	-
GLORYS2V4	39218	58.45%	43705	63.49%
GLORYS12V1	41768	62.26%	49935	72.54%

Table A6. Total number of anticyclonic and cyclonic eddies identified in the region of study over the evaluation period for SWOT, GLORYS2V4, and GLORYS12V1. The percentage of eddies identified in GLORYS2V4 and GLORYS12V1 with respect to SWOT is also provided, with a lifetime threshold of 28 days.

Statistics	GLORYS12V1	GLORYS2V4	Diff.	Diff.%
POD	0.464	0.380	0.084	22.1%
FAR	0.295	0.346	-0.051	-14.7%

Table A7. aggregated eddy verification statistics for the Probability of Detection (POD) and False Alarm Ratio (FAR) evaluated over the period, from 1st August 2023 to 1st May 2025, for the comparison with DUACS, with a minimum lifetime threshold of 28 days.

Statistics	GLORYS12V1	GLORYS2V4	Diff.	Diff.%
POD	0.457	0.379	0.078	20.5%
FAR	0.288	0.322	-0.034	-10.5%

Table A8. aggregated eddy verification statistics for the Probability of Detection (POD) and False Alarm Ratio (FAR) evaluated over the period, from 1st August 2023 to 1st May 2025, for the comparison with SWOT, with a minimum lifetime threshold of 28 days.

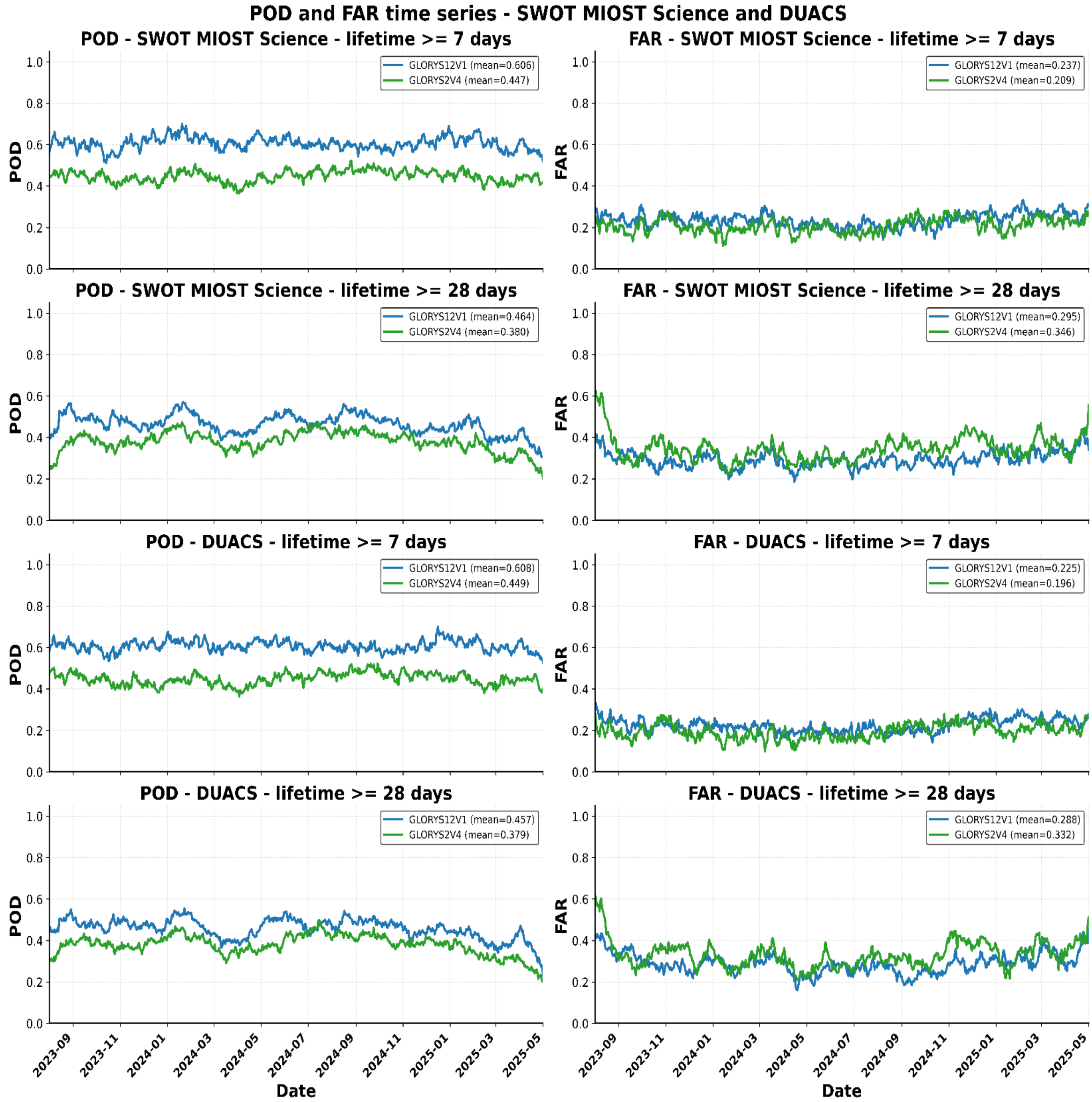
POD and FAR time series - SWOT MIOST Science and DUACS
POD - SWOT MIOST Science - lifetime >= 7 days
GLORYS12V1 (mean=0.606)
GLORYS2V4 (mean=0.447)
FAR - SWOT MIOST Science - lifetime >= 7 days
GLORYS12V1 (mean=0.237)
GLORYS2V4 (mean=0.209)
POD - SWOT MIOST Science - lifetime >= 28 days
GLORYS12V1 (mean=0.464)
GLORYS2V4 (mean=0.380)
FAR - SWOT MIOST Science - lifetime >= 28 days
GLORYS12V1 (mean=0.295)
GLORYS2V4 (mean=0.346)
POD - DUACS - lifetime >= 7 days
GLORYS12V1 (mean=0.608)
GLORYS2V4 (mean=0.449)
FAR - DUACS - lifetime >= 7 days
GLORYS12V1 (mean=0.225)
GLORYS2V4 (mean=0.196)
POD - DUACS - lifetime >= 28 days
GLORYS12V1 (mean=0.457)
GLORYS2V4 (mean=0.379)
FAR - DUACS - lifetime >= 28 days
GLORYS12V1 (mean=0.288)
GLORYS2V4 (mean=0.332)
POD
FAR
Date

(a)

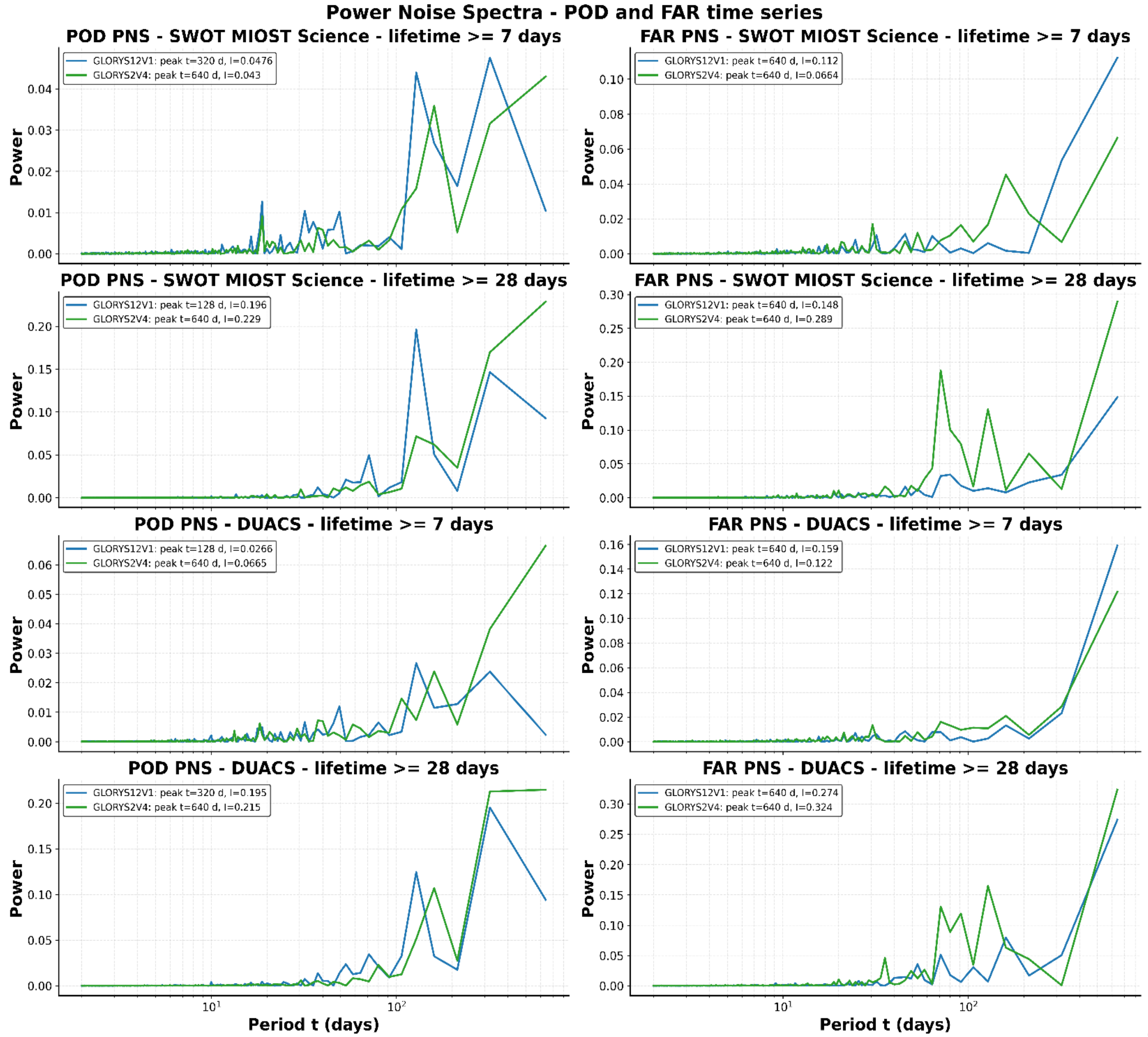

(b)

Fig. A1. Time series of matching statistics for GLORYS2V4 and GLORYS12V1, compared with SWOT and DUACS (a), over the period from 1st August 2023 to 1st May 2025, with a minimum lifetime of 7 and 28 days. In (b), the power spectra of each time series, for both products and comparisons.

At the 7-day threshold, POD decreases for both reanalyses. FAR increases for GLORYS2V4, whereas for GLORYS12V1 it decreases slightly against DUACS and remains essentially unchanged against SWOT. At the 28-day threshold, POD decreases and FAR increases relative to the 4-day configuration, while GLORYS12V1 retains higher POD and attains lower FAR than GLORYS2V4 for both references. This condition highlights not only the greater ability of GLORYS12V1 to capture observational eddies compared to GLORYS2V4, for both satellite datasets, but also its lower error rate in detecting and tracking false alarms. The GLORYS12V1 FAR becomes lower than that of GLORYS2V4 when only long-lived eddies are considered. However, the application of a longer lifetime threshold also leads to a substantial reduction in the total number of detected and tracked eddies compared to the lower lifetime cases, as shown in Tables A1, A2, A5, and A6. This reduction is stronger for the reanalyses than for the satellite datasets, producing an overall decrease in POD and an overall increase in FAR for both comparisons and for both reanalysis products with respect to the results discussed in Sect. 3.2 and reported in Tables 4 and 5. This behaviour indicates that, although the 28-day threshold isolates more stable eddy structures, it also exposes a significant discrepancy between the reanalyses and the observational datasets. In particular, some of the eddies matched in the reanalyses at lower lifetime thresholds appear to be less temporally stable than those observed in the satellite products. As a result, the number of hits clearly tends to decrease as the minimum lifetime threshold increases.

This sensitivity test therefore suggests that temporally more stable eddies tend to reduce the resolution-related gap between the two reanalysis products. Nevertheless, this does not lead to an increase in POD or to a systematic decrease in FAR. This confirms that both ocean reanalyses still show limitations in capturing observed eddies and in avoiding the generation of unmatched eddy-like structures. More generally, these results show that one of the main challenges is to identify a methodology able to remove spurious and unstable structures, for which it is not always clear whether they can be considered robust mesoscale eddies.

In panel (b), the power spectra show that, at short temporal scales, the variability of the verification-metric time series is almost similar across the different configurations. The spectral differences are mainly concentrated at the longest resolved periods. For FAR, GLORYS12V1 has the larger peak with the 7-day threshold, whereas GLORYS2V4 has the larger peak with the 28-day threshold. Because the analysed record is only 640 days long, peaks at periods of 320–640 days should be interpreted as low-frequency variability rather than as evidence of robust periodic or seasonal signals. It should also be noted that the axes do not have the same numerical range across all panels. In general, the numerical range of the FAR power spectra is larger than that of POD, indicating that the strongest spectral peaks are generally associated with FAR.

Appendix B

Sensitivity of bootstrap resampling results for verification metrics to the block length

To assess the sensitivity of the confidence intervals to temporal dependence, the coupled block-bootstrap analysis was repeated using block lengths of 7, 20, and 30 days, as well as block lengths derived from the mean lifetimes of the satellite-observed eddies. Results are reported for the 4-day and 7-day minimum-lifetime thresholds. Across the tested block lengths, GLORYS12V1 maintains higher POD than GLORYS2V4 for both observational references. The FAR difference also remains positive, although it becomes smaller for the 7-day minimum-lifetime threshold.

Verification Metric	GLORYS12V1	GLORYS2V4	Difference (12V1 − 2V4)
POD (Mean)	0.603	0.442	0.161
POD (95% CI)	[0.594, 0.611]	[0.431, 0.453]	[0.148, 0.173]
FAR (Mean)	0.234	0.200	0.034
FAR (95% CI)	[0.224, 0.245]	[0.189, 0.213]	[0.020, 0.048]

Table B1. Bootstrap resampling for SWOT, for a minimum lifetime threshold of 7 days and a block length of 7 days.

Verification Metric	GLORYS12V1	GLORYS2V4	Difference (12V1 − 2V4)
POD (Mean)	0.599	0.438	0.161
POD (95% CI)	[0.586, 0.610]	[0.430, 0.446]	[0.147, 0.174]
FAR (Mean)	0.241	0.208	0.034
FAR (95% CI)	[0.233, 0.250]	[0.197, 0.219]	[0.024, 0.043]

Table B2. Bootstrap resampling for DUACS comparison, for a minimum lifetime threshold of 7 days and a block length of 7 days.

Verification Metric	GLORYS12V1	GLORYS2V4	Difference (12V1 − 2V4)
POD (Mean)	0.620 0.603	0.455 0.444	0.165 0.159
POD (95% CI)	[0.608 , 0.632] [0.591 , 0.614]	[0.442 , 0.468] [0.429 , 0.460]	[0.149 , 0.183] [0.142 , 0.177]
FAR (Mean)	0.236 0.235	0.187 0.200	0.049 0.034
FAR (95% CI)	[0.228 , 0.244] [0.222 , 0.250]	[0.175 , 0.202] [0.182, 0.221]	[0.031 , 0.065] [0.011 , 0.054]

Table B3. Block-bootstrap estimates of POD and FAR using 20-day blocks for the comparison with DUACS. Values are reported for GLORYS12V1, GLORYS2V4, and their difference, together with 95% confidence intervals. In the first row, there is the calculation for the 4 days minimum lifetime threshold. In the second row, there is the calculation for 7 days minimum lifetime threshold.

Verification Metric	GLORYS12V1	GLORYS2V4	Difference (12V1 − 2V4)
POD (Mean)	0.617 0.598	0.450 0.440	0.167 0.158
POD (95% CI)	[0.603 , 0.633] [0.582, 0.614]	[0.440 , 0.459] [0.429, 0.451]	[0.151 , 0.187] [0.140, 0.178]
FAR (Mean)	0.236 0.242	0.192 0.207	0.044 0.035
FAR (95% CI)	[0.230, 0.241] [0.233, 0.251]	[0.180 , 0.207] [0.193, 0.225]	[0.031 , 0.056] [0.021, 0.046]

Table B4. Block-bootstrap estimates of POD and FAR using 20-day blocks for the comparison with SWOT MIOST. Values are reported for GLORYS12V1, GLORYS2V4, and their difference, together with 95% confidence intervals. In the first row, there is the calculation for the 4 days minimum lifetime threshold. In the second row, there is the calculation for 7 days minimum lifetime threshold.

Verification Metric	GLORYS12V1	GLORYS2V4	Difference (12V1 − 2V4)
POD (Mean)	0.620 0.603	0.452 0.441	0.168 0.162
POD (95% CI)	[0.604, 0.634] [0.589, 0.615]	[0.437, 0.466] [0.425, 0.459]	[0.148, 0.190] [0.142, 0.185]
FAR (Mean)	0.235 0.234	0.186 0.201	0.049 0.033
FAR (95% CI)	[0.227, 0.245] [0.223, 0.250]	[0.173, 0.200] [0.184, 0.217]	[0.031, 0.066] [0.011, 0.055]

Table B5. Block-bootstrap estimates of POD and FAR using 30-day blocks for the comparison with DUACS. Values are reported for GLORYS12V1, GLORYS2V4, and their difference, together with 95% confidence intervals. In the first row, there is the calculation for the 4 days minimum lifetime threshold. In the second row, there is the calculation for 7 days minimum lifetime threshold.

Verification Metric	GLORYS12V1	GLORYS2V4	Difference (12V1 − 2V4)
POD (Mean)	0.618 0.616	0.448 0.460	0.170 0.166
POD (95% CI)	[0.600, 0.636] [0.602, 0.626]	[0.438, 0.456] [0.448, 0.484]	[0.149, 0.194] [0.131, 0.173]
FAR (Mean)	0.236 0.240	0.191 0.206	0.045 0.035
FAR (95% CI)	[0.231, 0.240] [0.236, 0.245]	[0.180, 0.202] [0.194, 0.217]	[0.032, 0.056] [0.023, 0.046]

Table B6. Block-bootstrap estimates of POD and FAR using 30-day blocks for the comparison with SWOT. Values are reported for GLORYS12V1, GLORYS2V4, and their difference, together with 95% confidence intervals. In the first row, there is the calculation for the 4 days minimum lifetime threshold. In the second row, there is the calculation for 7 days minimum lifetime threshold.

For the sake of completeness, we also calculated the average lifetimes of the observed eddies for each satellite dataset using two different minimum lifetimes (4 and 7 days). The idea is to use these average lifetimes as the block lengths for the coupled bootstrap resampling. The mean eddy lifetime is calculated from the number of daily observations associated with each individual trajectory, using the “nb_obs_by_track” property provided by py-eddy-tracker. Tracks with zero observations are excluded.

For DUACS, we calculate the average lifetime of eddies:

- Anticyclonic eddies with a minimum lifetime threshold of 4 days: 18.03 days.
- Cyclonic eddies with a minimum lifetime threshold of 4 days: 18.23 days.
- Anticyclonic eddies with a minimum lifetime threshold of 7 days: 22.69 days.
- Cyclonic eddies with a minimum lifetime threshold of 7 days: 23.05 days.

Therefore, considering both anticyclonic and cyclonic eddies, we calculate an average eddy lifetime of: 18.13 days (minimum lifetime of 4 days) and 22.87 days (minimum lifetime of 7 days). Therefore, for the block bootstrap resample, we rounded up to the next whole day, setting a value of 19 days for a minimum lifetime of 4 days, and a value of 23 days for a minimum lifetime of 7 days.

For SWOT, we calculate the average lifetime of eddies:

- Anticyclonic eddies with a minimum lifetime threshold of 4 days: 17.51 days.
- Cyclonic eddies with a minimum lifetime threshold of 4 days: 17.58 days.
- Anticyclonic eddies with a minimum lifetime threshold of 7 days: 22.69 days.
- Cyclonic eddies with a minimum lifetime threshold of 7 days: 22.38 days.

Therefore, considering both anticyclonic and cyclonic eddies, we calculate an average eddy lifetime of: 17.54 days (minimum lifetime of 4 days) and 22.54 days (minimum lifetime of 7 days). Therefore, for the block bootstrap resample, we rounded up to the next whole day, setting a value of 18 days for a minimum lifetime of 4 days, and a value of 23 days for a minimum lifetime of 7 days.

Verification Metric	GLORYS12V1	GLORYS2V4	Difference (12V1 – 2V4)
POD (Mean)	0.620 0.602	0.452 0.443	0.168 0.159
POD (95% CI)	[0.608, 0.632] [0.589, 0.614]	[0.438, 0.466] [0.426, 0.460]	[0.153, 0.186] [0.143, 0.180]
FAR (Mean)	0.235 0.235	0.186 0.200	0.049 0.034
FAR (95% CI)	[0.228, 0.243] [0.223, 0.250]	[0.175, 0.199] [0.182, 0.221]	[0.035, 0.062] [0.011, 0.055]

Table B7. Block-bootstrap estimates of POD and FAR using 18 days and 23 days blocks for the comparison with DUACS. Values are reported for GLORYS12V1, GLORYS2V4, and their difference, together with 95% confidence intervals. In the first row, there is the calculation for the 4 days minimum lifetime threshold. In the second row, there is the calculation for 7 days minimum lifetime threshold.

Verification Metric	GLORYS12V1	GLORYS2V4	Difference (12V1 – 2V4)
POD (Mean)	0.618 0.598	0.448 0.441	0.170 0.157
POD (95% CI)	[0.601, 0.632] [0.576, 0.613]	[0.440, 0.457] [0.430, 0.452]	[0.153, 0.188] [0.139, 0.176]
FAR (Mean)	0.236 0.241	0.192 0.207	0.044 0.034
FAR (95% CI)	[0.229, 0.244] [0.234, 0.250]	[0.180, 0.204] [0.195, 0.220]	[0.032, 0.056] [0.019, 0.047]

Table B8. Block-bootstrap estimates of POD and FAR using 19 days and 23 days blocks for the comparison with SWOT. Values are reported for GLORYS12V1, GLORYS2V4, and their difference, together with 95% confidence intervals. In the first row, there is the calculation for the 4 days minimum lifetime threshold. In the second row, there is the calculation for 7 days minimum lifetime threshold.

Appendix C

Sensitivity of verification metrics to eddy amplitude thresholds.

To assess the sensitivity of the verification results to eddy amplitude, POD and FAR were recomputed using minimum amplitude thresholds of 5, 10, 15, and 20 cm. We also considered the complementary subset of eddies with amplitudes lower than or equal to 10 cm to isolate the contribution of low-amplitude features. The 10 cm value is used only as a diagnostic criterion and not as a physical boundary between different eddy regimes.

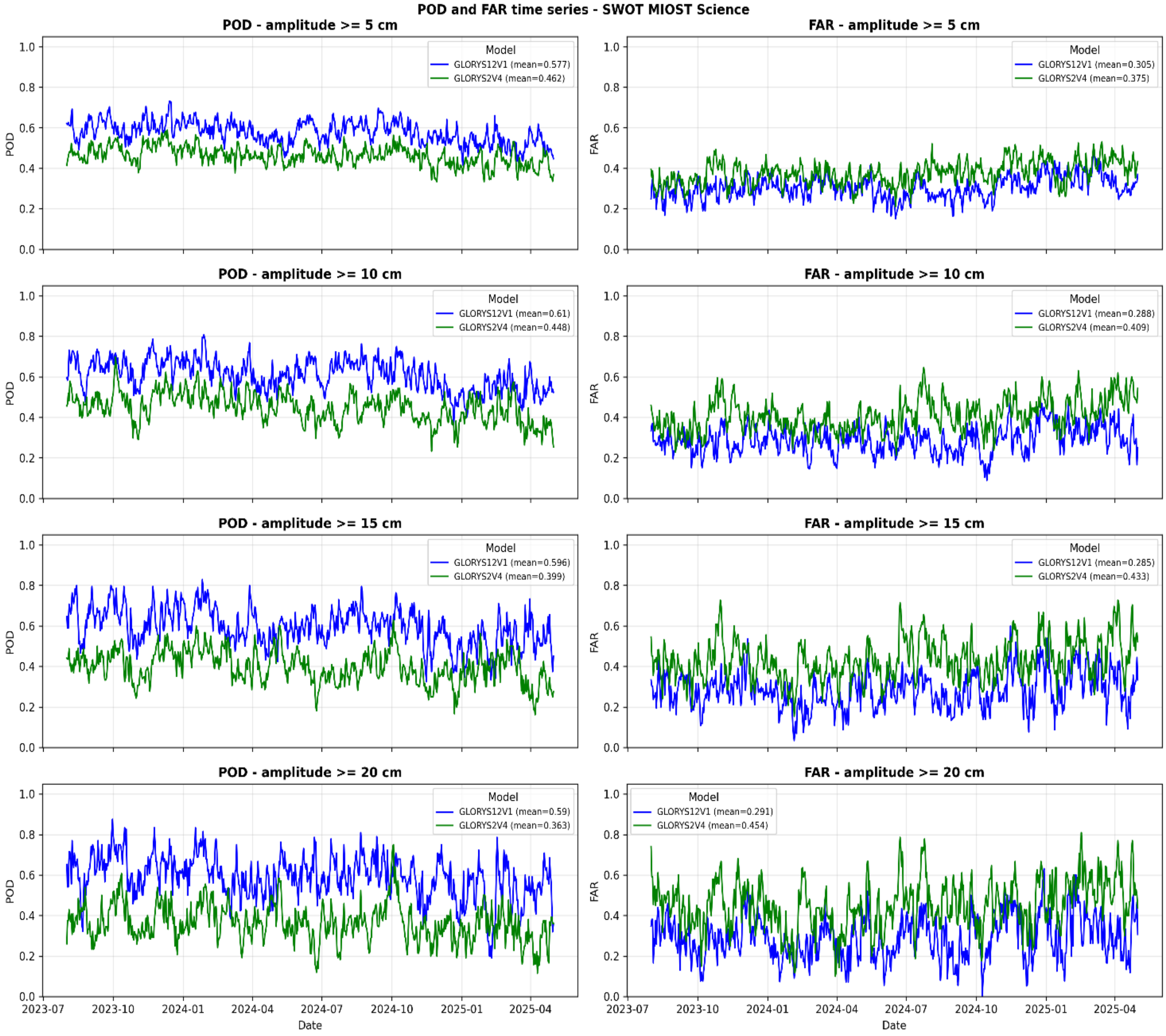
POD and FAR time series - SWOT MIOST Science
POD - amplitude >= 5 cm
FAR - amplitude >= 5 cm
Model
GLORYS12V1 (mean=0.577)
GLORYS2V4 (mean=0.462)
GLORYS12V1 (mean=0.305)
GLORYS2V4 (mean=0.375)
POD - amplitude >= 10 cm
FAR - amplitude >= 10 cm
GLORYS12V1 (mean=0.61)
GLORYS2V4 (mean=0.448)
GLORYS12V1 (mean=0.288)
GLORYS2V4 (mean=0.409)
POD - amplitude >= 15 cm
FAR - amplitude >= 15 cm
GLORYS12V1 (mean=0.596)
GLORYS2V4 (mean=0.399)
GLORYS12V1 (mean=0.285)
GLORYS2V4 (mean=0.433)
POD - amplitude >= 20 cm
FAR - amplitude >= 20 cm
GLORYS12V1 (mean=0.59)
GLORYS2V4 (mean=0.363)
GLORYS12V1 (mean=0.291)
GLORYS2V4 (mean=0.454)
POD
FAR
Date
2023-07
2023-10
2024-01
2024-04
2024-07
2024-10
2025-01
2025-04
(a)

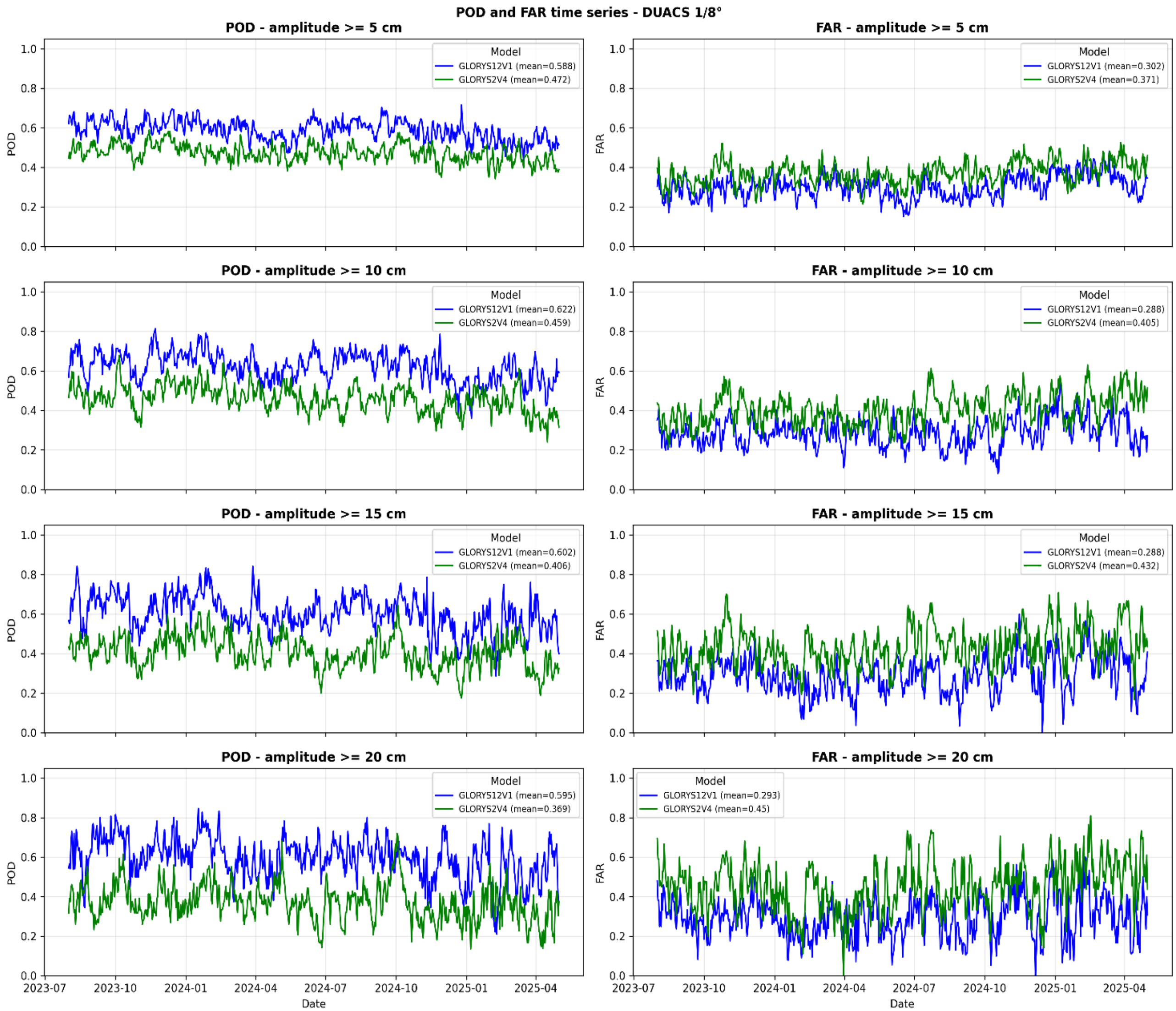

(b)

Fig. C1. Time series for POD & FAR by amplitude threshold: 5 cm, 10 cm, 15 cm, 20 cm, for SWOT comparison (a) and for DUACS 1/8° comparison (b), with a minimum lifetime threshold of 4 days.

The verification metrics do not improve monotonically as low-amplitude eddies are progressively excluded. For GLORYS12V1, POD remains approximately between 0.58 and 0.62, while FAR remains between about 0.27 and 0.31. For GLORYS2V4, POD decreases from approximately 0.46 to 0.47 at the 5 cm threshold to about 0.36 – 0.37 at 20 cm, while FAR increases from about 0.37–0.38 to approximately 0.45. The higher thresholds also retain fewer eddies, producing larger day-to-day variability. Therefore, these results do not indicate a uniform improvement in the representation of stronger eddies.

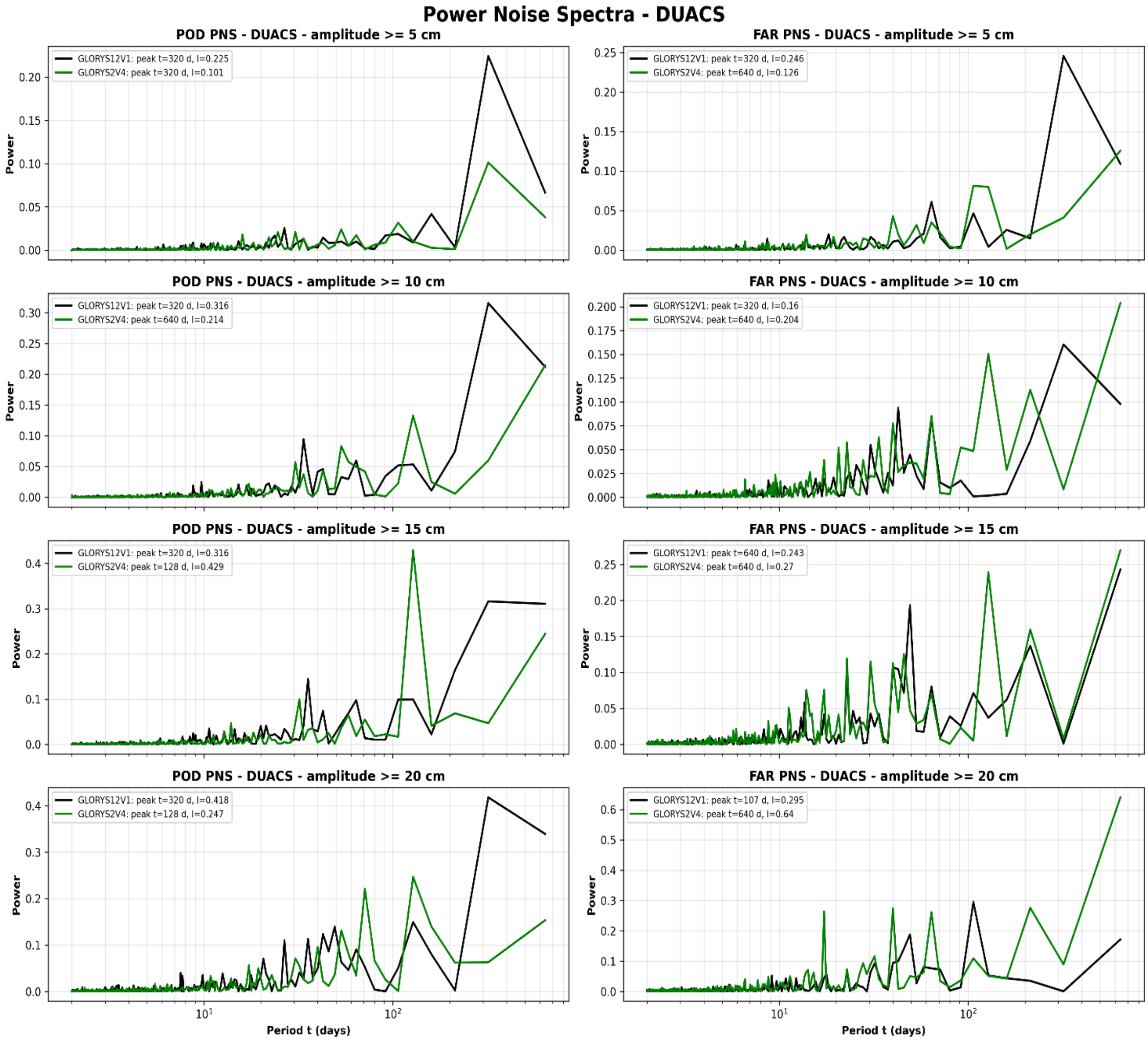

Power Noise Spectra - DUACS
POD PNS - DUACS - amplitude >= 5 cm
GLORYS12V1: peak t=320 d, I=0.225
GLORYS2V4: peak t=320 d, I=0.101
FAR PNS - DUACS - amplitude >= 5 cm
GLORYS12V1: peak t=320 d, I=0.246
GLORYS2V4: peak t=640 d, I=0.126
POD PNS - DUACS - amplitude >= 10 cm
GLORYS12V1: peak t=320 d, I=0.316
GLORYS2V4: peak t=640 d, I=0.214
FAR PNS - DUACS - amplitude >= 10 cm
GLORYS12V1: peak t=320 d, I=0.16
GLORYS2V4: peak t=640 d, I=0.204
POD PNS - DUACS - amplitude >= 15 cm
GLORYS12V1: peak t=320 d, I=0.316
GLORYS2V4: peak t=128 d, I=0.429
FAR PNS - DUACS - amplitude >= 15 cm
GLORYS12V1: peak t=640 d, I=0.243
GLORYS2V4: peak t=640 d, I=0.27
POD PNS - DUACS - amplitude >= 20 cm
GLORYS12V1: peak t=320 d, I=0.418
GLORYS2V4: peak t=128 d, I=0.247
FAR PNS - DUACS - amplitude >= 20 cm
GLORYS12V1: peak t=107 d, I=0.295
GLORYS2V4: peak t=640 d, I=0.64
Power
Period t (days)

(a)

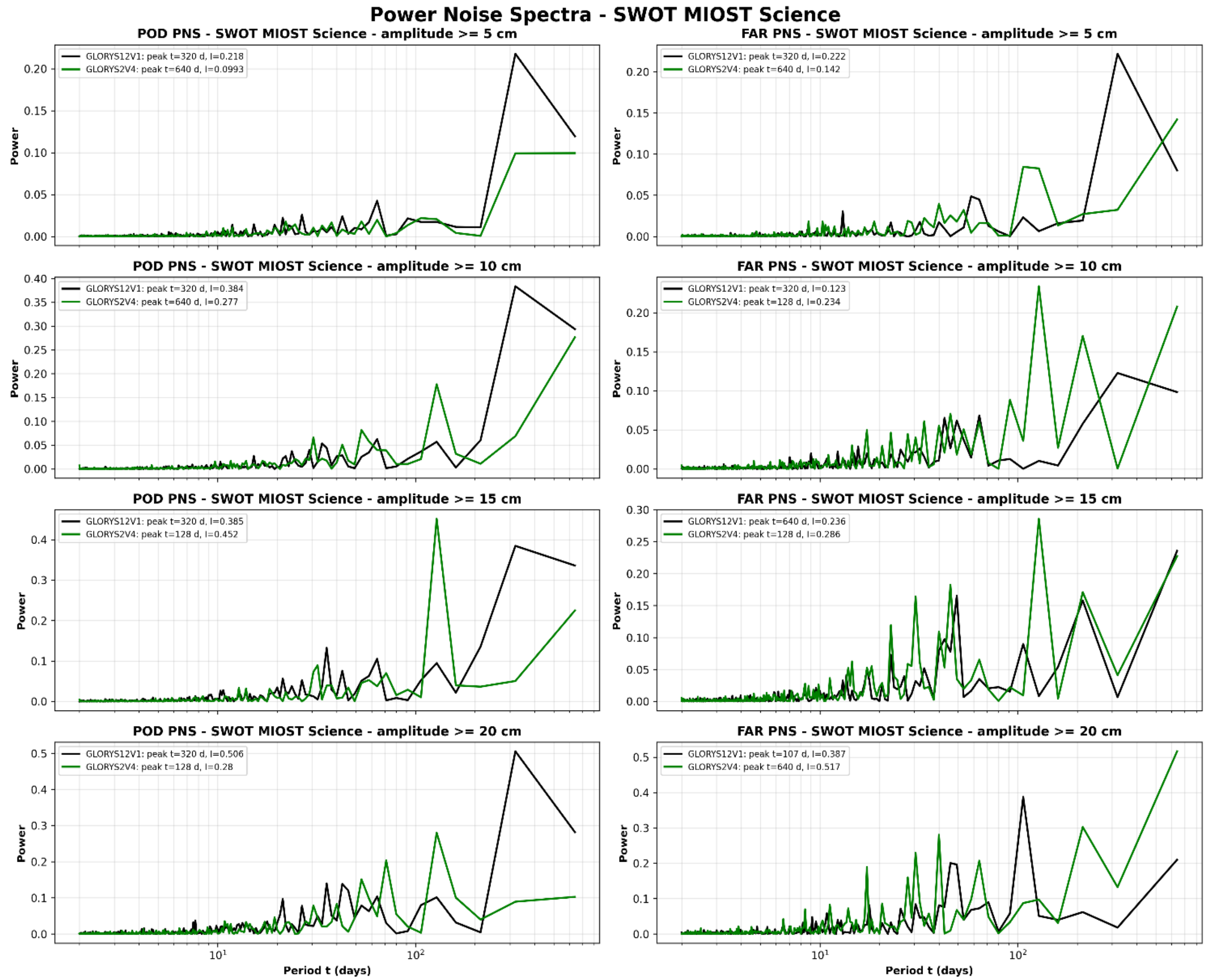

(b)

Fig. C2. Power Spectra of time series of both verification metrics for each reanalysis products, for DUACS (a) and SWOT MIOST Science comparison (b). It is shown that the agreement does not improve significantly compared with the more general case, namely that extended to all eddies. Generally, for both observational datasets, we observe that the agreement between the two reanalyses is never markedly better. Only in terms of FAR is it observed that GLORYS2V4 shows a net deterioration in agreement, as there is a clear increase in FAR, particularly at high amplitudes.

For higher amplitude thresholds, the metric values show much larger variations over time. On some days, the POD values are close to 1 and the FAR values are close to 0, while on other days they are much farther from these ideal values. This variability is mainly caused by the smaller number of eddies with amplitudes above 10 or 20 cm. For this reason, the POD and FAR time series can show large variations and can rapidly move towards values close to 0 or 1. These results suggest that the imperfect matching between the reanalyses and the observational datasets mainly concerns small ocean eddies. However, this improvement does not mean that the complete eddy field is better represented.

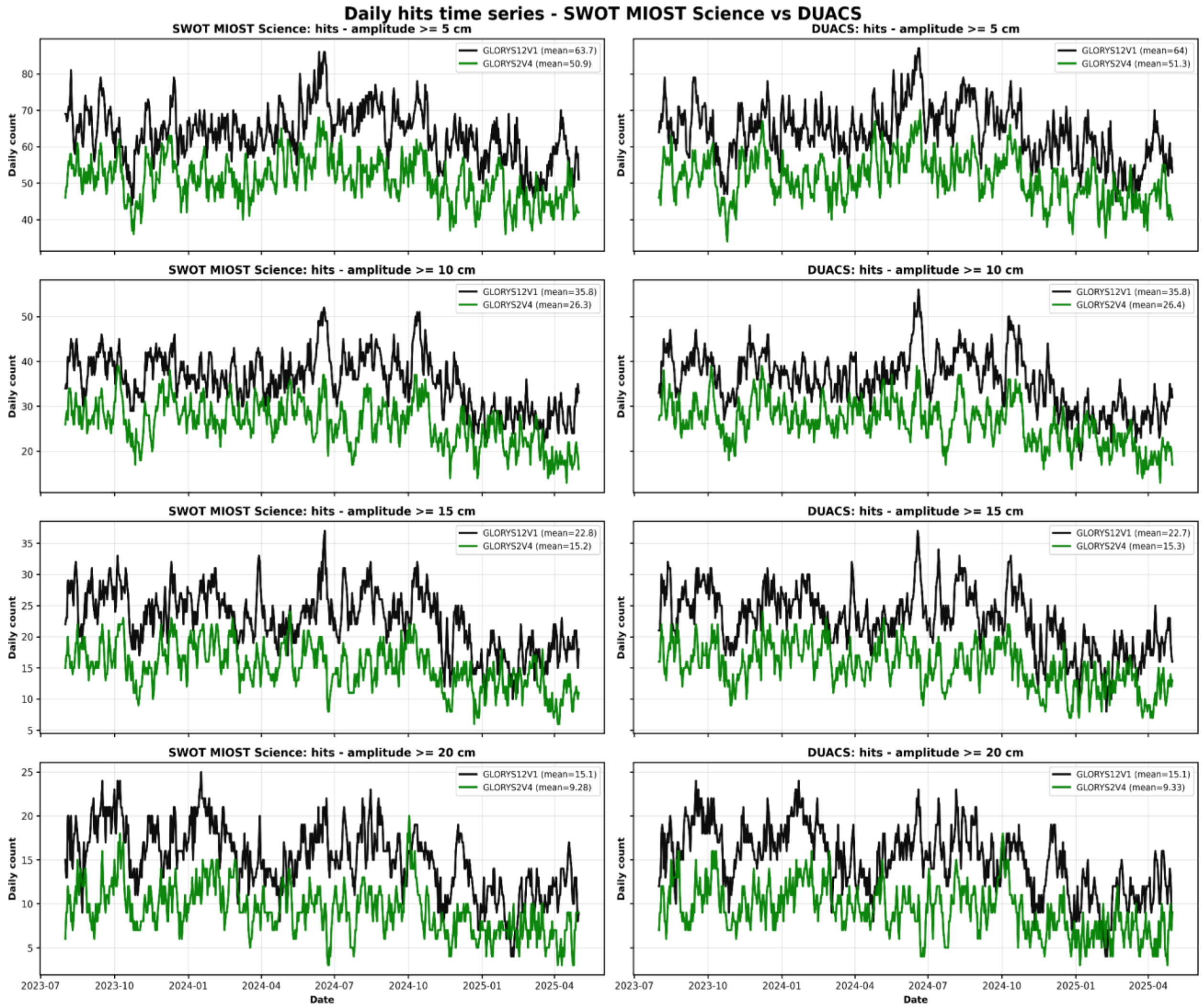
Daily hits time series - SWOT MIOST Science vs DUACS
SWOT MIOST Science: hits - amplitude >= 5 cm
GLORYS12V1 (mean=63.7)
GLORYS2V4 (mean=50.9)
DUACS: hits - amplitude >= 5 cm
GLORYS12V1 (mean=64)
GLORYS2V4 (mean=51.3)
SWOT MIOST Science: hits - amplitude >= 10 cm
GLORYS12V1 (mean=35.8)
GLORYS2V4 (mean=26.3)
DUACS: hits - amplitude >= 10 cm
GLORYS12V1 (mean=35.8)
GLORYS2V4 (mean=26.4)
SWOT MIOST Science: hits - amplitude >= 15 cm
GLORYS12V1 (mean=22.8)
GLORYS2V4 (mean=15.2)
DUACS: hits - amplitude >= 15 cm
GLORYS12V1 (mean=22.7)
GLORYS2V4 (mean=15.3)
SWOT MIOST Science: hits - amplitude >= 20 cm
GLORYS12V1 (mean=15.1)
GLORYS2V4 (mean=9.28)
DUACS: hits - amplitude >= 20 cm
GLORYS12V1 (mean=15.1)
GLORYS2V4 (mean=9.33)
Daily count
Date

(a)

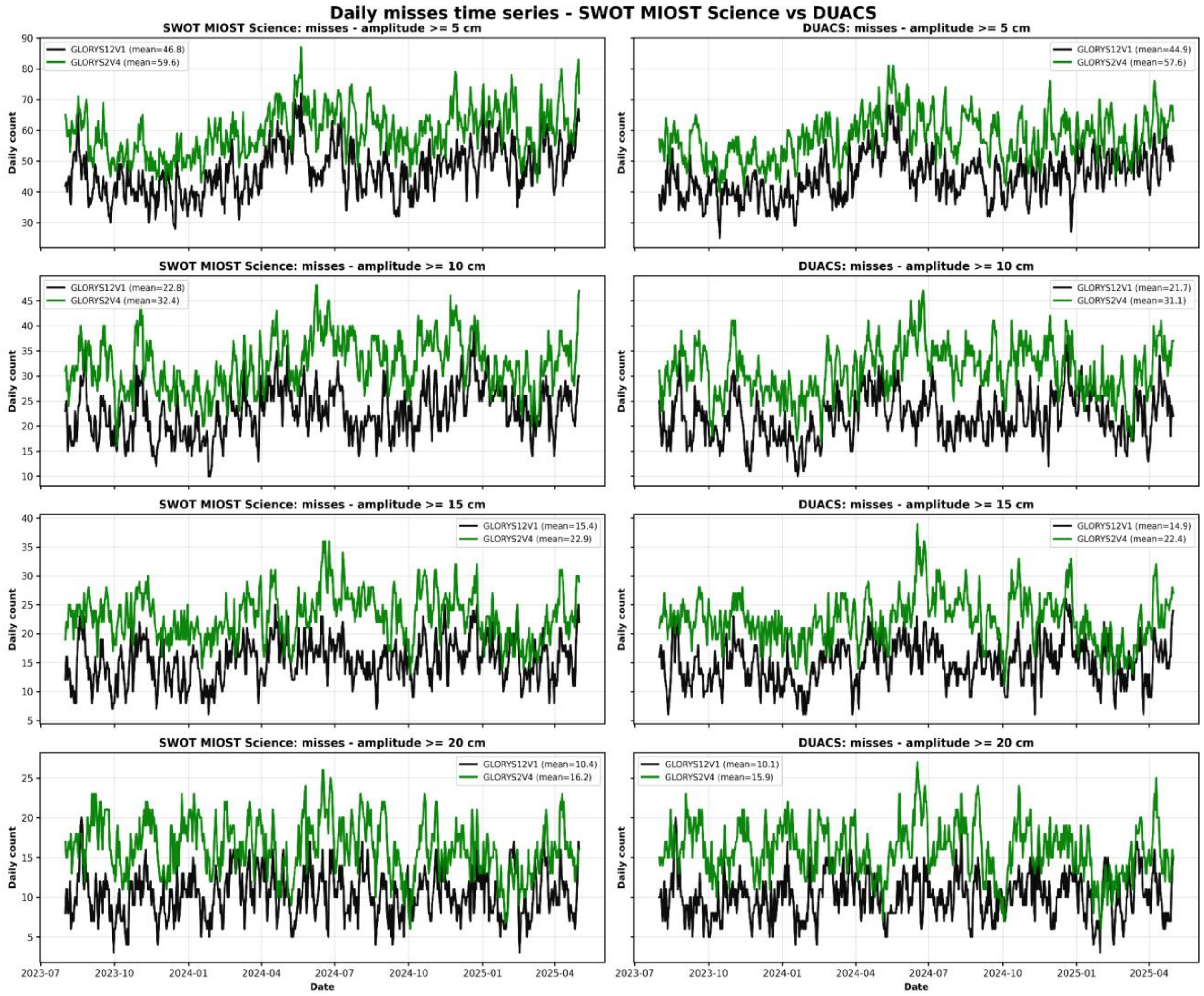

(b)

Fig. C3. Time series for daily number of hits (a), misses (b), for both satellite data compared to the reanalyses. On the left, the comparison with SWOT MIOST Science, while on the right, the comparison with DUACS.

As the minimum amplitude threshold increases, the absolute numbers of both hits and misses decrease because fewer eddies satisfy the criterion. For GLORYS12V1, the mean number of hits remains higher than the number of misses at all thresholds. For GLORYS2V4, misses remain more numerous than hits and their relative importance increases at higher thresholds. This behaviour is consistent with the reduction in POD observed for GLORYS2V4. The power spectra in Fig. C2 shows that temporal variability generally increases with the minimum amplitude threshold, mainly at longer periods, while differences remain limited at short periods. GLORYS12V1 generally shows larger POD spectral peaks, whereas GLORYS2V4 generally shows larger FAR peaks, with exceptions at 15 cm for POD and 5 cm for FAR. Fig. C3 shows that both hits and misses decrease in absolute number as the threshold increases because fewer eddies are retained. However, GLORYS12V1 maintains more hits than misses, whereas misses remain more numerous than hits for GLORYS2V4, indicating a greater reduction in matching performance for GLORYS2V4 at higher amplitude thresholds. We also evaluated POD and FAR for low-amplitude eddies (≤10 cm), whose weak SSH signatures make their detection and matching more sensitive to mapping, filtering, and background variability. This subset is therefore expected to show lower POD and higher FAR because small differences between observational and reanalysis fields can alter eddy position and contours or generate unmatched features.

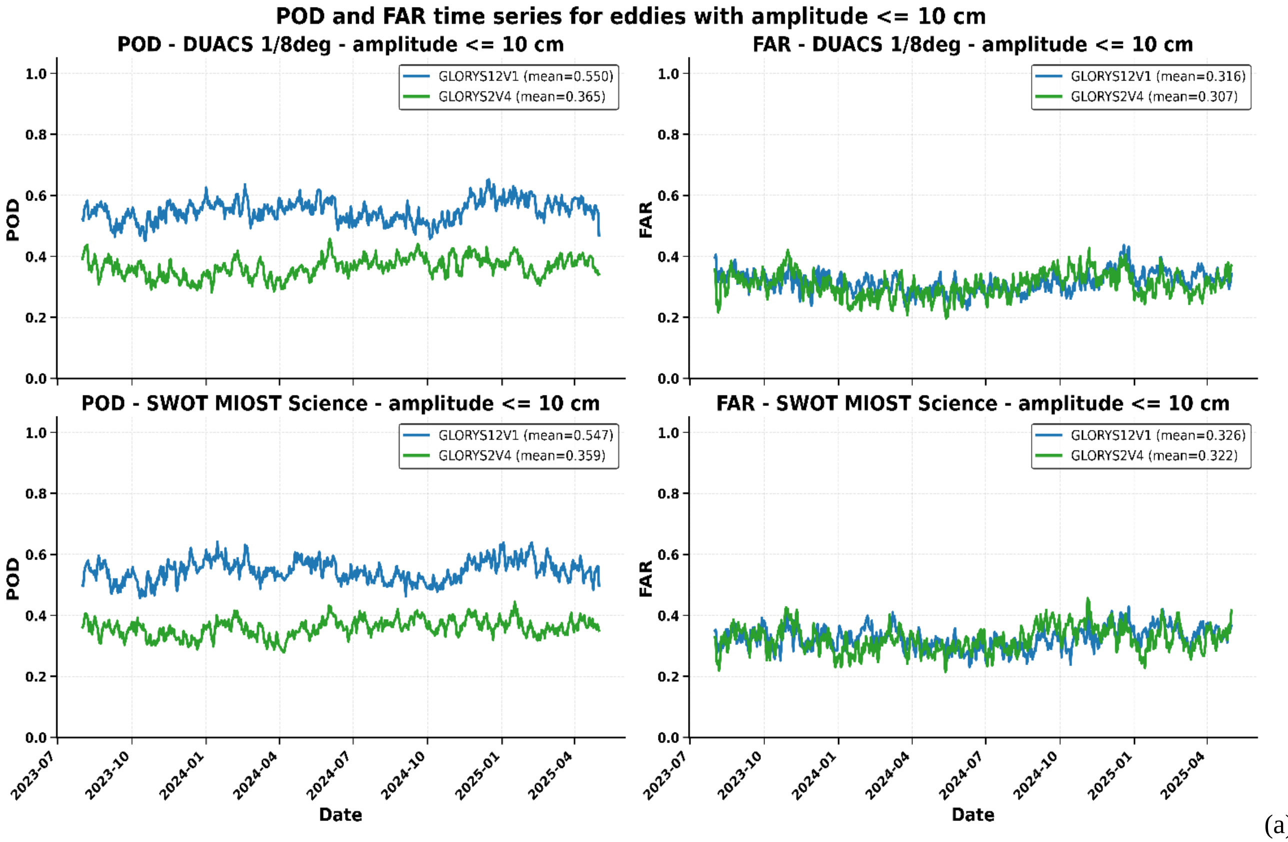

(a)

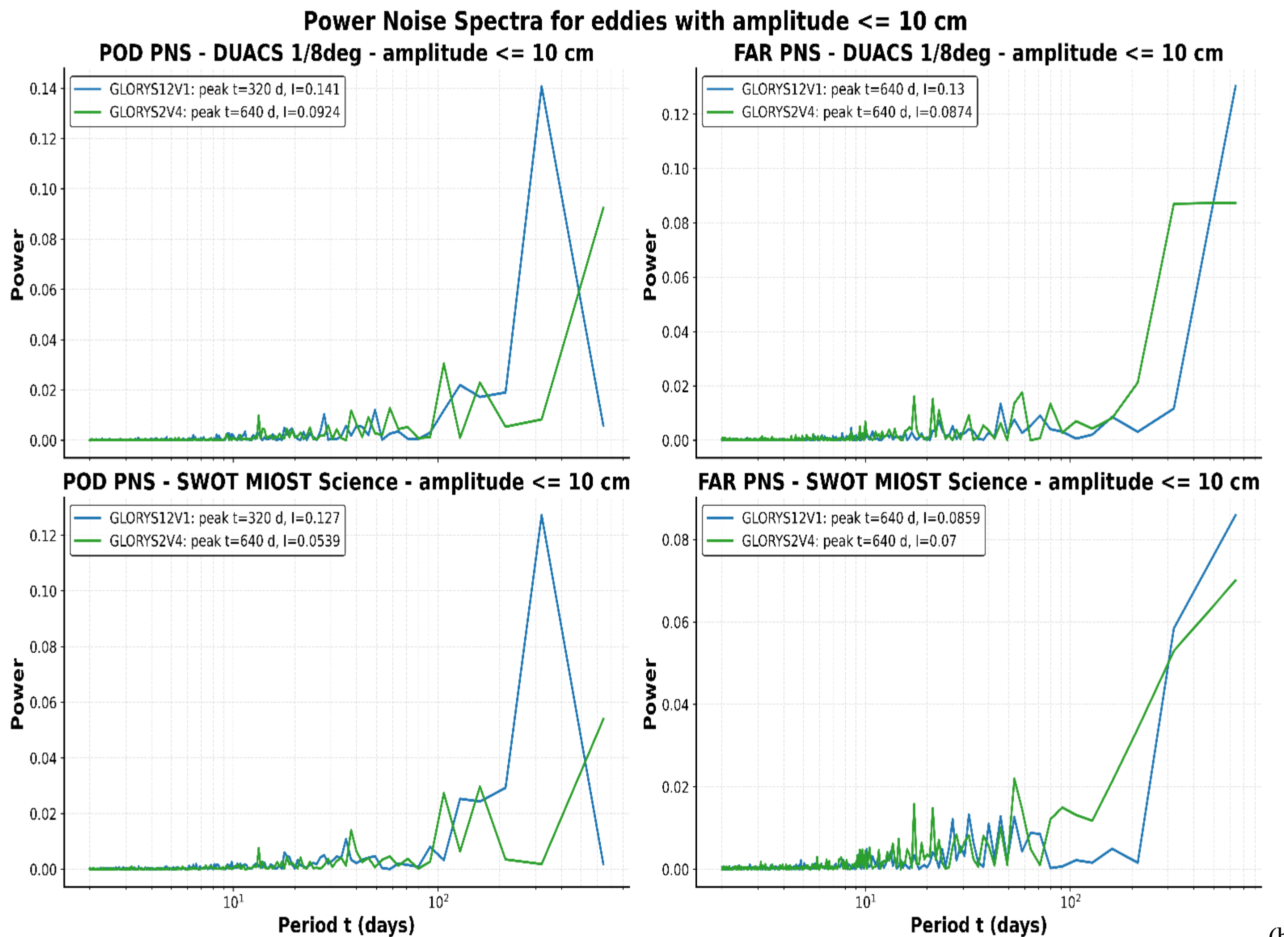

(b)

Fig. C4. **(a) POD and FAR time series for eddies with amplitudes ≤10 cm for the comparisons with DUACS 1/8° and SWOT MIOST Science. (b) Corresponding power spectra. A 4–day minimum–lifetime threshold is used.**

Fig. C5 shows the distributions of hits, misses, and false alarms as functions of eddy radius and amplitude.

We further introduce the histograms of the eddy matching statistics, namely hits, misses, and false alarms, as a function of both eddy radius and eddy amplitude. The aim is to provide a more detailed view, similar to a zoomed-in analysis, of how the matching statistics vary with the two main physical eddy features. This additional representation is useful because, on a linear scale, the histograms are not always able to clearly show the distinct behaviour of each matching statistic as eddy amplitude and radius increase. A logarithmic y-axis is used to distinguish the matching categories in bins containing fewer eddies. This is shown in Fig. C5.

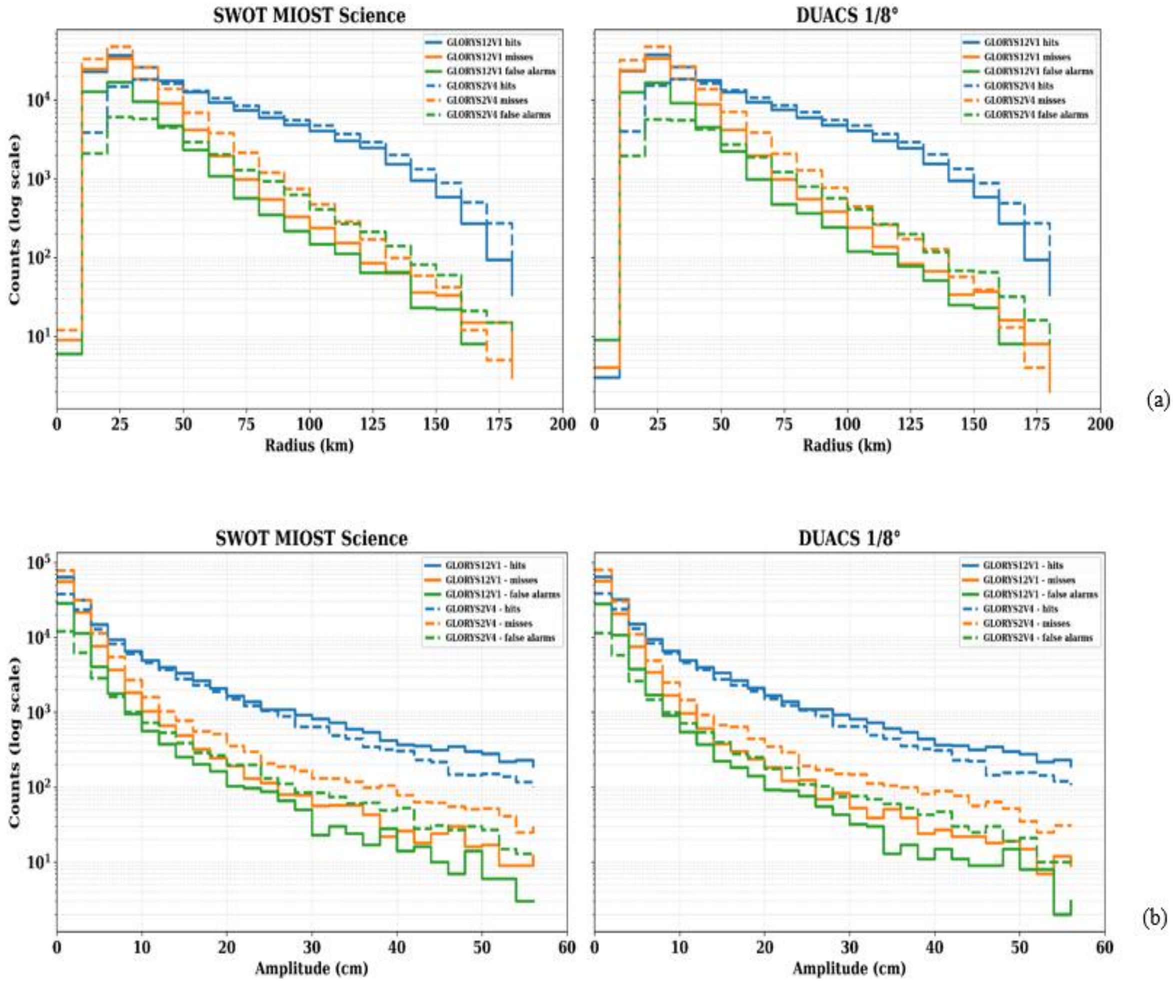

Fig. C5. Histograms for eddy matching statistics on a logarithmic scale, for both comparisons, for eddy radius (a) and eddy amplitude (b).

At the smallest radii and amplitudes, misses are particularly prominent, especially for GLORYS2V4, confirming its greater difficulty in representing small eddies. GLORYS12V1 produces more hits in these classes, although this is accompanied by more small false alarms. For eddy radius, GLORYS2V4 has more misses than GLORYS12V1 up to approximately 150 km, while its false alarms become more numerous above about 50 km. In the amplitude distributions, misses remain the main source of error for GLORYS2V4. Above radii of approximately 50 km and amplitudes of 8–10 cm, hits become the dominant category for both reanalyses and both observational references. The largest discrepancies are therefore concentrated among smaller and lower-amplitude eddies.

Appendix D

This appendix assesses the sensitivity of the verification results to two methodological choices: (i) the maximum centroid distance allowed in the eddy-matching procedure and (ii) the cutoff wavelength of the Bessel high-pass filter applied before eddy detection. The reference values are 125 km for the matching distance and 500 km for the filter cutoff wavelength. The alternative values tested here are 62.5 km for matching and 200 and 800 km for filtering. All other methodological settings, including the 4 days minimum lifetime threshold, remain unchanged.

Sensitivity to a different cost function distance threshold for the eddy matching process: 62.5 km.

The matching analysis was repeated using a maximum centroid distance of 62.5 km, corresponding to half of the reference value of 125 km. This more restrictive criterion allows only eddies with closer centroid positions to be matched. When a pair accepted with the 125 km threshold no longer satisfies the 62.5 km criterion, the reference eddy is classified as a miss and the corresponding reanalysis eddy as a false alarm.

Figure D1 shows an example for anticyclonic eddies on 1 January 2025. The stricter threshold reduces the number of hits and increases both misses and false alarms, demonstrating the sensitivity of the matching statistics to the maximum distance allowed between eddy centroids.

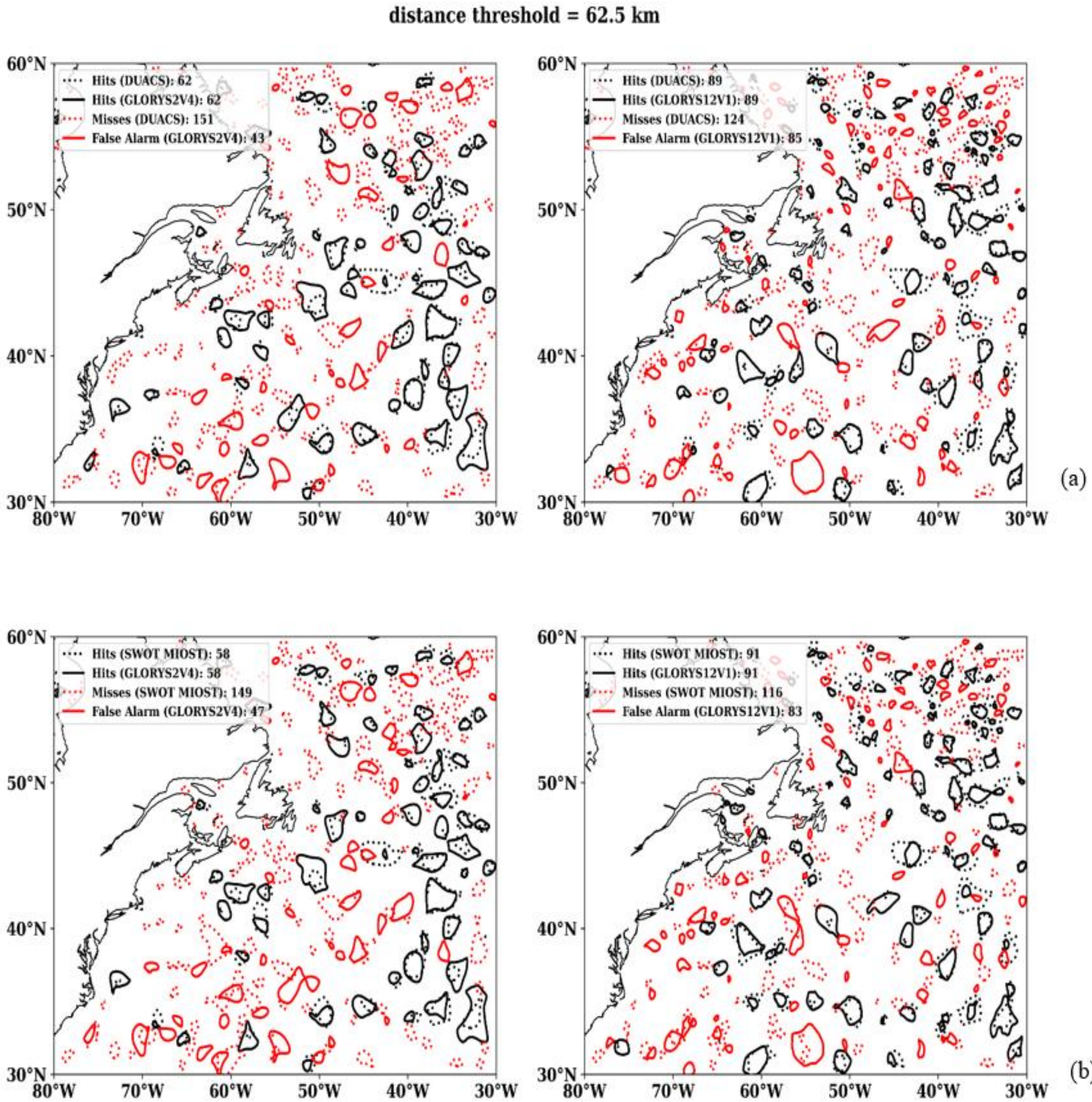

Fig. D1. Anticyclonic-eddy matching on 1 January 2025 using a maximum centroid distance of 62.5 km. GLORYS2V4 is shown on the left and GLORYS12V1 on the right, for the comparisons with (a) DUACS 1/8° and (b) SWOT MIOST Science.

The verification metrics are computed on a daily basis, following the same procedure described in Section 2.4 and Sect. 3.2, in order to evaluate the temporal evolution of the matching performance. Table D1 and Table D2 report the absolute and relative changes in the verification metrics for the two comparisons, respectively.

Verification metric	125 km threshold	62.5 km threshold	Difference	Difference %
POD 12V1	0.624	0.483	-0.141	-22.59%
FAR 12V1	0.237	0.409	0.172	72.57%
POD 2V4	0.455	0.307	-0.148	-32.52%
FAR 2V4	0.194	0.456	0.262	135.05%

Table D1. Aggregated eddy verification statistics for the Probability of Detection (POD) and False Alarm Ratio (FAR) for the comparison with SWOT using maximum matching distances of 125 and 62.5 km. Absolute and percentage differences are calculated as the 62.5 km result minus the 125 km result.

Verification metric	125 km threshold	62.5 km threshold	Difference	Difference %
POD 12V1	0.628	0.487	-0.141	-22.45%
FAR 12V1	0.230	0.402	0.172	74.78%
POD 2V4	0.460	0.310	-0.150	-32.60%
FAR 2V4	0.182	0.447	0.265	145.60%

Table D2. Aggregated eddy verification statistics for the Probability of Detection (POD) and False Alarm Ratio (FAR) for the comparison with DUACS using maximum matching distances of 125 and 62.5 km. Absolute and percentage differences are calculated as the 62.5 km result minus the 125 km result.

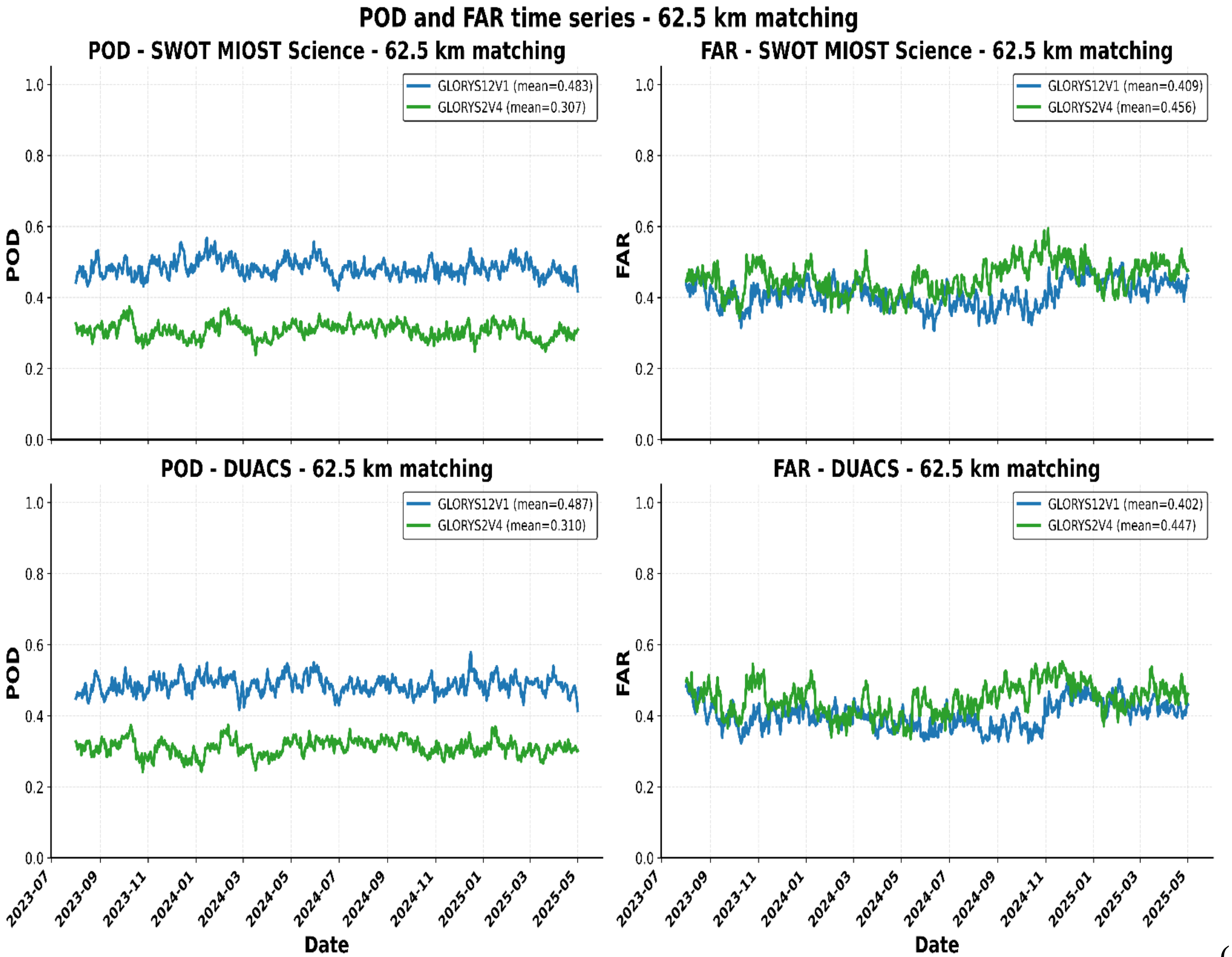

POD and FAR time series - 62.5 km matching
POD - SWOT MIOST Science - 62.5 km matching
FAR - SWOT MIOST Science - 62.5 km matching
GLORYS12V1 (mean=0.483)
GLORYS2V4 (mean=0.307)
GLORYS12V1 (mean=0.409)
GLORYS2V4 (mean=0.456)
POD - DUACS - 62.5 km matching
FAR - DUACS - 62.5 km matching
GLORYS12V1 (mean=0.487)
GLORYS2V4 (mean=0.310)
GLORYS12V1 (mean=0.402)
GLORYS2V4 (mean=0.447)
POD
FAR
Date

(a)

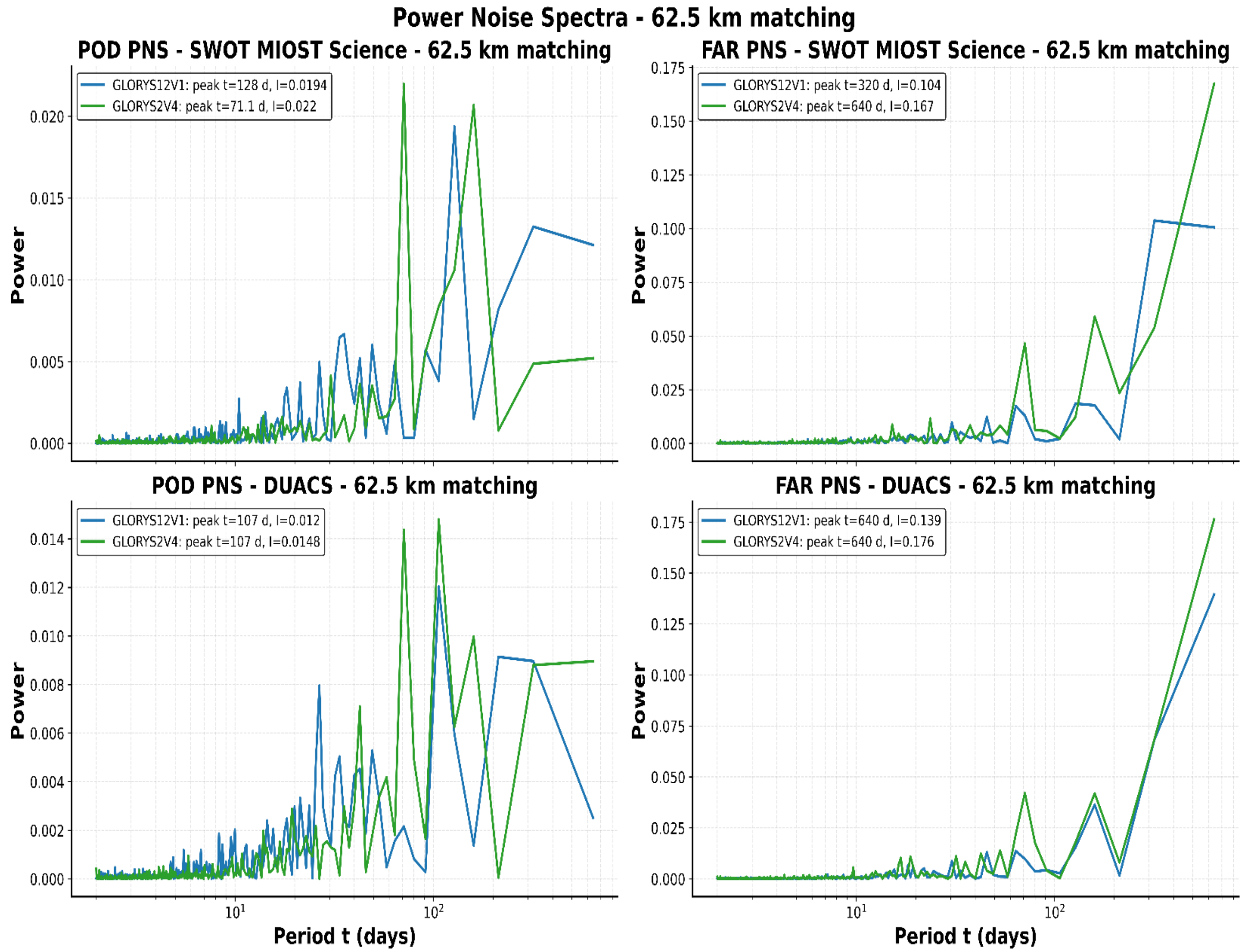

(b)

Fig. D2. (a) Time series for the verification metrics, for the comparison with SWOT MIOST Science and DUACS 1/8° comparison, with a minimum lifetime threshold of 4 days. In (b) power spectra for all the time series presented in (a).

Overall, when the maximum matching distance is reduced from 125 km to 62.5 km, FAR becomes higher for GLORYS2V4 than for GLORYS12V1, as shown in Table D1, Table D2, Fig. D1 and Fig. D2 (a). This does not necessarily mean that GLORYS2V4 produces a larger absolute number of false alarms. Rather, it reflects the relative nature of FAR, which depends on the proportion of unmatched reanalysis eddies with respect to the total number of reanalysis detections considered in the verification.

In contrast, POD remains higher for GLORYS12V1, indicating that the higher-resolution reanalysis is still able to match a larger fraction of the observed eddies, even under the more restrictive distance criterion. The most evident effect of reducing the matching distance is the strong increase in FAR, especially for GLORYS2V4, where FAR more than doubles in both satellite-based comparisons. A substantial increase is also found for GLORYS12V1, with FAR increasing by more than 70%. POD also decreases when the reduced distance threshold is applied, but the relative reduction is smaller than for FAR. The decrease is of the order of 20% for GLORYS12V1 and about 30% for GLORYS2V4. This indicates that the reduced distance threshold may affect the classification of unmatched reanalysis detections, leading to a large increase in false alarms, while the reduction in correctly matched observed eddies is less pronounced.

The power spectra in Fig. 2D (b) shows slightly larger main POD peaks for GLORYS2V4 than for GLORYS12V1. GLORYS2V4 also exhibits the larger FAR peak in both observational comparisons. In the SWOT comparison, the main POD peaks occur at approximately 71 days for GLORYS2V4 and 128 days for GLORYS12V1, whereas both are located near 107 days in the DUACS comparison. The strongest FAR peaks occur at longer resolved periods. Because the evaluation period is only approximately 640 days long, peaks at or near 640 days should be interpreted as low-frequency variability rather than as evidence of a robust periodic cycle.

Sensitivity to different Bessel filters for eddy detection process

The SSH or ADT fields of all products were high-pass filtered using a Bessel filter before eddy detection. The reference cutoff wavelength is 500 km. To assess the sensitivity of the detection and verification results to the retained spatial scales, the complete detection, tracking, and matching procedure was repeated using cutoff wavelengths of 200 and 800 km. The 200 km cutoff applies more restrictive spatial filtering, whereas the 800 km cutoff retains a broader range of large-scale variability.

Verification metric	500 km	200 km	Difference	Difference (%)
POD 12V1 (SWOT)	0.624	0.680	0.056	8.97%
POD 12V1 (DUACS)	0.628	0.679	0.051	8.12%
FAR 12V1 (SWOT)	0.237	0.197	-0.04	-16.88%
FAR 12V1 (DUACS)	0.230	0.189	-0.041	-17.83%
POD 2V4 (SWOT)	0.455	0.540	0.085	18.68%
POD 2V4 (DUACS)	0.460	0.541	0.081	17.61%
FAR 2V4 (SWOT)	0.194	0.129	-0.065	-33.51%
FAR 2V4 (DUACS)	0.182	0.118	-0.064	-35.16%

Table D3. Mean eddy verification metrics, difference and percentage difference, crossing from a cutoff wavelenght for Bessel filter of 500 km to 200 km for both comparisons.

Verification metric	500 km	800 km	Difference	Difference (%)
POD 12V1 (SWOT)	0.624	0.609	-0.015	-2.40%
POD 12V1 (DUACS)	0.628	0.614	-0.014	-2.23%
FAR 12V1 (SWOT)	0.237	0.248	0.011	4.64%
FAR 12V1 (DUACS)	0.230	0.243	0.013	5.65%
POD 2V4 (SWOT)	0.455	0.422	-0.033	-7.25%
POD 2V4 (DUACS)	0.460	0.428	-0.032	-6.96%
FAR 2V4 (SWOT)	0.194	0.198	0.004	2.06%
FAR 2V4 (DUACS)	0.182	0.190	0.008	4.40%

Table D4. Mean eddy verification metrics, difference and percentage difference, crossing from a cutoff wavelenght for Bessel filter of 500 km to 800 km for both comparisons.

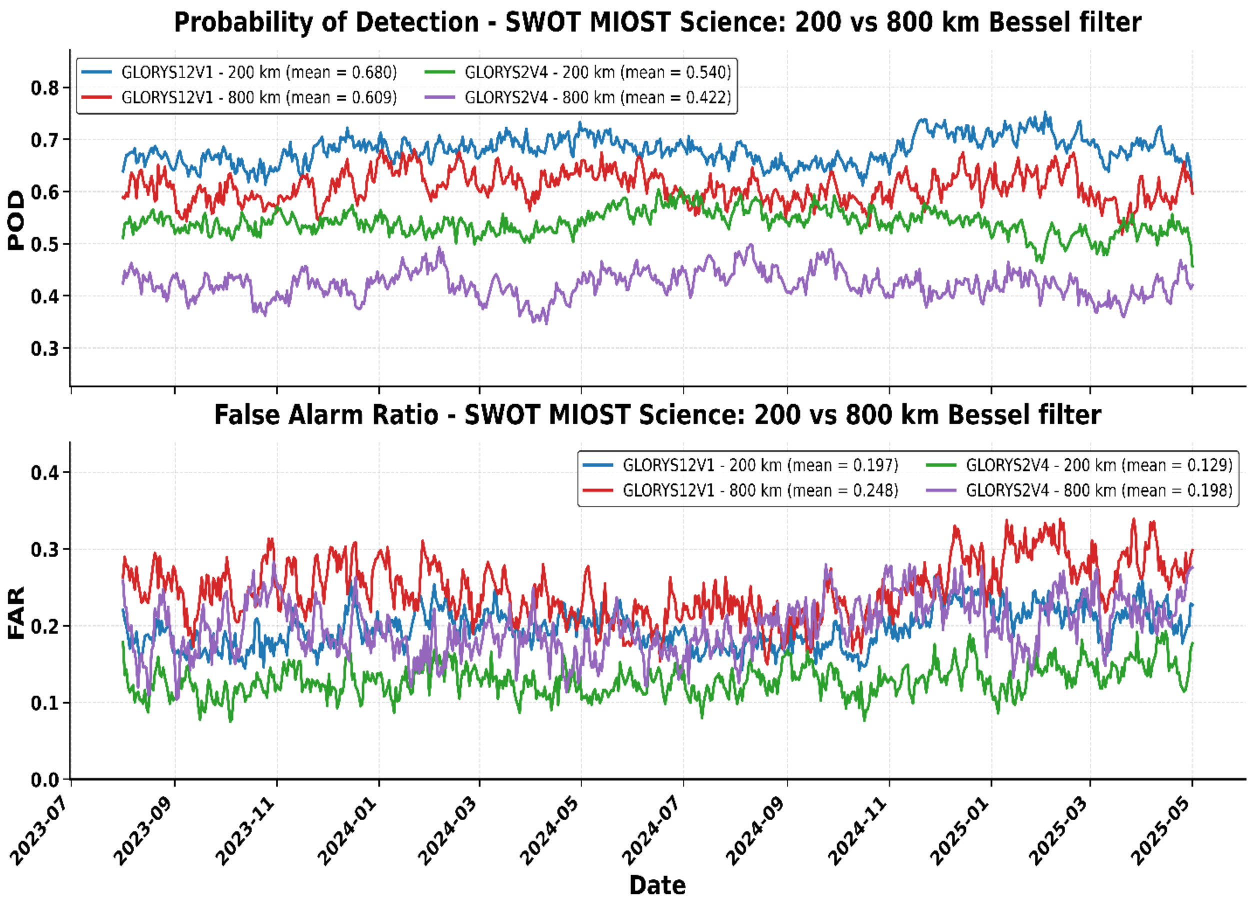

(a)

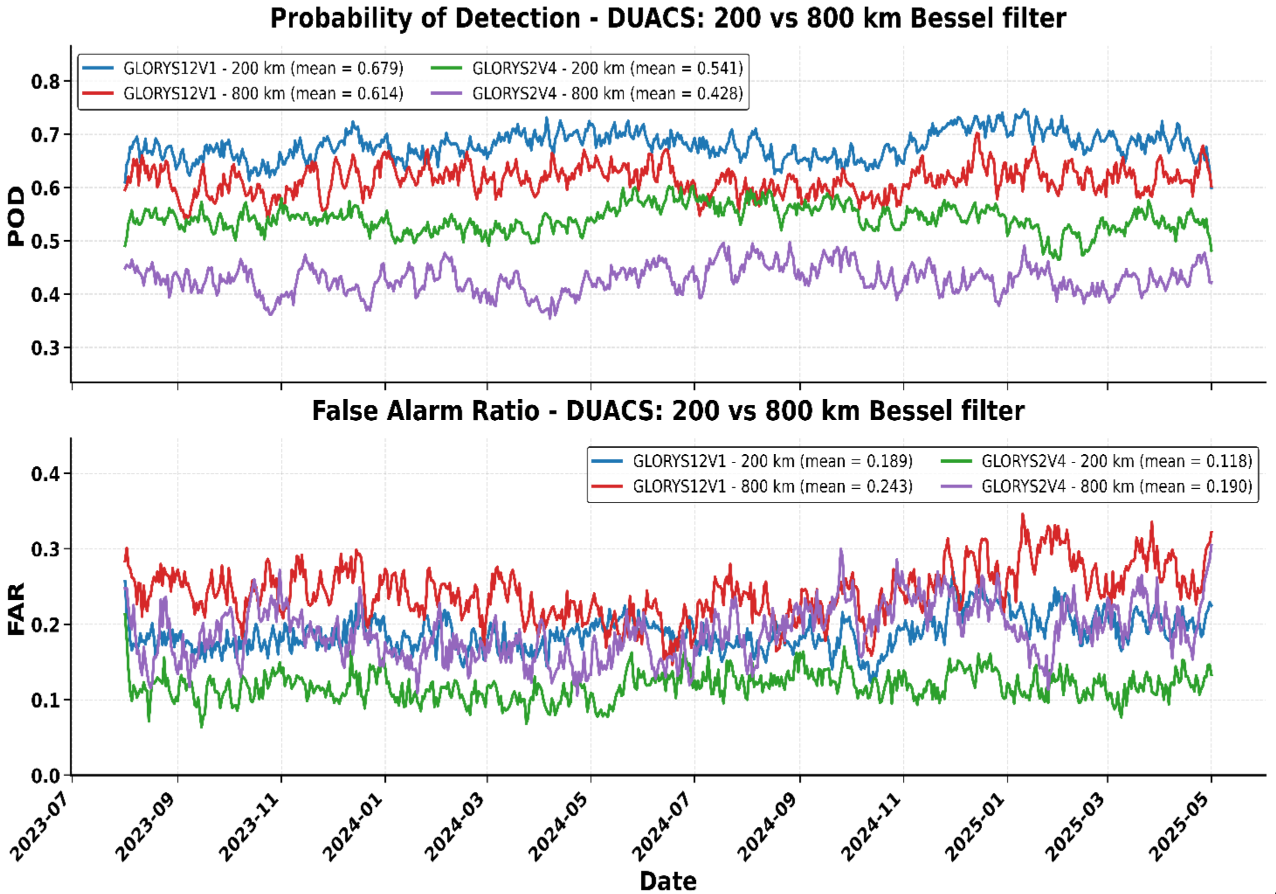
Probability of Detection - DUACS: 200 vs 800 km Bessel filter
GLORYS12V1 - 200 km (mean = 0.679)
GLORYS12V1 - 800 km (mean = 0.614)
GLORYS2V4 - 200 km (mean = 0.541)
GLORYS2V4 - 800 km (mean = 0.428)
POD
False Alarm Ratio - DUACS: 200 vs 800 km Bessel filter
GLORYS12V1 - 200 km (mean = 0.189)
GLORYS12V1 - 800 km (mean = 0.243)
GLORYS2V4 - 200 km (mean = 0.118)
GLORYS2V4 - 800 km (mean = 0.190)
FAR
Date

(b)

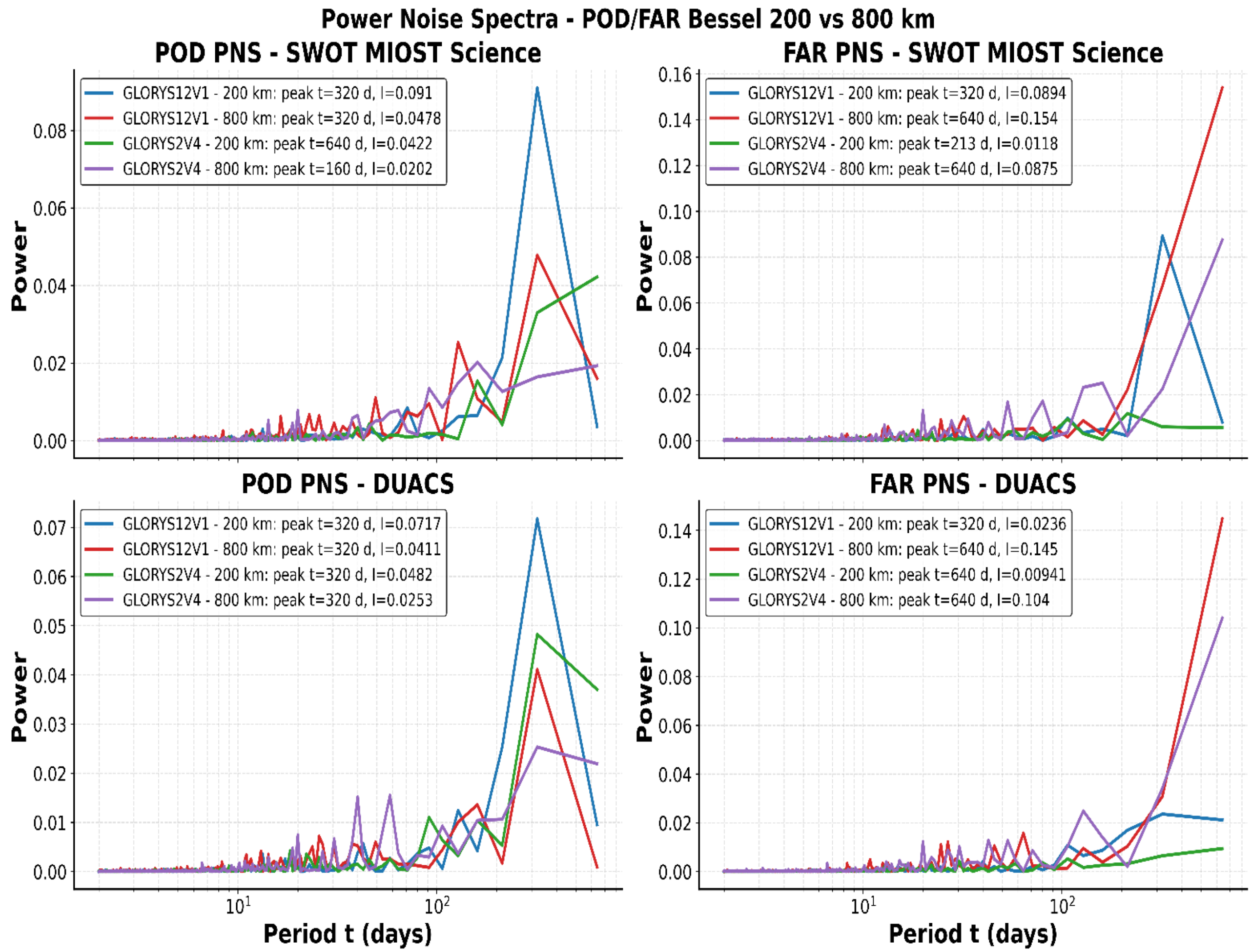

(c)

Fig. D3. POD and FAR time series obtained using Bessel-filter cutoff wavelengths of 200 and 800 km for the comparisons with (a) SWOT MIOST Science and (b) DUACS 1/8°. Panel (c) shows the corresponding power spectra. A 4-day minimum-lifetime threshold is used.

Reducing the Bessel-filter cutoff wavelength from 500 to 200 km increases POD and decreases FAR for both reanalyses and both observational comparisons. The changes are particularly pronounced for GLORYS2V4, for which POD increases by approximately 18% and FAR decreases by approximately 34–35%. For GLORYS12V1, POD increases by about 8–9% and FAR decreases by approximately 17–18%. Increasing the cutoff wavelength from 500 to 800 km produces smaller and opposite changes: POD decreases and FAR increases for both reanalyses. The POD reduction is larger for GLORYS2V4, whereas the FAR changes remain relatively small. For both cutoff tests, POD is slightly more sensitive in the SWOT comparison, while FAR is generally more sensitive in the DUACS comparison. These changes show that the verification metrics depend on the spatial scales retained before eddy detection. However, the better verification scores obtained with the 200 km cutoff wavelength do not necessarily demonstrate that this value is physically more appropriate, because stronger filtering may remove structures that would otherwise remain unmatched. Regarding the power spectra, the largest peaks for POD are observed for GLORYS12V1 using the 200 km filter cutoff, at temporal scales of the order of several hundred days, approximately 320 days. For FAR, the highest values are instead found for GLORYS12V1 with the 800 km filter cutoff, with enhanced power around 640 days. At shorter temporal scales, the variability is nearly similar across all datasets and filter configurations. Overall, in terms of noise power, the strongest peak is found for the POD of GLORYS12V1 with the 200 km filter cutoff in the comparison with SWOT MIOST.

Data availability

The datasets used in this study are available from the following sources. The DUACS 1/8° global gridded altimetry product is distributed by the Copernicus Marine Service under product ID SEALEVEL_GLO_PHY_L4_MY_008_047 (https://doi.org/10.48670/moi-00148). The data were accessed and downloaded on 31 October 2025 (Global Ocean Gridded L 4 Sea Surface Heights And Derived Variables Reprocessed 1993 Ongoing | Copernicus Marine Service). The SWOT MIOST Science product corresponds to the AVISO/DUACS experimental delayed-time global Level-4 gridded sea-level dataset combining nadir and SWOT wide-swath observations, version 2.0.1 (https://doi.org/10.24400/527896/A01-2025.001). The product is distributed by AVISO through the ODATIS THREDDS server (SWOT MIOST Science). We used files from the science period covering 1 August 2023 to 1 May 2025. The data were accessed and downloaded on 1 November 2025. The GLORYS12V1 reanalysis is distributed by the Copernicus Marine Service under product ID GLOBAL_MULTIYEAR_PHY_001_030 (https://doi.org/10.48670/moi-00021). GLORYS2V4 was obtained as a member of the Copernicus Marine Service Global Ocean Ensemble Physics Reanalysis product, GLOBAL_MULTIYEAR_PHY_ENS_001_031 (Global Ocean Ensemble Physics Reanalysis | Copernicus Marine Service). GLORYS2V4 has a horizontal resolution of 1/4° and 75 vertical levels. The data were accessed and downloaded on 1 November 2025. For both reanalyses, daily fields covering 1 August 2023 to 1 May 2025 were used.

Code availability

The eddy detection methodology is based on the publicly available Python package py-eddy-tracker (Mason et al., 2014; Faghmous et al., 2015; Mason et al., 2019; Pegliasco et al.,2021), available at: https://py-eddy-tracker.readthedocs.io. The feature-based verification methodology follows Smith and Fortin (2022). Initial analysis scripts were provided by GCS and were further developed by PM for the present study. The custom analysis scripts are available in the following GitHub repository:quantitative_evaluation_ocean_mesoscale_eddies_north_atlantic/scripts at main · Mauriello1997/quantitative_evaluation_ocean_mesoscale_eddies_north_atlantic

Competing interests

At least one of the (co-)authors serves as editor for the special issue to which this paper belongs.

Author Contributions

PM developed the analysis code, under suggestions of GCS, CY and AS. The methodology is built upon initial scripts provided by GCS, and further implemented by PM, GCS, AS, CY. PM performed the data analysis and led the writing of the manuscript. Significant contributions to the interpretation of results and manuscript preparation were provided by AS, GCS, CY. All authors have reviewed and approved the final version of the manuscript.

References

Abernathey, R. and Haller, G.: Transport by Lagrangian vortices in the eastern Pacific, J. Phys. Oceanogr., 48, 667–685, https://doi.org/10.1175/JPO-D-17-0102.1, 2018.

Amores, A., Jordà, G., Arsouze, T., and Le Sommer, J.: Up to what extent can we characterize ocean eddies using present-day gridded altimetric products?, J. Geophys. Res.-Oceans, 123, 7220–7236, https://doi.org/10.1029/2018JC014140, 2018.

Ballarotta, M., et al.: DUACS DT2018: Improved altimeter sea level products for monitoring mesoscale ocean variability, Ocean Sci., 15, 1091–1109, https://doi.org/10.5194/os-15-1091-2019, 2019.

Ballarotta, M., Ubelmann, C., Bellemin-Laponnaz, V., Le Guillou, F., Meda, G., Anadon, C., Laloue, A., Delepoulle, A., Faugère, Y., Pujol, M.-I., Fablet, R., and Dibarboure, G.: Integrating wide-swath altimetry data into Level-4 multi-mission maps, Ocean Sci., 21, 63–80, https://doi.org/10.5194/os-21-63-2025, 2025

Beauchamp, M., Febvre, Q., Georgenthum, H., and Fablet, R.: 4DVarNet-SSH: end-to-end learning of variational interpolation schemes for nadir and wide-swath satellite altimetry, Geosci. Model Dev., 16, 2119–2147, https://doi.org/10.5194/gmd-16-2119-2023, 2023.

Bonaduce, A., Cipollone, A., Johannessen, J. A., Staneva, J., Raj, R. P., and Aydogdu, A.: Ocean mesoscale variability: a case study on the Mediterranean Sea from a re-analysis perspective, Front. Earth Sci., 9, 724879, https://doi.org/10.3389/feart.2021.724879, 2021.

Cabanes, C., Grouazel, A., von Schuckmann, K., Hamon, M., Turpin, V., Coatanoan, C., Paris, F., Guinehut, S., Boone, C., Ferry, N., de Boyer Montégut, C., Carval, T., Reverdin, G., Pouliquen, S., and Le Traon, P.-Y.: The CORA dataset: validation and diagnostics of in-situ ocean temperature and salinity measurements, Ocean Sci., 9, 1–18, https://doi.org/10.5194/os-9-1-2013, 2013.

Ciani, D., Santoleri, R., Liberti, G. L., Prigent, C., Donlon, C., and Buongiorno Nardelli, B.: Copernicus Imaging Microwave Radiometer (CIMR) benefits for the Copernicus Level 4 sea-surface salinity processing chain, Remote Sens., 11, 1818, https://doi.org/10.3390/rs11151818, 2019.

Ciani, D., Fanelli, C., and Buongiorno Nardelli, B.: Estimating ocean currents from the joint reconstruction of absolute dynamic topography and sea surface temperature through deep learning algorithms, Ocean Sci., 21, 199–216, https://doi.org/10.5194/os-21-199-2025, 2025.

Chelton, D. B., Gaube, P., Schlax, M. G., Early, J. J., and Samelson, R. M.: The influence of nonlinear mesoscale eddies on near-surface oceanic chlorophyll, Science, 334, 328–332, https://doi.org/10.1126/science.1208897, 2011a.

Chelton, D. B., Schlax, M. G., and Samelson, R. M.: Global observations of nonlinear mesoscale eddies, Prog. Oceanogr., 91, 167–216, https://doi.org/10.1016/j.pocean.2011.01.002, 2011b.

Chenillat, F., Franks, P. J. S., and Combes, V.: Biogeochemical properties of eddies in the California Current System, Geophys. Res. Lett., 43, 5812–5820, https://doi.org/10.1002/2016GL069009, 2016.

Cullen, V. L.: Columbus Iselin and oceanographic research in the western North Atlantic, Oceanography, 18, 30–33, 2005.

CLS and CNES: DUACS Experimental Products Handbook: SSALTO/DUACS Level-4 Sea Surface Height and Derived Variables Gridded Products – Including SWOT MIOST Science, Version 1.2, April 2025, available at: https://www.aviso.altimetry.fr/fileadmin/documents/data/tools/hdbk_duacs_experimental.pdf, 2025.

Conti, D., Orfila, A., Mason, E., Sayol, J. M., Simarro, G., and Balle, S.: An eddy tracking algorithm based on dynamical systems theory, Ocean Dynam., 66, 1415–1427, https://doi.org/10.1007/s10236-016-0990-7, 2016.

Copernicus Marine Service: CMEMS-GLO-QUID-001-030: Quality Information Document for Global Ocean Reanalysis Product GLORYS12V1, Mercator Ocean International, available at https://documentation.marine.copernicus.eu/QUID/CMEMS-GLO-QUID-001-030.pdf, 2024.

Copernicus Marine Service: Product User Manual for Sea Level L4 NRT and MY Products, CMEMS-SL-PUM-008-046-047-060-068, Issue 1.0, Mercator Ocean International, available at: CMEMS-SL-PUM-008-046-047-060-068.pdf, 2025.

Copernicus Marine Service: Synthesis Quality Overview Document for Sea Level Products, CMEMS-SL-SQO-008-033-068, Issue 14.0, Mercator Ocean International, available at: CMEMS-SL-PUM-008-032-068.pdf, 2025.

de Vos, M., Backeberg, B., and Counillon, F.: Using an eddy-tracking algorithm to understand the impact of assimilating altimetry data on the eddy characteristics of the Agulhas system, Ocean Dynam., 68, 1071–1091, https://doi.org/10.1007/s10236-018-1174-4, 2018.

Droghei, R., Buongiorno Nardelli, B., and Santoleri, R.: A new global sea surface salinity and density dataset from multivariate observations (1993–2016), Front. Mar. Sci., 5, 84, https://doi.org/10.3389/fmars.2018.00084, 2018.

EO Portal: SWOT (Surface Water and Ocean Topography) Satellite Mission, available at: https://www.eoportal.org/satellite-missions/swot (last access: 15 April 2026), 2024.

Ezraty, R., Girard-Ardhuin, F., Piollé, J.-F., Kaleschke, L., and Heygster, G.: Arctic and Antarctic sea ice concentration and Arctic sea ice drift estimated from Special Sensor Microwave data, User's manual, Version 2.1, Département d'Océanographie Physique et Spatiale, IFREMER, Brest, France, and Institute of Environmental Physics, University of Bremen, Bremen, Germany, 2007.

Fablet, R., Chapron, B., Drumetz, L., Mémin, E., Pannekoucke, O., and Rousseau, F.: Learning variational data assimilation models and solvers, J. Adv. Model. Earth Syst., 13, e2021MS002572, https://doi.org/10.1029/2021MS002572, 2021

Faghmous, J. H., Frenger, I., Yao, Y., Warmka, R., Lindell, A., and Kumar, V.: A daily global mesoscale ocean eddy dataset from satellite altimetry, Sci. Data, 2, 150028, https://doi.org/10.1038/sdata.2015.28, 2015.

Fouchet, E., Benkiran, M., Le Traon, P.-Y., and Remy, E.: Comparison of a global high-resolution ocean data assimilation system with SWOT observations, Front. Mar. Sci., 12, 1563934, https://doi.org/10.3389/fmars.2025.1563934, 2025.

Fu, L.-L. and Ubelmann, C.: On the transition from profile altimeter to swath altimeter for observing global ocean surface topography, J. Atmos. Ocean. Technol., 31, 560–568, https://doi.org/10.1175/JTECH-D-13-00109.1, 2014.

Le Guillou, F., Metref, S., Cosme, E., Ubelmann, C., Ballarotta, M., Le Sommer, J., and Verron, J.: Mapping altimetry in the forthcoming SWOT era by back-and-forth nudging a one-layer quasigeostrophic model, J. Atmos. Ocean. Tech., 38, 697–710, https://doi.org/10.1175/JTECH-D-20-0104.1, 2021.

Le Traon, P. Y. and Morrow, R.: Ocean currents and eddies, in: Satellite Altimetry and Earth Sciences, Academic Press, 171–210, https://doi.org/10.1016/B978-012431551-4/50007-0, 2001.

Lellouche, J.-M., Le Galloudec, O., Drévillon, M., Régnier, C., Greiner, E., Garric, G., Ferry, N., Desportes, C., Testut, C.-E., Bricaud, C., Bourdallé-Badie, R., Tranchant, B., Benkiran, M., Drillet, Y., Daudin, A., and De Nicola, C.: Evaluation of global monitoring and forecasting systems at Mercator Océan, Ocean Sci., 9, 57–81, https://doi.org/10.5194/os-9-57-2013, 2013.

Lellouche, J.-M., Greiner, E., Le Galloudec, O., Garric, G., Regnier, C., Drevillon, M., Benkiran, M., Testut, C.-E., Bourdalle-Badie, R., Gasparin, F., Hernandez, O., Levier, B., Drillet, Y., Remy, E., and Le Traon, P.-Y.: Recent updates to the Copernicus Marine Service global ocean monitoring and forecasting real-time 1/12° high-resolution system, Ocean Sci., 14, 1093–1126, https://doi.org/10.5194/os-14-1093-2018, 2018.

Lellouche, J.-M., Greiner, E., Bourdallé-Badie, R., Garric, G., Melet, A., Drévillon, M., Bricaud, C., Hamon, M., Le Galloudec, O., Regnier, C., Candela, T., Testut, C.-E., Gasparin, F., Ruggiero, G., Benkiran, M., Drillet, Y., and Le Traon, P.-Y.: The Copernicus global 1/12° oceanic and sea ice GLORYS12 reanalysis, Front. Earth Sci., 9, 698876, https://doi.org/10.3389/feart.2021.698876, 2021.

Leroux, S., Brankart, J.-M., Albert, A., Brodeau, L., Molines, J.-M., Jamet, Q., Le Sommer, J., Penduff, T., and Brasseur, P.: Ensemble quantification of short-term predictability of the ocean dynamics at a kilometric-scale resolution: a Western Mediterranean test case, Ocean Sci., 18, 1619–1644, https://doi.org/10.5194/os-18-1619-2022, 2022.

López-Álzate, M. E., Sayol, J.-M., Hernández-Carrasco, I., Osorio, A. F., Mason, E., and Orfila, A.: Mesoscale eddy variability in the Caribbean Sea, Ocean Dynam., 72, 679–693, https://doi.org/10.1007/s10236-022-01525-9, 2022.

Ma, C., Guo, X., Zhang, H., Di, J., and Chen, G.: An investigation of the influences of SWOT sampling and errors on ocean eddy observation, Remote Sens., 12, 2682, https://doi.org/10.3390/rs12172682, 2020.

Madec, G. and Imbard, M.: A global ocean mesh to overcome the North Pole singularity, Clim. Dynam., 12, 381–388, https://doi.org/10.1007/BF00211684, 1996.

Madec, G. and the NEMO System Team: NEMO Ocean Engine Reference Manual, Zenodo [code], https://doi.org/10.5281/zenodo.1464816, 2024.

Martin, M. J., Hoteit, I., Bertino, L., and Moore, A. M.: Data assimilation schemes for ocean forecasting: state of the art, in: Ocean prediction: present status and state of the art (OPSR), edited by: Álvarez Fanjul, E., Ciliberti, S. A., Pearlman, J., Wilmer-Becker, K., and Behera, S., Copernicus Publications, State Planet, 5-opsr, 9, https://doi.org/10.5194/sp-5-opsr-9-2025, 2025.

Mason, E., Pascual, A., and McWilliams, J. C.: A new sea surface height–based code for oceanic mesoscale eddy tracking, J. Atmos. Ocean. Technol., 31, 1181–1188, https://doi.org/10.1175/JTECH-D-14-00019.1, 2014.

Mason, E., Pascual, A., Gaube, P., Ruiz, S., Pelegrí, J. L., and Delepoulle, A.: Subregional characterization of mesoscale eddies across the Brazil-Malvinas Confluence, J. Geophys. Res.-Oceans, 122, 3329–3357, https://doi.org/10.1002/2016JC012611, 2017.

Mason, E., Ruiz, S., Bourdalle-Badie, R., Reffray, G., García-Sotillo, M., and Pascual, A.: New insight into 3-D mesoscale eddy properties from CMEMS operational models in the western Mediterranean, Ocean Sci., 15, 1111–1131, https://doi.org/10.5194/os-15-1111-2019, 2019.

Morrow, R., Fu, L.-L., Ardhuin, F., Benkiran, M., Chapron, B., Cosme, E., d'Ovidio, F., Farrar, J. T., Gille, S. T., Lapeyre, G., Le Traon, P.-Y., Pascual, A., Ponte, A., Qiu, B., Rascle, N., Ubelmann, C., Wang, J., and Zaron, E. D.: Global observations of fine-scale ocean surface topography with the Surface Water and Ocean Topography (SWOT) mission, Front. Mar. Sci., 6, 232, https://doi.org/10.3389/fmars.2019.00232, 2019.

Mulet, S., Rio, M.-H., Etienne, H., Artana, C., Cancet, M., Dibarboure, G., Feng, H., Husson, R., Picot, N., Provost, C., and Strub, P. T.: The new CNES-CLS18 global mean dynamic topography, Ocean Sci., 17, 789–808, https://doi.org/10.5194/os-17-789-2021, 2021.

Pegliasco, C., Chaigneau, A., Morrow, R., and Dumas, F.: Detection and tracking of mesoscale eddies in the Mediterranean Sea: A comparison between the Sea Level Anomaly and the Absolute Dynamic Topography fields, Adv. Space Res., 68, 401–419, https://doi.org/10.1016/j.asr.2020.03.039, 2021.

Pegliasco, C., Delepoulle, A., Mason, E., Morrow, R., Faugère, Y., and Dibarboure, G.: META3.1exp: a new global mesoscale eddy trajectory atlas derived from altimetry, Earth Syst. Sci. Data, 14, 1087–1107, https://doi.org/10.5194/essd-14-1087-2022, 2022.

Rhines, P. B. and Young, W. R.: Homogenization of potential vorticity in planetary gyres, J. Fluid Mech., 122, 347–367, https://doi.org/10.1017/S0022112082002250, 1982.

Richardson, P. L.: Eddy kinetic energy in the North Atlantic from surface drifters, J. Geophys. Res.-Oceans, 88, 4355–4367, https://doi.org/10.1029/JC088iC07p04355, 1983.

Rogé, M., Morrow, R., Ubelmann, C., and Dibarboure, G.: Using a dynamical advection to reconstruct a part of the SSH evolution in the context of SWOT, application to the Mediterranean Sea, Ocean Dynam., 67, 1047–1066, https://doi.org/10.1007/s10236-017-1073-0, 2017.

Sangrà, P., Pascual, A., Rodríguez-Santana, Á., Machín, F., Mason, E., McWilliams, J. C., Pelegrí, J. L., Dong, C., Rubio, A., Arístegui, J., Marrero-Díaz, Á., Hernández-Guerra, A., Martínez-Marrero, A., and Auladell, M.: The Canary Eddy Corridor: A major pathway for long-lived eddies in the subtropical North Atlantic, Deep-Sea Res. Pt. I, 56, 2100–2114, https://doi.org/10.1016/j.dsr.2009.08.008, 2009.

Souza, J. M. A. C., de Boyer Montégut, C., and Le Traon, P.-Y.: Comparison between three implementations of automatic identification algorithms for the quantification and characterization of mesoscale eddies in the South Atlantic Ocean, Ocean Sci., 7, 317–334, https://doi.org/10.5194/os-7-317-2011, 2011.

Smith, G. C. and Fortin, A.-S.: Verification of eddy properties in operational oceanographic analysis systems, Ocean Model., 172, 101982, https://doi.org/10.1016/j.ocemod.2022.101982, 2022.

SSALTO/DUACS: Experimental Product Handbook: Gridded Sea Level Heights and geostrophic velocities computed with SWOT Level-3 products (using both KaRIn and nadir instruments), available at: https://www.aviso.altimetry.fr/fileadmin/documents/data/tools/hdbk_duacs_experimental_miost_swot.pdf, 2024.

Stephens, C. and Marshall, J.: Dynamical influence of air–sea buoyancy fluxes on the thermohaline circulation, J. Phys. Oceanogr., 29, 3042–3056, https://doi.org/10.1175/1520-0485(1999)029<3042:DIOASB>2.0.CO;2, 1999.

SWOT Science Team: SWOT Science Data Products User Handbook, NASA/JPL, available at: https://www.earthdata.nasa.gov/s3fs-public/2024-06/D-109532_SWOT_UserHandbook_20240502.pdf, 2024.

Szekely, T., Gourrion, J., Pouliquen, S., and Reverdin, G.: CORA, Coriolis Ocean Dataset for Reanalysis, SEANOE [data set], https://doi.org/10.17882/46219, 2019.

Taburet, G., Sanchez-Roman, A., Ballarotta, M., Pujol, M.-I., Legeais, J.-F., Fournier, F., Faugere, Y., and Dibarboure, G.: DUACS DT2018: 25 years of reprocessed sea level altimetry products, Ocean Sci., 15, 1207–1224, https://doi.org/10.5194/os-15-1207-2019, 2019.

Thoppil, P. G., Frolov, S., Rowley, C. D., et al.: Ensemble forecasting greatly expands the prediction horizon for ocean mesoscale variability, Commun. Earth Environ., 2, 89, https://doi.org/10.1038/s43247-021-00151-5, 2021.

Ubelmann, C., Klein, P., and Fu, L.-L.: Dynamic interpolation of sea surface height and potential applications for future high-resolution altimetry mapping, J. Atmos. Ocean. Tech., 32, 177–184, https://doi.org/10.1175/JTECH-D-14-00152.1, 2015.

Ubelmann, C., Cornuelle, B., and Fu, L.-L.: Dynamic mapping of along-track ocean altimetry: Method and performance from observing system simulation experiments, J. Atmos. Ocean. Technol., 33, 1691–1699, https://doi.org/10.1175/JTECH-D-15-0163.1, 2016.

Ubelmann, C., Dibarboure, G., Gaultier, L., Ponte, A., Ardhuin, F., Ballarotta, M., and Faugère, Y.: Reconstructing ocean surface current combining altimetry and future spaceborne Doppler data, J. Geophys. Res.-Oceans, 126, e2020JC016560, https://doi.org/10.1029/2020JC016560, 2021.

Walsh, K.: Objective detection of tropical cyclones in high-resolution analyses, Mon. Weather Rev., 125, 1767–1779, https://doi.org/10.1175/1520-0493(1997)125<1767:ODOTCI>2.0.CO;2, 1997.

Wang, G., Zhao, B., Qiao, F., and Zhao, C.: Rapid intensification of Super Typhoon Haiyan: the important role of a warm-core ocean eddy, Ocean Dynam., 68, 1649–1661, https://doi.org/10.1007/s10236-018-1217-x, 2018.

Wu, C., Lee, C., and Lin, I.: The effect of the ocean eddy on tropical cyclone intensity, J. Atmos. Sci., 64, 3562–3578, https://doi.org/10.1175/JAS4051.1, 2007.

Xie, J., de Vos, M., Bertino, L., Zhu, J., and Counillon, F.: Impact of assimilating altimeter data on eddy characteristics in the South China Sea, Ocean Model., 155, 101704, https://doi.org/10.1016/j.ocemod.2020.101704, 2020.

Xu, X., McClean, J. L., and Moore, A. M.: Assessing the predictability of mesoscale eddies in the Southern California Current System using an ensemble of regional ocean model simulations, Ocean Model., 122, 35–50, https://doi.org/10.1016/j.ocemod.2017.12.005, 2018.

Yang, C., Bricaud, C., Drévillon, M., Storto, A., Bellucci, A., and Santoleri, R.: The role of eddies in the North Atlantic decadal variability, Front. Mar. Sci., 9, 781788, https://doi.org/10.3389/fmars.2022.781788, 2022.

Yang, C., Bourdallé-Badie, R., Drevillon, M., Amaya, D., Aouf, L., Aydogdu, A., Barton, B., Bell, M., Boyer, T., Blauw, A., Carton, J., Candela, T., Cossarini, G., Dabrowski, T., de Boisseson, E., de Mora, L., Fablet, R., Forget, G., Fujii, Y., Garric, G., Giunta, V., Salamon, P., Hersbach, H., Juza, M., Le Sommer, J., Martin, M., McAdam, R., Menendez Garcia, M., Morim, J., Nicolì, D., Reppucci, A., Samuelsen, A., Sauzède, R., Slivinski, L., Specq, D., Storto, A., Tuomi, L., Vandenbulcke, L., Aznar, R., Beuvier, J., Cipollone, A., Clementi, E., Di Biagio, V., Escudier, R., Giesen, R., Greiner, E., Guihou, K., Korabel, V., Lamouroux, J., Law Chune, S., Lellouche, J.-M., Levier, B., Lima, L., Mangin, A., Mayer, M., Melet, A., Miraglio, P., Oikonomou, C., Pfeffer, J., Renshaw, R., Ringgaard, I., Thual, S., Titaud, O., Tonani, M., van Gennip, S., von Schuckmann, K., Drillet, Y., and Le Traon, P.-Y.: Gathering users and developers to shape together the next-generation ocean reanalyses, Bull. Amer. Meteorol. Soc., 106, E419–E429, https://doi.org/10.1175/BAMS-D-24-0034.1, 2025.

Zadra, A., McTaggart-Cowan, R., Vaillancourt, P. A., Roch, M., Bélair, S., and Leduc, A.-M.: Evaluation of tropical cyclones in the Canadian global modeling system: Sensitivity to moist process parameterization, Mon. Weather Rev., 142, 1197–1220, https://doi.org/10.1175/MWR-D-13-00124.1, 2014.

Zhang, Z., Wang, W., and Qiu, B.: Oceanic mass transport by mesoscale eddies, Science, 345, 322–324, https://doi.org/10.1126/science.1252418, 2014.